HU-P-D195

Dosimetry and dose planning in boron neutron capture therapy:
Monte Carlo studies

Hanna Koivunoro

Department of Physics
Faculty of Science
University of Helsinki
Helsinki, Finland

ACADEMIC DISSERTATION

To be presented, with the permission of
the Faculty of Science of the University of Helsinki,
for public examination in Auditorium D101,
Physicum, Gustav Hällströmin katu 2 A
on August 10th, 2012, at 12 noon

Helsinki 2012

SUPERVISED BY:

Professor Sauli Savolainen, PhD
Department of Physics
University of Helsinki
Finland

HUS Helsinki Medical Imaging Center
Helsinki University Central Hospital
Finland

REVIEWED BY:

Docent Maunu Pitkänen, PhD
Department of Oncology
Tampere University Hospital
Finland

Docent Antero Koivula, PhD
Department of Oncology
Oulu University Hospital
Finland

OPPONENT:

Docent Simo Hyödynmaa, PhD
Department of Oncology
Tampere University Hospital
Finland

Abstract

Boron neutron capture therapy (BNCT) is a biologically targeted radiotherapy modality. So far, 249 cancer patients have received BNCT at the Finnish Research Reactor 1 (FiR 1) in Finland. The effectiveness and safety of radiotherapy are dependent on the radiation dose delivered to the tumor and healthy tissues, and on the accuracy of the doses. At FiR 1, patient dose calculations are performed with the Monte Carlo (MC) -based treatment-planning system (TPS), Simulation Environment for Radiotherapy Applications (SERA). Initially, BNCT was applied to head and neck cancer, brain tumors, and malignant melanoma. To evaluate the applicability of the new target tumors for BNCT, calculation dosimetry studies are needed. So far, clinical BNCT has been performed with the neutrons from a nuclear reactor, while an accelerator based neutron sources applicable for hospital operation would be preferable.

In this thesis, BNCT patient dose calculation practice in Finland was evaluated against reference calculations and experimental data in several cases. Calculations with two TPSs applied in clinical BNCT were compared. The suitability of the deuterium-deuterium (D-D) and deuterium-tritium (D-T) fusion reaction-based compact neutron sources for BNCT were evaluated. In addition, feasibility of BNCT for noninvasive liver tumor treatments was examined.

The deviation between SERA and the reference calculations was within 4% in the phantoms studied and in a brain cancer patient model elsewhere, except on the phantom or skin surface, for the boron, nitrogen, and photon dose components. These dose components produce 99% of the tumor dose and > 90% of the healthy tissue dose at points of relevance for treatment at the FiR 1 facility. The reduced voxel cell size (≤ 0.5 cm) in the SERA edit mesh improved calculation accuracy on the surface. The erratic biased fast-neutron run option in SERA led to significant underestimation (up to 30–60%) of the fast-neutron dose, while more accurate fast-neutron dose calculations without the biased option are too time-consuming for clinical practice. The SERA calculations for thermal neutron fluence are also accurate (within 5%) in comparison to the activation foil measurements at FiR 1. Large (> 5%) deviation was found between the measured and calculated photon doses, which produces from 25% up to > 50% of the healthy tissue dose at certain depths.

The MCNP5 code is applicable for ionization chamber response within an accuracy of 2% ± 1%, which is sufficient for BNCT. The compact fusion-based neutron generators are applicable for BNCT treatments, if yields of $>10^{13}$ neutrons per second could be obtained. Noninvasive liver BNCT with epithermal neutron beams can deliver high tumor dose (about 70 Gy (W)) into the shallow depths of the liver, while tumor doses at the deepest parts of the organ remains low (about 10 Gy (W)), if the accumulation of boron in the tumor compared with that in the healthy liver is sixfold or less.

The patient dose calculation practice is accurate against reference calculation methods for the major dose components induced by thermal neutrons in the FiR 1 beam. Calculation of the thermal neutron fluence, which creates the most crucial patient dose, is also accurate against experimental data. Final verification of the fast neutron and photon dose calculation is restricted to high levels of uncertainty in existing measurement methods.

Preface

This thesis was carried out at various institutes: at the Department of Physics, University of Helsinki, the Lawrence Berkeley National Laboratory (LBNL) in Berkeley California, the Department of Oncology in Helsinki University Central Hospital, and the Boneca Corporation in Helsinki, Finland. All of these institutions are gratefully acknowledged.

Completion of this thesis work has been a long journey, which could not have been accomplished without the successful co-operation and generous help of many people, to whom I would like to express my sincere gratitude.

Particularly, I wish to thank the Head of the Department of Physics, Professor Juhani Keinonen, PhD, for supporting my studies and my thesis advisor Chief Physicist of HUS Helsinki Medical Imaging Center, Professor Sauli Savolainen, PhD, for initially introducing me to boron neutron capture therapy (BNCT) research, and for his patience, support and encouragement.

I owe my gratitude to Academy Professor Heikki Joensuu, MD, and Head of the Department of Oncology, Petri Bono, MD, for the opportunity to work in the inspiring environment of Oncology Clinic and for supporting my research. I am also grateful to Docent Mikko Tenhunen, PhD, for sharing his immense knowledge of radiotherapy and for his great efforts to explain things clearly.

I sincerely thank former Managing Director of Boneca Corporation, Mr. Markku Pohjola, MSc, and emeritus leader of the Plasma & Ion Source Technology Group at LBNL, Ka-Ngo Leung, PhD, for supporting my thesis research and providing me the opportunity to work on exciting projects.

I am deeply thankful to Docent Maunu Pitkänen, PhD, and Docent Antero Koivula, PhD, for careful review of this thesis and for their sound comments.

I am indebted to my many colleagues for providing a stimulating and fun environment in which to learn and work. Especially, I'm grateful to Petri Kotiluoto, PhD, for his dedicated support and interest in my research, his wise advice, and lots of helpful conversations during my thesis project. I thank Tiina Seppälä, PhD, for accommodating guidance and for numerous enthusiastic, thus helpful, debates related to dose calculations, and for being a friend over the years. I am thankful to Head of the FiR 1, Iiro Auterinen, TechMSc, for the opportunity to visit regularly the FiR 1 reactor, for the stimulating conversations and for clever counseling on my research. I also wish to thank Leena Kankaanranta, MD, for co-operation and insightful comments on my scientific investigations. I also thank Iiro and Leena for amusing company during various scientific trips over the past years. I am grateful to Tom Serén, TechLic, for sound conversations and for teaching me a great deal of neutron dosimetry.

I am thankful to the Head of the Radiation Metrology Laboratory of STUK, Docent Antti Kosunen, PhD, for introducing me to clinical dosimetry and making me interested in ionization chamber modeling. I wish to thank Docent Mika Kortesniemi, PhD, and Jouni Uusi-Simola, PhD, for helpful conversations related to ionization chamber measurements and BNCT dosimetry, and for delightful team work. I am deeply thankful to Teemu Siiskonen, PhD and Eero Hippeläinen, PhL, for fruitful cooperation during my ionization chamber odyssey.

My sincere thanks goes to Elisabetta Durisi, PhD, for good company and for pleasant alliance at LBNL and later on, for offering me the opportunity to visit and work with her research group at the University of Torino. I also deeply appreciate Hiroaki Kumada, PhD, for inviting me to work with him at the Japan Atomic Energy Agency, and for the smooth and interesting research collaboration.

I thank my fellow labmates in the Plasma & Ion Source Technology Group at LBNL. Especially, I am grateful to Tak Pui Lou, PhD, for kindly sharing his knowledge on Monte Carlo simulations as well as a tiny office with me for almost 3 years. I warmly thank Jani Reijonen, PhD, for teaching me about fusion neutron sources and for friendship during my years at LBNL. In addition, I am grateful to Darren Bleuel, PhD, for introducing me with BNCT dose calculations, for patiently reviewing my early scientific articles, and for good company during my years in California.

I wish to thank my friends, especially Anna, Paula, Ritva, Sanna, and Minttu for all the emotional support, comradeship, entertainment, and caring they have provided. In addition, I am grateful to Marko, who besides being a friend, also shares my interest in physics and recently, more specifically, in medical physics.

I am grateful to my dear brother Jussi, who probably taught me both to co-operate and argue persistently since a very early age. Special thanks are dedicated to my caring husband Mika for his love and patience during the past difficult years, and also for stopping my attempts to work during holidays by hiding my computer.

Lastly, and most importantly, I wish to thank my parents, Terttu and Heikki, for their care and support. Especially I owe gratitude to my Dad, who passed away too young for both of us one year ago and whom I miss terribly. Since the very beginning, Dad helped to make physics fun for me and without him, this thesis would not have happened. To him I dedicate this thesis.

4

Contents

LIST OF ORIGINAL PUBLICATIONS

I   Koivunoro H, Auterinen I, Kosunen A, Kotiluoto P, Seppälä T and Savolainen S 2003 Computational study of the required dimensions for standard sized phantoms in boron neutron capture therapy dosimetry *Physics in Medicine and Biology* **48** N291-300

II   Durisi E, Koivunoro H, Visca L, Borla O and Zanini A 2010 Comparison of different MC techniques to evaluate BNCT dose profiles in phantom exposed to various neutron fields *Radiation Protection Dosimetry* **138** 213-22

III   Koivunoro H, Kumada H, Seppälä T, Kotiluoto P, Auterinen I, Kankaanranta L and Savolainen S 2009 Comparative study of dose calculations with SERA and JCDS treatment planning systems *Applied Radiation and Isotopes* **67** S126-9

IV   Koivunoro H, Seppälä T, Uusi-Simola J, Merimaa K, Kotiluoto P, Serén T, Kortesniemi M, Auterinen I and Savolainen S 2010 Validation of dose planning calculations for boron neutron capture therapy using cylindrical and anthropomorphic phantoms *Physics in Medicine and Biology* **55** 3515-33

V   Koivunoro H, Bleuel DL, Nastasi U, Lou TP, Reijonen J and Leung KN 2004 BNCT dose distribution in liver with epithermal D-D and D-T fusion-based neutron beams *Applied Radiation and Isotopes* **61** 853-9

VI   Koivunoro H, Siiskonen T, Kotiluoto P, Hippeläinen E, Auterinen I and Savolainen S 2012 Accuracy of the electron transport in MCNP5 and its suitability for ionization chamber response simulations: A comparison with the EGSnrc and PENELOPE codes *Medical Physics* **39** 1335-1344

The author prepared the manuscripts of Publications I, III–VI, and contributed to the study design. The author participated in preparation of the Publication II manuscript at all stages. In addition, in the Publication I, the author performed the MCNP calculations and data analysis. In Publication II, the author gave conceptual advice and participated in the data analysis. In Publication III, the author performed the SERA calculations, and analyzed the data. In Publication IV, the author performed the simulations, analyzed the calculated data, and participated in carrying out the experiments. In Publication V, the author performed the calculations, and analyzed the results. In Publication VI, the author performed the MCNP calculations and analyzed the data.

SYMBOLS AND ABBREVIATIONS

2-D	Two-dimensional
3-D	Three-dimensional
4-D	Four-dimensional
ABNS	Accelerator-Based Neutron Source
ANSI/ANS	American National Standards Institute/American Nuclear Society
ASD	Aperture-to-Surface-Distance or Aperture-to-Skin-Distance
Au-RR	^{197}Au(n,γ)^{198}Au activation reaction rate
BAGINS	Birmingham Accelerator-Generated epIthermal Neutron Source
BNCT	Boron neutron capture therapy
BNCT_Rtpe	BNCT Radiation Treatment-Planning Environment, a Monte Carlo –based treatment planning software for BNCT
BNL	Brookhaven National Laboratory
BPA	^{10}B-boronophenylalanine
BSA	Beam-shaping assembly
BSH	Sodium borocaptate
BUGLE	Broad User Group Library ENDF/B, coupled neutron and gamma-ray cross-section library
CAVRZnrc	User code in EGSnrc software
CBE	Compound biological effectiveness factor
C-BENS	Cyclotron-Based Epithermal Neutron Source at the Kyoto University
CH	Condensed history (algorithm)
CSDA	Continuous slowing down approximation
CT	Computed tomography
CTV	Clinical target volume
D_B	Total absorbed dose from boron neutron capture
D_{fast}	Total absorbed dose caused by fast neutrons, mainly recoil protons from hydrogen
D_g	Total absorbed photon dose
D_N	Total absorbed dose from nitrogen neutron capture
DBCN	Debug information card in MCNP
D-D	Deuterium-deuterium
DORT	A two-dimensional discrete ordinate (deterministic) transport code
DOSRZnrc	User code in EGSnrc software
D-T	Deuterium-tritium
E	Energy
EGS	Electron Gamma Shower, a Monte Carlo simulation system
EGS4	A Monte Carlo code from the EGS system
EGSnrc	A Monte Carlo code from the EGS system
ENDF	Evaluated nuclear data file, cross-section data library

EPDL97	Evaluated Photon Data Library 97
ESTEP	Parameter on the MCNP material card, that describes the number of electron substeps per energy step
ETRAN	A Monte Carlo transport code for coupled electron-photon transport
^{18}F-FBPA	4-borono-2 [^{18}F] fluoro-L-phelyalanine
FiR 1	Nuclear research reactor located in Otaniemi, Espoo
Fluental^{TM}	Neutron moderator material developed at VTT
FLUKA	Fluktuierende kaskade, a Monte Carlo code
FLURZnrc	User code in EGSnrc software
GB-10	Polyhedral borane dianion
GEANT4	Geometry and tracking 4, a toolkit for the Monte Carlo simulation of the passage of particles through matter
GTV	Gross tumor volume
Gy (W)	Weighted Gray
HN	Head and neck
HU	Hounsfield unit
HVJ	Hemaggulutinating virus of Japan
IBA	Ion Beam Applications S. A.
IC	Ionization chamber
ICRU	International Commission on Radiation Units and Measurements
IND	Investigational new drug
INL	Idaho National Laboratory
IPPE	Institute for Physics and Power Engineering in Obninsk, Russia
IRDF	International reactor dosimetry file, a nuclear cross-section library
ITS	Integrated TIGER series of coupled electron/photon Monte Carlo transport codes
JAEA	Japan Atomic Energy Agency
JCDS	JAEA Computational Dosimetry System
JCDS-FX	JCDS based on PHITS code
KERMA	Kinetic Energy Released in MAtter by charged particles
KUR	Kyoto University Research Reactor
KURRI	Kyoto University Research Reactor Institute
LBNL	Lawrence Berkeley National Laboratory
L-BPA	4-borono-L-phenylalanine
LET	Linear energy transfer
MACLIB	Macrolibrary, a nuclear cross-section library
MacNCTPlan	Macintosh neutron capture therapy, a MCNP-based treatment planning software, successor of NCT_plan
McPTRAN.MEDIA	A Monte Carlo algorithm based on PTRAN
McPTRAN.CAVITY	A Monte Carlo algorithm based on PTRAN for ion chamber calculations

MIT	Massachusetts Institute of Technology
MC	Monte Carlo
MCNP	General Monte Carlo N-Particle Transport Code
MCNPX	Monte Carlo N-Particle Code extended
MCNP5	Version 5 of the MCNP code
$MCNP5_{ITS}$	ITS code based electron energy indexing algorithm in MCNP5
$MCNP5_{new}$	New algorithm for electron energy-loss straggling in MCNP5
MCNP6	A Monte Carlo code based on MCNPX and MCNP5
Mg(Ar)	Argon gas-filled ionization chamber with magnesium walls
MLV	Multistep Lattice-Voxel
Mn-RR	$^{55}Mn(n,\gamma)^{56}Mn$ activation reaction rate
MPM	Malignant pleural mesothelioma
MR	Magnetic resonance
MRS	Magnetic resonance spectroscopy
MultiTrans	A three-dimensional simplified spherical harmonics (deterministic) transport code
NCT_Plan	Monte Carlo-based treatment planning code for boron neutron capture therapy
NCT	Neutron capture therapy
NIST	National Institute of Standards and Technology
NRI	Nuclear Research Institute
PENELOPE	Penetration and Energy Loss of Positrons and Electrons, a Code System for Monte Carlo Simulation of Electron and Photon Transport
PENGEOM	Subroutine of PENELOPE for modeling of geometries and materials
PENMAIN	A generic main program of PENELOPE
PET	Positron emission tomography
PHITS	Japanese Particle and Heavy-Ion Transport code System, a Monte Carlo code
PMMA	Polymethyl-methacrylate plastic
ppm	Part per million
PRESTA	Parameter Reduced Electron Stepping Algorithm, an electron transport algorithm in EGS code for ionization chamber calculations
PSDL	Primary standard dosimetric laboratory
PTRAN	A Proton Transport Monte Carlo code
PTV	Planning target volume
Q value	Energy released in nuclear interaction: a difference of energies of parent and daughter nuclides
R_0	Continuous slowing down approximation range of electrons
RBE	Relative biological effectiveness
RE	Radioembolization
RF	Radio frequency

RSVP^{TM}	Radio Surgery Verification Phantom developed by the Phantom Laboratory
S(α,β)	Optional thermal neutron scattering treatment in MCNP, which accounts the molecular binding effects of hydrogen in the materials
SBRT	Stereotactic body radiation therapy
SERA	Simulation Environment for Radiation Applications
seraMC	Monte Carlo engine of SERA system
SIRT	Selective internal radiation therapy
SPRRZnrc	User code in EGSnrc software
TD 5/5	Tolerance dose, 5% probability of complications within five years
TE(TE)	Tissue equivalent ionization chamber
THOR	Tsing Hua Open-Pool Reactor in Hsinchu City, Taiwan
THORplan	A MCNP-based treatment planning software developed at National Tsing Hua University in Taiwan
TLD	Thermoluminescence dosimeter
TPS	Treatment planning system
TRIGA	Training, Research, Isotopes, General Atomics research reactor type
Univel	Uniform-volume element reconstruction method
VTT	Technical Research Center of Finland
w_i	Weighting factor
XCOM	Photon Cross-section Database

1 Introduction

In radiotherapy, a large dose of radiation is delivered to the tumor with the aim of destroying or damaging the cancer cells, while the dose to the surrounding healthy tissues is limited to a tolerable level. Conventional external radiotherapy is usually delivered via high-energy (megavoltage) photons or electrons produced by a linear accelerator. The effectiveness of the treatment is dependent on the radiation dose delivered to the tumor location and on the accuracy of the dose. If the dose falls along the steepest region of the dose-response curves, 5% changes in dose can already result in 10−20% changes in tumor control probability or up to 20−30% changes in normal tissue complication probabilities (Goitein and Busse 1975, Stewart and Jackson 1975). The International Commission on Radiation Units and Measurements (ICRU) recommends that the radiation dose delivered should be within 5% of the prescribed dose (ICRU 1978). This means that uncertainty at each step within the treatment process, including patient positioning, *dose planning* and *reference dosimetry measurements*, should be significantly smaller than 5%. The dose distribution computed can be considered accurate enough, if it differs from the relative dose measurements by less than 2% at points of relevance for the treatment (ICRU 1987).

The idea of neutron capture therapy (NCT) is to selectively target the tumor cells by high-linear energy transfer (high-LET) heavy particle radiation, which is released when the tumor-seeking compound is exposed to an externally applied neutron field (Locher 1936). In boron neutron capture therapy (BNCT), a ^{10}B containing compound is applied, since ^{10}B has an unusually high thermal neutron (E < 0.4 eV) capture reaction cross-section of up to 3843 barns (Chadwick *et al.* 2006). During neutron irradiation, ^{10}B disintegrates emitting highly energetic short-range (< 10 μm ~ cell diameter) particles, an α particle and ^{7}Li nucleus, via the ^{10}B(n,α)^{7}Li reaction (Q = 2.79 MeV). Thermal neutrons have little effect on normal cells, since the capture cross-sections of the major tissue elements ^{16}O, ^{12}C, ^{1}H, and ^{14}N are only 1.9×10^{-4} barns, 3.4×10^{-3} barns, 3.32×10^{-1} barns and 7.5×10^{-2} barns, respectively (Chadwick *et al.* 2006).

The initial clinical BNCT trials were carried out with the thermal neutron beams on highly malignant brain tumors in the United States, at Brookhaven National Laboratory (BNL, Upton, NY, USA) and Massachusetts Institute of Technology (MIT, Cambridge, MA, USA) during the years 1951–1961 (Slatkin 1991). The thermal neutrons penetrated insufficiently into the deep tumors, damaging the scalp, and the ^{10}B carrier accumulated inadequately in the tumor cells. Later on, clinical brain tumor trials continued in Japan in 1968 (Nakagawa and Hatanaka 1997). To avoid the thermal neutron penetration problem, the brain tumors were treated under anesthesia via an open craniotomy procedure and a new improved compound, sodium borocaptate (BSH) was applied as the ^{10}B carrier (Hatanaka and Sano 1973). In the 1980s, the melanoma-seeking ^{10}B compound ^{10}B-boronophenylalanine (BPA) was utilized for intravenous administration in cutaneous and intracerebral melanoma, combined still with the thermal neutron beams in Japan (Mishima *et al.* 1989).

In the 1990s, thermal neutrons were substituted with the higher energy epithermal (0.4 eV < E < 10 keV) neutrons for treatments of metastatic subcutaneous melanoma of the extremities in combination with orally taken BPA at MIT (Madoc-Jones *et al.* 1996). During the same decade, clinical BNCT trials were initialized in Europe, combining BSH and epithermal neutron beams in brain cancer treatments in Petten, The Netherlands (Hideghéty *et al.* 1999, Sauerwein *et al.* 2002). Soon after, BPA and epithermal neutrons were applied in brain cancer treatments at BNL (Coderre *et al.* 1997, Chanana *et al.* 1999), at MIT (Busse *et al.* 2003), in Sweden (Henriksson *et al.* 2008), in Japan (Imahori *et al.* 1998), and in Finland (Joensuu *et al.* 2003). Epithermal neutron beams combined with BPA have also been applied in head and neck (HN) cancer treatments in Japan (Aihara *et al.* 2006) and in Finland (Kankaanranta *et al.* 2007, 2011). In 2003, a clinical cutaneous melanoma trial was initiated utilizing BPA and a mixed thermal-epithermal neutron beam in Bariloche, Argentina (Menéndez *et al.* 2009). In Japan, both current boron carriers, BPA and BSH, were applied simultaneously with epithermal neutrons in brain tumor and HN cancer BNCT (Kato *et al.* 2004, Miyatake *et al.* 2005, Yamamoto *et al.* 2008), while BNCT was combined with conventional fractionated photon radiotherapy in primary treatment of brain tumors (Matsumura *et al.* 2009).

The first human liver cancer patients were treated with thermal neutrons in an isolated liver after surgical removal of the organ from the patient at the research reactor in Pavia, Italy (Pinelli *et al.* 2002). Few years later, the first noninvasive liver tumor BNCT was carried out at Kyoto University Research Reactor (KUR) in Japan: a patient with multiple inoperable liver tumors received BNCT without surgical procedure, using a newly developed boron delivery system, intra arterial administration of the boron compound with a vessel-embolizing agent, lipiodol, in the hepatic arteria (Suzuki *et al.* 2007). Both BPA and BSH were used as the ^{10}B carriers and the irradiation was given with an epithermal neutron beam. Suzuki *et al.* (2008) also treated the first lung cancer patients, a malignant pleural mesothelioma (MPM) and another malignant short spindle cell tumor, with BPA-mediated BNCT.

Originally, BNCT was applied as the last salvage therapy for heavily pretreated HN patients with recurrent cancer (Aihara *et al.* 2006, Kankaanranta *et al.* 2007, 2012). In 2010, BNCT was successfully applied as the first-line treatment of a large inoperable HN tumor in combination with intensity-modulated chemoradiotherapy in Finland (Kankaanranta *et al.* 2011).

To date, all the clinical BNCT trials have been carried out using reactor-based neutrons due to the high epithermal neutron flux (about 10^9 n cm^{-2} s^{-1}) required. The development of an accelerator-based neutron source (ABNS), which could be safely installed in a hospital, has been of interest for almost 3 decades (Barth *et al.* 1989, Blue and Yanch 2003, Barth and Joensuu 2007, Barth 2009). Development of such ABNSs comprises three challenging tasks (Blue and Yanch 2003). A high-power accelerator for producing a high-current charged particle beam is required. An appropriate neutron-producing target needs to be developed with an efficient heat removal system. A beam-shaping assembly (BSA) to reduce the initial neutron energy into an optimal epithermal neutron beam needs to be

designed. So far, the closest to the clinical ABNS for BNCT is the Cyclotron-Based Epithermal Neutron Source (C-BENS) built at the Kyoto University Research Reactor Institute (KURRI) in Osaka, Japan by Sumitomo Heavy Industries (Tokyo, Japan) (Tanaka *et al.* 2009). C-BENS produces neutrons through the ^{9}Be(p,n)^{9}B reaction, utilizing the 30 MeV proton beam at 1 mA current. Compact accelerators that produce neutrons through ^{2}H(d,n)^{3}He (deuterium-deuterium, D-D) or ^{3}H(d,n)^{4}He (deuterium-tritium, D-T) fusion reaction, developed at the Lawrence Berkeley National Laboratory (LBNL, Berkeley, CA, USA), have also been suggested for BNCT use (Reijonen *et al.* 2004, 2005).

In Finland, clinical BNCT trials were initiated by applying BPA as a ^{10}B carrier and epithermal neutrons from Finnish Research Reactor 1 (FiR 1, Otaniemi, Espoo, Finland), in malignant brain cancer patients in 1999 (Joensuu *et al.* 2003). So far, 249 patients have been treated with BNCT in 308 sessions, since some patients have received two or three treatments. Before initializing the clinical trials, the epithermal neutron beam was reconstructed at the 250 kW FiR 1 Training, Research, Isotopes, General Atomics (TRIGA) MARK II reactor, the radiobiological studies were carried out, the patient position system was developed, and the procedures for primary beam dosimetry, treatment planning, and blood ^{10}B concentration evaluation were established (Auterinen *et al.* 2001, Serén *et al.* 1999, Benczik 2000, Seppälä 2002, Kortesniemi 2002, Ryynänen 2002, Vähätalo 2004, Savolainen *et al.* 2012). Later on, complimentary dosimetric methods were examined (Aschan 1999, Karila 2006, Uusi-Simola 2009).

At FiR 1, fission neutrons of up to 15 MeV are slowed down to the epithermal energy range with Fluental^{TM} (69 w-% of AlF$_3$, 30 w-% of metallic Al, 1-w% ^{7}LiF, density about 3 g/cm^3) moderator material developed at the VTT Technical Research Center of Finland (VTT, Finland) (Auterinen *et al.* 2001). The moderated neutrons are collimated and gamma-shielded with bismuth into the high-intensity forward-directed (current-to-fluence ratio 0.77) epithermal neutron beam with low gamma, thermal neutron, and fast neutron contamination (Seppälä 2002). The FiR 1 beam model was established and verified for brain cancer patient dose planning in the PhD thesis study by Seppälä (2002). In addition, a new deterministic three-dimensional (3-D) neutral and charged particle transport code, MultiTrans, was developed for BNCT dosimetry and dose planning calculations within the Finnish BNCT project (Kotiluoto *et al.* 2001, Kotiluoto 2007).

The beam characteristics and intensity were confirmed with the measurements performed by the Finnish dosimetry team and by visiting teams from the Nuclear Research Institute (NRI), Rez, Czech Republic (Marek and Viererbl 2004), Idaho National Laboratory (INL), Idaho Falls, ID, USA (Nigg *et al.* 1999a) and MIT, USA (Binns *et al.* 2005). Neutron activation foils are used as the primary dosimetry method (Serén *et al.* 1999, Auterinen *et al.* 2004) and the dual ionization chamber (IC) technique as the secondary method (ICRU 1989, Kosunen *et al.* 1999). The feasibility and accuracy of the dual IC technique were evaluated in the PhD thesis work by Kosunen (1999). The uncertainties estimated for IC measurements are not satisfactory and should be improved to be closer to the requirements of conventional radiotherapy (Kosunen *et al.* 1999, Uusi-Simola 2009). Particularly, the

high level of uncertainty (4–20%) in photon dose (D_g) detection increases the uncertainty of the total patient dose (Seppälä 2002). The applicability of thermoluminescence dosimeters (TLDs) for detection of D_g was studied in two works: in the PhD thesis by Aschan (1999) and in the Licentiate thesis by Karila (2006). They concluded that the absorbed D_g can be measured with the TLDs within 20% in the mixed neutron-photon field, which enables *in vivo* measurements with approximately the same accuracy.

Current dosimetric practice was evaluated and complementary dosimeter types, a microdosimeter and polymer gels, were studied in the PhD thesis by Uusi-Simola (2009). The microdosimeter provided 10% lower D_g results than the IC measurements, but were roughly within measurement uncertainties, which were rather high (8%). The two gel dosimeter types studied were found suitable for measuring the relative two-dimensional (2-D) dose distribution in BNCT.

The dosimetry system was analyzed further and the blood boron concentration estimation system during the patient treatments, as well as the patient-positioning system, were developed within the PhD thesis by Kortesniemi (2002). The suitability of the mathematical models for predicting the kinetic behavior of ^{10}B in the patient during BNCT treatment were evaluated in the PhD thesis study of Ryynänen (2002). In addition, two PhD thesis works were published related to the ^{10}B carrier BPA. In one, 4-borono-L-phenylalanine (L-BPA) was evaluated for clinical BNCT trials and a radiolabeled analogue of L-BPA, 4-borono-2[^{18}F]fluoro-L-phenylalanine (^{18}F-FBPA), was developed for clinical positron emission tomography (PET) imaging studies (Vähätalo 2004). In another work, the magnetic resonance spectroscopy (MRS) imaging of BPA distribution in phantoms and in patients was examined (Timonen 2010).

In addition to several studies carried out in relation to BNCT dosimetry in Finland, challenges remain in both experimental and computational dosimetry. The dosimetric methods were investigated in the international Code of Practice in BNCT Dosimetry in Europe project (Voorbraak and Järvinen 2003) and in intercontinental BNCT dosimetry exchange collaboration (Binns *et al.* 2005, Riley *et al.* 2008). Among the other dosimetric goals, one aim was to define dimensions for the reference phantom used for beam verification and a large scanning phantom used for full characterization of the beam parameters in the BNCT beams.

To improve the D_g and the total dose detection accuracy with the dual IC method, it has been suggested that the perturbation effects and relative response of the chambers for the BNCT beam should be determined through computer simulations of an actual measurement situation (Munck *et al.* 2002, Kosunen *et al.* 1999). Primarily, the D_g detection accuracy should be improved, since the thermal and epithermal neutrons can be measured accurately with the activation foils. Modeling of the IC response for photons in a neutron field requires transport of electrons, in addition to neutrons and photons. An accurate simulation of the chamber response is a challenging task for the simulation codes, since it requires correct modeling of boundary crossing of electrons between media of highly different densities and electron backscatter from the chamber walls. Few codes that

have been verified for chamber response simulations at clinically required accuracy are not able to simulate neutron transport, whereas a coupled neutron-photon-electron transport code Monte Carlo N-Particle (MCNP) (Briesmeister 2000) utilized in BNCT dosimetry, has not been verified for the IC response simulations.

So far, beam characterization measurements and calculations have been performed in regular cylindrical or cubical phantoms with the flat ends attached to the beam port. This set up has been a valid verification method for treatments of regular targets, such as the brain. However, near the curvature boundary regions, discrepancy between the calculated and the measured dose is potentially greater. Therefore, verification of the measurements and calculations with more realistic anthropomorphic phantoms is recommended, when the treatments are extended from the brain to the HN area or elsewhere in the body (Kortesniemi 2004).

The treatment planning systems (TPSs) used currently in Finnish clinical trials miscalculates the dose near the surfaces of two very different densities, such as air or bone and soft tissue (Seppälä *et al.* 2002, Seppälä 2002). It has been suggested that reliability of the dose calculation could be enhanced if smaller voxel cells were applied in calculation edit mesh near the boundary regions (Seppälä 2002).

Each epithermal neutron beam applied for BNCT worldwide is unique and various dose-determining methods are available. Intercomparison measurements have shown that systematic differences of up to 10% are obtained between different institutes in determining the biologically weighted BNCT dose (Binns *et al.* 2005, Uusi-Simola 2009). To compare the clinical outcomes between the institutes, comparison of the beam parameters, applied dosimetry methods and the TPSs are necessary.

This thesis focuses on BNCT dosimetric studies, using Monte Carlo (MC) simulations. In the first part of the thesis, the computer simulations and main dosimetric methods used in external beam therapy are introduced. Afterwards, the dosimetric methods and simulation codes applied in BNCT, as well as neutron sources and target tumors suggested for BNCT, are summarized. Finally, six publications included in this thesis are reviewed with some unpublished additional data, and the conclusions and discussions of the study outcomes are provided.

2 Aims of the study

The aims of this thesis were, using MC simulations, to evaluate existing patient dose calculation practices applied in Finnish clinical BNCT trials against reference dose calculation methods and measurements, to establish new dosimetric methods for more accurate dose determination, and to evaluate the suitability of the compact accelerator-based neutron sources for BNCT. The specific aims were:

1. To determine the dimensions of a dosimetric reference phantom for neutron beam calibrations and a large water-scanning phantom for full characterization of the beam parameters (Publication I) and to evaluate the suitability of the MCNP code version 5 for IC response simulations (Publication VI).

2. To evaluate the dose calculations with the BNCT TPS in comparison to other dose calculation methods or measurements in different phantom geometries (Publication II and Publication IV), by comparing the cross-section libraries in function of neutron energy (Publication II), with different treatment distances (Publication IV), and in brain cancer patient treatment (Publication III).

3. To determine the applicability of accelerator-based fusion neutrons for BNCT treatments and the feasibility of treating liver tumors with external beam BNCT (Publication V).

In addition to the data published in the Publications I-VI, some previously unpublished simulation results are presented in Sections 6.1, 6.2, 7.2, and 8.1 of this thesis.

3 BACKGROUND

3.1 Computer applications in medical physics

Computer applications were originally developed to give faster and more accurate results in medical dosimetric problems that were at first handled by manual methods. Later on, computer techniques have been used more extensively and have enabled the solving of new problems, that could not have been considered without the aid of computers. The range of MC applications is very wide in medical physics (Rogers 2006). Computer simulations are used e.g. in TPSs for external beam radiotherapy, in photodynamic therapy, in nuclear medicine imaging, diagnostic X-ray applications, brachytherapy, in calculation of radiation protection quantities, and in modeling radiation detector response. This thesis focuses on computer simulation-based dose calculation in radiotherapy.

3.2 External beam therapy

3.2.1 Reference dosimetry

The purpose of clinical dosimetry is beam calibration and verification of the dose planning calculations. Current clinical dosimetry of external beam radiation therapy is based on determination of the absorbed dose to water, since it relates closely to the biological effects of radiation in tissue. Three basic dosimeters that are accurate enough for primary standard are the calorimeter, chemical dosimetry, and IC (ICRU 2001, Andreo *et al.* 2000). The ICs are usually applied at hospitals, since they are the most easily used instruments (Carrier and Cormack 1995). A cylindrical IC type may be used for the calibration of radiotherapy beams of medium-energy (above 80 kV) X-rays, ^{60}Co gamma beams, high-energy (MeV scale) photon beams, electron beams with energy above 10 MeV, and therapeutic proton and heavy-ion beams. The plane-parallel chambers are recommended for all electron energies and below 10 MeV their use is mandatory (Andreo *et al.* 2000).

Primary standard dosimetric laboratories (PSDLs) determine the absorbed dose to water, using water calorimeters, and provide calibration factors for the ICs in terms of absorbed dose to water for use in radiotherapy beams (Andreo *et al.* 2000). The reference conditions, which affect the absorbed dose measurement, are the geometrical arrangements such as distance from the radiation source to the detector and to the phantom surface, measurement depth in the phantom, phantom size and material, radiation field size, dose rate, and the ambient temperature, pressure, and relative humidity. The calibration measurements are typically performed under full-scattering conditions at the reference depth in a reference phantom. The reference medium recommended for electron and photon measurements is liquid water, whereas solid phantoms in slab form may be used for low-energy electron beams and are recommended for low-energy X-ray dosimetry (Andreo *et al.* 2000). The dose determination must always be referred to *the*

absorbed dose to water at the *reference depth* in a liquid water phantom (Andreo *et al.* 2000). The *reference phantom* size must extend to at least 5 cm beyond all four sides of the largest field size determined at the measurement depth and there should be a margin of at least 5 g/cm^2 (10 g/cm^2 for medium-energy X rays) beyond the maximum measurement depth (Andreo *et al.* 2000). The *reference depth* is on the beam axis in the phantom at the depth at which full backscattering is achieved. Typically, for a high-energy electron or photon beam, the reference measurement depth is at 5 g/cm or at 10 g/cm (Andreo *et al.* 2000).

3.2.2 Dose planning

Computerized radiotherapy TPSs are used in external beam radiotherapy to generate radiation beam shapes and dose distribution within the patient. For dose planning, the patient is imaged with computed tomography (CT) and often also with magnetic resonance (MR) or PET scanners. The medical images are used to determine the gross tumor volume (GTV) (ICRU 1993), often defined according to images taken before tumor resection, and clinical target volume (CTV), which contains GTV and subclinical microscopic malignancies to be treated adequately (ICRU 1993). The planning target volume (PTV) includes CTV and the surrounding margin, which is added to take into account all possible geometrical variations and inaccuracies to ensure delivery of the prescribed dose in the CTV (ICRU 1993). The CT images of the patient not only illustrate the locations of the PTV and healthy tissues, but also contain data on the tissues' electron density matrix, which can be utilized in dose distribution calculations in photon and electron beam therapy (Schneider *et al.* 1996). The dose planning determines the number, orientation, type, and characteristics (size and shape) of the radiation beams needed to deliver the desired radiation dose to the PTV, while dose to the surrounding healthy tissues remains at a tolerable level. The dose planning process consists of beam data acquisition from the measurements and entry into the TPS, patient anatomical data acquisition from the medical images, dose calculation, and the final transfer of data to the treatment machine. The beam data are acquired from the measurements in the reference condition. The reference condition is a beam, usually defined by a square aperture, directed at the surface of the reference phantom (ICRU 1987). Currently, 3-D image-based dose planning is the most common practice in the clinics. Recently, four-dimensional (4-D) image-based dose planning has also been used (Simpson *et al.* 2009).

In the current algorithms, the radiation beam data are decomposed into primary and secondary radiation components and are handled independently. In this way, changes in scattering due to beam shape, beam intensity, patient geometry, and tissue heterogeneities are taken into account in the dose distribution (IAEA 2005). The dose deposited by the photons can be calculated from the total photon-energy fluence distribution within the medium. The fluence distribution can be presented mathematically with the Boltzmann transport equation, which mathematically describes particle transport through the host medium (Duderstadt and Martin 1979). In current clinical applications, the Boltzmann equation is usually solved, using radiation kernels based on either convolution or

superposition methods. The kernel superposition methods are either point spread functions or pencil beams (ICRU 1987, Tillikainen *et al.* 2008). A weakness of kernel approaches is that they are only valid at points within the media at which charged particle equilibrium is reached in photon and electron beams. Disequilibrium of electrons exists near the interfaces between materials of highly differing densities such as lung, bone, and air.

An accurate method for solving the particle transport equation in full patient geometry is using either stochastic or deterministic methods. Rapid deterministic methods, such as the discrete ordinate method, are not currently available for clinical use (Gifford *et al.* 2006, Wareing *et al.* 2007, Kotiluoto *et al.* 2001). The MC method is stochastic and thus does not solve the Boltzmann transport equation numerically, but simulates a particle's probable behavior within the medium, using statistical sampling. MC methods are very accurate in complex treatment geometries and in cases of tissue heterogeneities, but are time-consuming, since a huge number of particles needs to be simulated to achieve results with low statistical uncertainty. Until recent times, MC methods have been too slow for routine clinical use (Chetty *et al.* 2007). Fast MC calculations often require utilizing variance reduction techniques and efficiency-enhancing methods (Kawrakow and Fippel 2000). Such fast MC algorithms have enabled clinical MC-based dose planning and are being implemented in various widely used commercial TPSs (Fragoso *et al.* 2010, Grofsmid *et al.* 2010, Heath *et al.* 2004, Künzler *et al.* 2008, Leal *et al.* 2003).

Currently, MC methods are considered the most accurate way to determine the dose in radiotherapy (Rogers 2006). These methods are used e.g. for determining beam parameters (energy deposition kernels) for radiotherapy dose planning and calculation of dosimetric parameters, such as water-to-air stoppingpower ratios and a variety of correction factors for IC measurements (Verhaegen and Seuntjens 2003, Chetty *et al.* 2007, Rogers *et al.* 2006).

3.2.3 Ionization chamber response simulations

The simulation of IC responses has been considered one of the most difficult calculation problems for MC codes (Nahum 1988, Kawrakow 2000, Rogers 2006). The code must correctly simulate electron transport through a gas-solid interface and electron backscatter from the chamber walls. In case of a neutron or charged particle beam, chamber response simulation also requires accurate transport of neutrons and often other charged particles initiated within the measurement geometry by neutrons.

Explicit simulation of electron transport interaction by interaction is often not feasible in practice, since an electron undergoes a huge number of small interactions during its lifetime. Electron transport simulations are usually solved with condensed history (CH) algorithms (Berger 1963). In CH algorithms, the cumulative effect of multiple collisions is condensed into a single "step" of electron path length, instead of modeling every interaction. This can be done, since most of the single collisions between electrons and atoms occur very closely together and result in very small changes in direction and energy

loss. During each CH step, angular scattering and energy loss processes of the particle transport equation are sampled from probability distributions based on multiple-scattering theories. For the multiple-scattering theories to be valid, the electron steps need to be long enough to represent many collisions, but short enough that the mean energy loss during each step is small.

Invention of the CH algorithm enabled the MC simulation of charged particle transport (Kawrakow 2000). In the class I CH algorithm, all collisions are simulated in the predetermined energy grid. One disadvantage of the algorithm is that most of the electron steps correspond to an energy that does not equal any of the grid energies and interpolations are needed. Another disadvantage is that the energy and direction of the primary particle are not affected by the secondary particles created along its path and therefore energy and momentum are not conserved in a single interaction. In the class II CH algorithm, all the interactions are divided into hard and soft collisions. The soft collisions are treated as in the class I approach, while the hard collisions (inelastic collisions above a certain threshold energy of the secondary electrons) are simulated explicitly collision by collision. The class I approach is used to describe multiple scattering and the class II approach to simulate radiative energy loss in the electron transport MC codes Couple Electron-Photon Transport (ETRAN) (Berger 1963, Seltzer 1988, 1991), Integrated Tiger Series (ITS) (Halbleib *et al.* 1992), MCNP (Briesmeister 2000), Geometry and Tracking 4 (GEANT4), (Agostinelli *et al.* 2003, Carrier *et al.* 2004) and Electron Gamma Shower (EGS) based codes (Nelson *et al.* 1985, Kawrakow and Rogers 2003, Kawrakow 2000a, Kawrakow 2000b). EGS4, EGSnrc, and GEANT4 employ the class II approach also to simulate collisional energy loss. Penetration and Energy Loss of Positrons and Electrons (PENELOPE) (Sempau *et al.* 1997, Salvat *et al.* 2006) implements the class II scheme for all electron interactions.

The first MC code able to simulate the IC response at the 0.1% level of accuracy (with respect to its own cross-sections) was EGSnrc (Kawrakow 2000a, 2000b). The precursor of the code, EGS4 and specially its Parameter Reduced Electron Stepping Algorithm (PRESTA), showed strong electron step size dependence of the calculated dose in a small low-density cavity (Rogers 1993). Thus the EGSnrc code was specially tailored for accurate IC response and electron-backscattering simulations by implementing various new algorithms in the code: a new any-angle multiple elastic-scattering theory, an improved electron step algorithm, a correct cross-section method for sampling distances between discrete interactions, a more accurate evaluation of energy loss, and an exact boundary-crossing algorithm (Kawrakow 2000a, 2000b). The EGSnrc code has been used extensively in determination of a wide variety of correction factors in radiation dosimetry (Mainegra-Hing *et al.* 2003, Capote *et al.* 2004, La Russa and Rogers 2006, La Russa *et al.* 2007, Wang and Rogers 2007, 2008a, 2008b). By definition, a more recent MC code, PENELOPE, is also an accurate tool for IC response simulations, since the boundary-crossing artifacts are avoided in the code (the surface-limiting scoring regions are not real boundaries) and electron transport can be performed fully explicitly (Salvat *et al.* 2003). Consequently, PENELOPE has provided IC response results within 0.2% from the analogue simulation of the same problem (Sempau and Andreo 2006). Neither the EGSnrc

nor the PENELOPE code is able to handle neutron transport, and thus for the IC response simulations in the neutron or charged particle beams, another code needs to be applied. The IC response simulations in the proton or heavy ion beam have been solved by applying an analytical model or the MC codes Fluktuierende Kaskade (FLUKA) (Kirby *et a.l* 2010), Proton Transport (PTRAN) (Berger 1993) or its MC algorithms McPTRAN.MEDIA and McPTRAN.CAVITY (Palmans 2004 and 2006, Palmans *et al.* 2002). The McPTRAN.MEDIA and McPTRAN.CAVITY are based on the transport algorithm of PTRAN that simulates proton pencil beams in homogenous water.

3.3 BNCT

3.3.1 Neutron sources

The optimum neutron beam energy for treating deep-seated tumors with BNCT is from the 4 eV to 40 keV energy spectrum peaking at 10 keV (Yanch *et al.* 1991). Since the most penetrating neutron beam can be easily moderated further to be less penetrating if needed, e. g. by placing a tissue-equivalent (TE) material on the patient's skin (Seppälä *et al.* 2004), the most penetrating neutron beam can be considered the optimum and the most usable for BNCT treatments of different tumor types. To date, all clinical BNCT trials have been carried out using reactor-based neutrons due to the high neutron flux required, while there is urgent need for hospital-based neutron sources (Barth and Joensuu 2007). The development of ABNSs, which could be safely installed at the hospital, has been of interest for almost three decades (Barth *et al.* 1989, Wang *et al.* 1990, Yanch *et al.* 1992, Barth 2009). Many different neutron-producing reactions could be exploited with an accelerator. The neutron-producing reactions are induced by accelerated protons, deuterons, or tritons targeting ^{7}Li, ^{9}Be, ^{13}C, ^{12}C, ^{2}H, or ^{3}H nuclei, via the reactions listed in Table 1.

Table 1 *Characteristics of charged particle reactions considered for acceleralor-based BNCT. The data were obtained from Bleuel (2003), Blue and Yanch (2003), and Tanaka et al. (2009).*

Reaction	Bombarding energy (MeV)	Average neutron energy (MeV)	Maximum neutron energy (MeV)	Neutron production rate (n mA^{-1} s^{-1})
^{7}Li(p,n)^{7}Be	2.5	0.55	0.79	9.1×10^{11}
^{9}Be(p,n)^{9}B	4.0	1.06	2.12	1.0×10^{12}
^{9}Be(p,n)^{9}B	30		28	1.9×10^{14}
^{9}Be(d,n)^{10}B	1.5	2.01	5.81	3.3×10^{11}
^{13}C(d,n)^{14}N	1.5	1.08	6.77	1.9×10^{11}
^{2}H(d,n)^{3}He	0.15	2.5	2.5	4.7×10^{8}
^{3}H(d,n)^{3}He	0.15	14.1	14.1	5.0×10^{10}

Probably, the most studied ABNS application is the ^{7}Li(p,n)^{7}Be reaction at approximately 2.5 MeV proton energy, because sufficiently low accelerator current (10 mA) is needed

for producing a high intensity of reasonably low-energetic neutrons (up to 1 MeV). Such BNCT beams with functional lithium target and BSA have been built at the University of Birmingham in the UK (Culbertson *et al.* 2004) and at the Institute for Physics and Power Engineering (IPPE) in Obninsk, Russia (Kononov *et al.* 2004). However, the neutron yields of these accelerator devices do not reach the reactor-based neutron beam intensity, probably because these accelerators were not originally designed for BNCT application. For the Birmingham Accelerator-Generated epIthermal Neutron Source (BAGINS, University of Birmingham, Birmingham, UK), the beam parameters measured are 17% lower than expected theoretically for the 1 mA proton beam at a potential of 2.8 MV, due to poor proton beam collimation, causing part of the proton beam to miss the Li target (Culbertson *et al.* 2004). In addition, there was an attempt by Ion Beam Applications S. A. (IBA, Louvain-La-Neuve, Belgium) to build a $^7Li(p,n)^7Be$ reaction-based accelerator device for BNCT (Forton *et al.* 2009). The accelerator was built to operate with a 20 mA proton beam current at 2.5 MeV, whereasthe measured neutron production data for the device have not been published.

A common problem for all neutron sources in BNCT is that, in contrast to other beam therapies (e.g. proton, fast neutron, photon, or electron sources), considerable moderation of the source neutrons is usually required, since the efficient ways of producing neutrons usually yields neutrons of high energy (> 0.7 MeV). The only way to slow these high-energy neutrons down is through nuclear interactions, and thus during the moderation, neutron intensity is reduced by about four orders of magnitude. Consequently, the BNCT neutron source needs to be operated at considerably higher power than a proton therapy accelerator. For example, the $^7Li(p,n)^7Be$ neutron source with 2.5 MeV protons requires 20 mA current for BNCT, whereas a typical proton therapy unit with proton energy up to 250 MeV operates at approximately 500 nA current. The high-intensity neutron source results in strong activation of the materials within the device. The higher the proton (and resulting neutron) energy the more likely that elements near the accelerator and within the BSA get activated. The binding energy of all nuclides found in nature is from 1.1 MeV to 8.8 MeV. At energies above 8.8 MeV, every possible element becomes activated. Thus, lower proton beam energy would be preferable in practice. In addition, difficulties in reducing the fast neutron and photon components from the clinical neutron beam are experienced (Tsukamoto *et al.* 2011), if high (up to 30 MeV) initial neutron energy is utilized.

A compact neutron source based on $^2H(d,n)^3He$ (D-D) or $^3H(d,n)^4He$ (D-T) fusion reactions yielding 2.45 MeV and 14.1 MeV neutrons, respectively, has been suggested for BNCT use (Verbeke *et al.* 2000, Cerullo *et al.* 2004, Publication V, Reijonen *et al.* 2005, Durisi *et al.* 2007). These reactions have positive Q values and thus, low bombarding energy is required in comparison to the other neutron-producing reactions. The fusion neutron source is compact in size and also safe for hospital use. The fusion-based neutron sources are commercially available. Such neutron sources used to be very common in neutron research facilities and at universities, and thus, the technology required is well known. For clinical BNCT, the yield required with D-D fusion neutrons is estimated to be on the order of 10^{12} neutrons per second and with the D-T fusion neutrons 10^{13} neutrons

per second (Reijonen *et al.* 2005). The neutron yield of commercially available fusion neutron sources is usually a maximum of about 10^8 neutrons per second.

The Plasma and Ion Source Technology group, team at the Ion Beam Technology Group, at LBNL has developed high-current D-D fusion neutron generators for various applications with neutron yields up to 10^{11} neutrons per second. The generators are of various designs, but all are operated with radio-frequency (RF) induction discharge, which ensures high efficiency and long lifetime (Reijonen *et al.* 2005). Basically, RF induction generates the deuterium plasma in the discharge chamber, usually with an external antenna. An advantage of RF induction discharge is its ability to generate high fractions of atomic ions from molecular gases and to generate high plasma densities for high extractable ion currents from relatively small discharge volumes (Reijonen *et al.* 2004). The RF discharge has demonstrated ion species nearly mono atomic. In the accelerator part of the generator, the ions are accelerated from the source to impinge on a metallic, usually titanic, target with voltages of about 120 kV or above. The ion beam self-loads the target surface with H^+ ions where the fusion reaction occurs. At an energy of 120 keV, the $^2H(d,n)^3He$ fusion reaction cross-section is already sufficiently high, while it further increases up to 2.4 MeV, as shown in Figure 1. The $^3H(d,n)^4He$ fusion reaction cross-section peaks at about 120 keV, which is clearly a favorable voltage for D-T neutron production. The D-T fusion reaction cross-section is about 200 times that of the D-D fusion reaction, and so the same ion beam current and voltage with D-T fusion provides 200 times higher neutron yield. The most powerful compact D-D neutron generator developed at LBNL is designed to operate with a 330 mA ^2H ion current and 120 kV acceleration voltage providing about 10^{11} neutrons per second (Reijonen *et al.* 2005). The same neutron generator is aimed to run with mixed ^2H and ^3H gas to yield about 10^{13} D-T fusion neutrons per second.
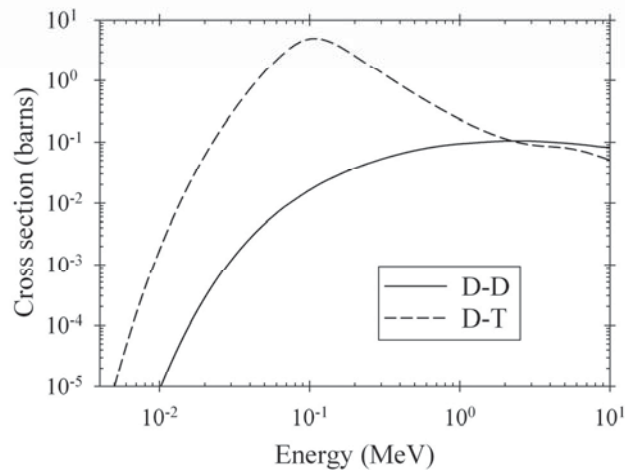
Figure 1 *$^2H(d,n)^3He$ (D-D) and $^3H(d,n)^3He$ (D-T) fusion reaction cross-sections plotted according to ENDF-B/VII.0 library data (Chadwick et al. 2006).*

3.3.2 Target tumors

In theory, some tumors are resistant to low-LET radiation. Some has suggested that high-LET radiation may offer a biological advantage in these tumors, since high-LET particle-induced cell killing is less dependent on oxygen levels than cell killing by low-LET beams (Warenius *et al.* 2000). In addition, high-LET radiation is densely ionizing and repair of potentially lethal damage occurs less frequently in cancer cells after high-LET irradiation (Gragg *et al.* 1977). In radiation-resistant tumors, the cells undergo slow cycling and are redistributed poorly, and the cell cycles are dominated by cells in resistant phases (Griffin and Phillips 1997). Radiation-resistant tumors include melanoma, sarcoma of the bone and soft tissues, adenocarcinoma of the thyroid, respiratory system, and alimentary systems and peripheral nerve tumors, such as gliomas.

As a source of high-LET radiation, BNCT has been used to treat radiation-resistant tumors. In the early days, BNCT was applied to high-grade gliomas and malignant inoperable melanoma in the brain and extremities. Due to the high gradient between healthy tissue dose and tumor dose, it has been possible to apply BNCT to recurrent tumors in patients who have previously received full dose of conventional radiation therapy. Later on, other brain tumors such as malignant recurrent inoperable meningiomas have also been natural candidates for BNCT due to extensive early research on BNCT effects on brain tissue (Miyatake *et al.* 2006). Lately, large recurrent inoperable HN tumors, including thyroid and oral cancer, have been treated with BNCT (Kouri *et al.* 2004, Kato *et al.* 2004, Kankaanranta *et al.* 2007, Kankaanranta *et al.* 2011). Since the prognosis in MPM is dismal, lung cancer has been of interest among BNCT researchers (Suzuki *et al.* 2006 and 2008, Protti *et al.* 2009, Bortolussi *et al.* 2010) and the first patients have been treated in Japan (Suzuki *et al.* 2007).

The liver is the most common target of metastases from many primary tumors (e.g. colorectal cancer, breast, lung, etc. (Vitale *et al.* 1986). The response rate for inoperable liver tumors to traditional radiation treatment or chemotherapy is poor, while surgical resection of limited metastatic liver tumors is effective in selected patient groups (Nordlinger *et al.* 1978, Fong *et al.* 1997, Singletary *et al.* 2003). With conventional techniques, radiation therapy for liver was not considered meaningful, since the tolerance dose (TD 5/5, 5% probability of complications within five years) is only 30 Gy for fractionated (from 1.8 to 2 Gy dose per day) whole liver irradiation (Emami *et al.* 1991). However, development of stereotactic body radiation therapy (SBRT) has enabled investigations of radiotherapy of selected liver metastases, since the SBRT method allows delivery of high radiation doses precisely focused on the target. Either a single dose or a small number of fractions has been utilized in liver tumor SBRT (Herfarth *et al.* 2004, Blomgren *et al.* 1995, Timmerman *et al.* 2003, Schefter *et al.* 2005). In SBRT studies, the mean doses to healthy liver remain low (maximum of 24 Gy), even in the highest dose group (Schefter *et al.* 2005). The high-dose study (60 Gy in three fractions) required that 700 ml of normal liver should receive less than 15 Gy and reported high (92%) local control rate at 2 years with mild acute toxicity (Rusthoven *et al.* 2009).

Previous clinical BNCT studies indicate that whole-liver BNCT could be an effective way to destroy liver metastases (Pinelli *et al.* 2002, Zonta *et al.* 2009). The first human liver cancer patient was treated with thermal neutrons in a liver with several adenocarcinoma metastases removed surgically from the patient (Pinelli *et al.* 2002). Due to the high concentration ratio between tumor and healthy cells (6:1) and their different responses to high-LET radiation, much higher boron dose (D_B) in the tumor than in healthy liver cells were delivered. However, due to the complexity of surgical removal of the liver and its high risks of complications, noninvasive BNCT given without removing the liver from the body may be preferable, if low dose to healthy tissue and sufficient tumor dose can be assured.

During recent decades, another new innovative targeting radiotherapy modality, radioembolization (RE) with yttrium-90 microspheres, often called selective internal radiation therapy (SIRT), has been introduced for liver cancer treatments (Dancey *et al.* 2000, Sarfaraz *et al.* 2003). The idea of SIRT is to deliver radioactive ^{90}Y isotope-containing microspheres directly into the tumor via the hepatic arteria, which is possible since the tumors are often more vascular than the normal liver (Dancey *et al.* 2000). In SIRT, it is possible to deliver high radiation doses up to >1000 Gy selectively in the tumor, while sparing healthy surrounding liver tissue (Dancey *et al.* 2000, Sarfaraz *et al.* 2003 and 2004, Stubbs *et al.* 2001). Nonetheless, while high tumor response rates have been reported, SIRT is a still palliative treatment modality (Prompers *et al.* 2011).

4. Overview of BNCT dosimetry

4.1 Dose components

An incident BNCT beam consists of neutrons and photons with wide energy spectra. Four distinct dose components with different biological effects are important when the beam enters tissue: the D_g, fast neutron dose (D_{fast}), nitrogen dose (D_N), and D_B (IAEA 2001). These dose components must be quantified, using special dosimetry procedures. The D_g consists of two components, primary photons initiated from the reactor core and BSA structures and secondary photons from the nuclear reactions within the tissue. The D_{fast} is primarily caused by fast but also epithermal neutrons through the ^{1}H(n,n')p reaction in tissue (also called the hydrogen dose or proton recoil dose). The D_N consists of a locally deposited dose from emitted protons and recoiling ^{14}C nuclei from the thermal neutron absorption reaction ^{14}N(n,p)^{14}C in tissue. The D_B consists of high-energy α and ^{7}Li particles. In 94% of the ^{10}B(n,α)^{7}Li reactions, 477 keV gamma rays are emitted, which are ignored in dosimetric evaluation, because they are about two orders of magnitude less significant than the gamma rays from the hydrogen capture reaction, although these characteristic gammas are utilized for ^{10}B analysis purposes.

All of the dose components have their own *relative biological effectiveness (RBE)*, and thus, to compare the BNCT dose with the fractionated absorbed dose in photon radiotherapy, each dose component needs to be multiplied with the *weighting factor* (w_i). Using w_i, the total *weighted absorbed dose* in photon dose equivalent units, *weighted Gray* (Gy (W)), can be defined as follows (Bleuel *et al.* 1998, Savolainen *et al.* 2001, Seppälä *et al.* 2001):

$$D_W = w_g D_g + w_B D_B + w_N D_N + w_{fast} D_{fast}$$

The w_i are energy- and dose rate-dependent and thus, are also dependent on individual beam characteristics and scattering conditions (location in the body or in the phantom). In addition, the biological effectiveness is dependent on the tissue. Moreover, synergy between the various radiation components is indicated, which results in a greater biological effect than would be in the case of independent action of the various radiation types (Phoenix *et al.* 2009). Nonetheless, constant values for the w_i values of 1 for D_g and 3.2 for D_{fast} and D_N are commonly applied, regardless of the tissue (Coderre and Morris 1999, Seppälä 2002).

D_{fast} and D_N are dependent on the hydrogen and nitrogen mass fraction and the mass density of the tissue. Most commonly, elemental compositions of tissues are defined according to ICRU Report 46 (ICRU, 1992), while in Finnish clinical protocol, the hydrogen and nitrogen compositions of the brain are defined according to Brooks *et al.* (1980) (10.6 mass-% of hydrogen and 1.84 mass-% of nitrogen), as in the Brookhaven clinical trials (Chanana *et al.* 1999, Seppälä 2002). In Finland, neutron transport is performed through ICRU-based tissues, but the difference in the hydrogen and nitrogen

mass fraction between the Brookhaven brain and the ICRU based brain is taken into account in the corresponding w_i values (Seppälä *et al.* 2001).

The w_i for D_B is called the *compound biological effectiveness factor* (CBE), since it is not only dependent on the radiosensitivity of the tissue, but also on the boron carrier applied. The CBE factors of 1.3, 3.8, and 2.5 for BPA in brain, tumor, and skin, respectively, are recommended (Coderre and Morris 1999) and applied in the Finnish clinical protocols (Seppälä 2002).

For calculation of the physical D_B, the boron concentration of tissue needs to be evaluated. The boron concentration of blood during neutron irradiation has been from about 11 parts per million (ppm) to 30 ppm, depending on the BPA infusion dose in the clinical BNCT trials in Finland (Kankaanranta *et al.* 2007, 2011, 2012).

4.2 Phantoms

BNCT dosimetry is performed in air to characterize the neutron beam and in the phantom to calibrate the beam model and normalize and verify the computational treatment planning. At the FiR 1 reactor, the dose planning normalization and validation are performed in a cylindrical phantom with dimensions (diameter 20 cm, length 24 cm) similar to those of the human head, because the clinical trials have been focused on the brain and HN tumor treatments. A solid polymethyl-methacrylate (PMMA) plastic phantom is used for dose planning normalization and a water-filled phantom for validation (Seppälä 2002). The dose planning normalization measurement is performed at the reference depth, which is located 2 cm deep along the central beam axis in the phantom for the FiR 1 beam, wherein the thermal neutron fluence maximum is reached. The solid plastic was chosen as the phantom material for beam normalization, instead of water, for more exact detector (activation foil) positioning and practicality, while water simulates BNCT doses in brain tissue better than PMMA (Seppälä 2002, Seppälä *et al.* 1999). Water is a suitable phantom material for dosimetry of epithermal neutron beams, since it is practical and provides scattering conditions similar to those of tissue (Seppälä *et al.* 1999, Raaijmakers *et al.* 1995, Wojnecki and Green 2001).

In dosimetry of external radiotherapy, the beam calibration measurements are typically performed under full scattering conditions at the reference point in a *reference phantom*. Full characterization of the dose components for beam model verifications in dosimetric and dose planning calculations must be performed in a *scanning phantom*, which is sufficiently large to approximate an infinite scattering medium at each measurement point. The *reference phantoms* or the large *scanning phantoms* recommended for photon, electron, fast neutron, and heavy ion therapy cannot be adopted directly in BNCT dosimetry, due to very different scattering and attenuation characteristics. To define the reference and scanning phantom dimensions for BNCT, each of the dose components needs to be considered separately, since they have independent spatial distributions. In Publication I, the minimum dimensions of a reference phantom and a large scanning

phantom were determined for beam calibration and neutron source characterization measurements at FiR 1. The study was performed as part of the Code of Practice in BNCT Dosimetry in Europe project (Voorbraak and Järvinen 2003).

The large homogenous phantoms are geometrically very unlike the patient, and thus anatomical phantoms have been applied for geometric considerations of the beam parameters. Water-filled Snyder (Snyder *et al.* 1969) or other similar ellipsoidal head phantoms have been used for comparisons of measurements and calculations (Kortesniemi 2002), to compare the treatment planning codes (Wojnecki and Green 2002, Goorley *et al.* 2002), or to study the BNCT beam parameters during beam optimization (Bleuel *et al.* 1998). The Snyder head phantom with anatomical structures (skin, skull, brain and possibly tumor) has been used to test the important aspects of the treatment planning codes such as dose volume calculations and calculation accuracy near material boundaries (Goorley *et al.* 2002, Albritton and Kiger 2006, Durisi *et al.* 2009).

In brain tumor BNCT, a beam aperture-to-skin surface distance (ASD) of nearly zero centimeters has been applied, and thus most phantom studies have been performed with the phantom attached to the beam aperture. However, for treatment of tumors located in the other parts of the body, increased ASD may be required. Although the beams are usually forward-directed at the beam aperture plane (at FiR 1, neutron current-to-flux ratio 0.77), changes in the ASD may lead to changes in the patient dose distribution. An irregular surface shape (face structures and jawline) also influences the dose distribution in typical HN cancer treatment, and thus validation of dose planning in the anthropomorphic phantoms is essential.

4.3 Primary dosimetry: activation foil technique

The D_B and D_N are not measured directly, but are calculated from the thermal neutron fluence measured with the neutron activation technique. At the FiR 1 facility, the thermal neutron and epithermal neutron fluence are determined through the $^{55}Mn(n,\gamma)^{56}Mn$ and $^{197}Au(n,\gamma)^{198}Au$ activation reaction rates (RR) (denoted from here on as Mn-RR and Au-RR, respectively) measurements with diluted Mn-Al and Au-Al foils (1 w-% of Mn and Au, respectively) (Nigg *et al.* 1999a, Seppälä 2002, Voorbraak and Järvinen 2003). The uncertainty of the Mn-RR and Au-RR measurements is only 3% (Seppälä 2002, Serén *et al.* 1999). Au-RR is used to normalize the beam model in a phantom, since the uncertainty of the $^{197}Au(n,\gamma)^{198}Au$ reaction cross-section is very low (< 1%) in comparison to the $^{55}Mn(n,\gamma)^{56}Mn$ reaction cross-section (< 4.5%) at the energy range of interest in BNCT (Seppälä 2002). The D_{fast} can be determined from the fast neutron fluence characterized via $^{115}In(n,n')$ (threshold 430 keV), $^{27}Al(n,\alpha)^{24}Na$ (threshold 6.5 MeV), $^{54}Fe(n,p)^{54}Mn$ (threshold 800 keV), or $^{58}Ni(n,p)^{58}Co$ (threshold 1.9 MeV) activation reaction measurements (Serén *et al.* 1999, Auterinen *et al.* 2004b, Nigg *et al.* 1999a, Chadwick *et al.* 2006). However, due to relatively low reaction cross-sections (Figure 2) and typically low contamination of the fast neutrons in the epithermal BNCT beams, fast neutron

activation of the elements is small, and thus the uncertainty of the fast neutron fluence rate measured is high (> 30%) (Serén *et al.* 1999).
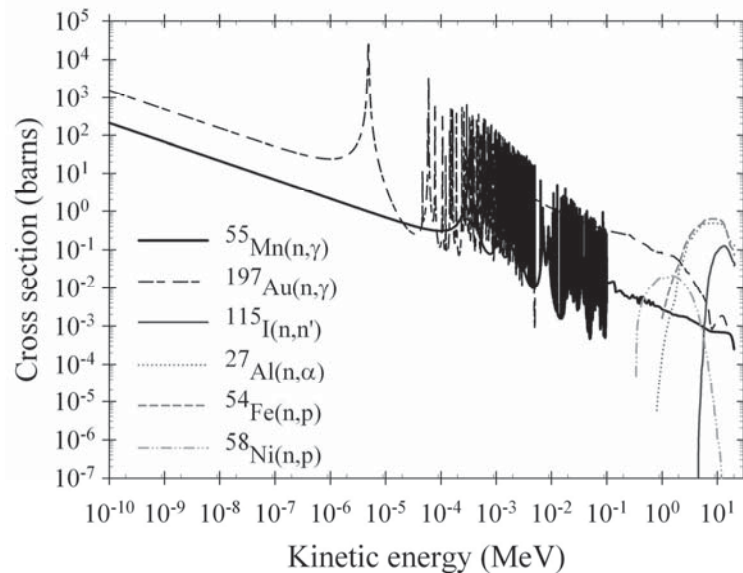

Figure 2 *Neutron activation reaction cross-sections utilized in BNCT neutron beam characterization plotted from ENDF/B-VII.0 library data (Chadwick et al. 2006).*

4.4 Secondary dosimetry: dual ionization chamber method

The dual IC method described in ICRU Report 45 (ICRU 1989) for fast neutron beam dosimetry is the recommended method for direct measurements of the total neutron and photon dose in BNCT (Rogus *et al.* 1994, Raaijmakers and Konijnenberg 1995, Kosunen *et al.* 1999, Kortesniemi 2002, IAEA 2001, Riley *et al.* 2003). The total dose is measured with the tissue-equivalent TE(TE) chamber and the photon dose with the nominally neutron-insensitive Mg(Ar) or the C(CO_2) chamber (Binns *et al.* 2005). The neutron dose is estimated by subtracting the measured photon dose from the measured total dose, which causes high uncertainty in the neutron dose measurement with the TE(TE) chamber (Kosunen *et al.* 1999). Uncertainties of the IC measurements in the BNCT beams are 4–20% for the photon dose and 5–30% for the fast neutron dose (Binns *et al.* 2005). Due to low fast neutron contamination of the BNCT beams, the high uncertainty of the fast neutron dose determination is accepted. The percentage contribution of the individual dose components to the weighted total brain dose at various depths calculated in the cylindrical water phantom is shown in Figure 3. Improvement of the photon dose detection accuracy is essential, since at certain depths in tissue (depending on the boron concentration), > 50% of the total weighted healthy tissue dose is due to the photon dose component. Moreover, photon dose covers over 80% of the total physical absorbed dose in water.
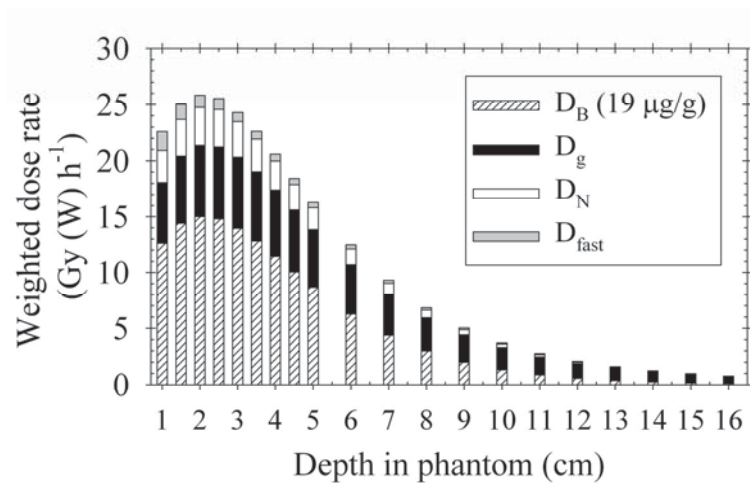
Figure 3 *Percentage contribution of the individual dose components to the weighted total brain dose at various depths in the cylindrical water phantom, when irradiated with a 14 cm diameter circular FiR 1 beam. The brain is assumed to contain 19 ppm of ^{10}B, 1.84 mass-% of nitrogen, and 10.6 mass-% of hydrogen. The weighting factors are: 3.2 for D_N and D_{fast}, 1 for D_g, and 1.3 for D_B.*

The relative photon sensitivity for the Mg(Ar) detector was previously defined through calibrations in water in a ^{60}Co gamma source and in a 6 MV linear accelerator photon beam (Kosunen *et al.* 1999). However, at the FiR 1 beam, the photons in the water phantom are mainly (90–98%) created within the medium, and they may have very different energies and angle distributions than the photons from a high-energy accelerator. Moreover, the existence of the chamber structures in the phantom changes the neutron and photon field in water compared with situations without the presence of the chamber (Kosunen 1999, Kosunen *et al.* 1999). Thus, determination of the IC sensitivity through measurements in a high-energy accelerator photon beam may be inaccurate and should be determined with computer simulations of the actual irradiation situation, mentioned already in the Introduction, as suggested by Munck af Rosenschöld *et al.* (2002) and Kosunen *et al.* (1999).

4.5 Dose planning

The absorbed dose in BNCT is due to nuclear interactions and thus the computational approximations in use for photon and electron therapy cannot be adopted for BNCT dose planning. Thus, specialized TPSs have been developed for BNCT use. To calculate the neutron interactions within the body, the elemental composition of the organs needs to be modeled, since the electron density information of the medical images cannot be utilized for dose calculation.

Regardless of the interest in developing a TPS based on faster deterministic calculation methods (Kotiluoto and Hiismäki 2001), only MC-based software programs have been applied in clinical BNCT. Four TPSs have been developed for BNCT purposes: NCT_Plan (Zamenhof *et al.* 1996), Simulation Environment for Radiation Applications (SERA) (Nigg *et al.* 1999b), Japan Atomic Energy Agency (JAEA) computational dosimetry system (JCDS) (Kumada *et al.* 2004) and THORplan (Lin and Liu 2006, Li *et al.* 2009). The precursors of the NCT_Plan and SERA were MacNCTPlan and BNCT_Rtpe with minor differences from the recent versions.

Three of the TPSs (NCT_Plan, JCDS and the THORplan) utilize the MCNP code for particle transport calculations and use a voxel reconstruction technique to produce a geometric description of the patient. In the voxel reconstruction technique, the medical image data are partitioned into uniform cubes and each cube is assigned appropriate material properties. Basically, each of these systems has unique procedures to convert patient medical data into a voxel model and assign the elemental composition within the model. Each system produces the input file for the MCNP calculations, and processes the output file data, such as dose volume histograms and the isodose contour plots over the medical images. The SERA system differs from these MCNP-based systems in its way of creating the patient model and performing the MC transport. The SERA system is described in detail in Section 5.1 and the JCDS system in Section 5.3.

The performance of the MacNCTPlan (Zamenhof *et al.* 1996) and BNCT_Rtpe (Nigg *et al.* 1997) have been compared in a phantom study by Goorley *et al.* (2002), mainly focusing on the voxel size in the patient model. Wojnecki and Green (2002) performed a dose calculation comparison between the MacNCTPlan and SERA systems (Nigg, 2003) in the phantom geometries. More recently, Casal *et al.* (2004) compared the calculations performed with the NCTPlan (González *et al.* 2005) and SERA systems to the measurements in a phantom at the RA-6 reactor facility in Argentina. The dose calculations with the THORPlan have been compared with the NCTplan, SERA, and MCNP in the modified Snyder head phantom (Li *et al.* 2009).

5 Summary of the applied Monte Carlo codes

5.1 *SERA* − treatment planning system

The SERA system consists of several software modules, including an image formatter and editor, 3-D viewer, dose-contouring and -plotting tools, particle transport-modeling interface, and a dose postprocessing function (Wessol *et al.* 2001). As mentioned in the previous section, the SERA system differs from the other BNCT TPSs in its way of producing the patient model and in tracking particles through this geometry. The patient model is reconstructed using a pixel-by-pixel uniform-volume element (univel) reconstruction method, and SERA's own MC algorithm, seraMC, is applied for neutron and photon transport calculations (Nigg 2003).

Any medical image modality can be used to create the patient model, since the model is independent of the initial image data. Anatomical regions are delineated on the 2-D medical images, and the delineated image slices are combined to form a 3-D patient model. The regions are assigned manually with the tissue data, typically obtained from ICRU Report 46 (ICRU 1992). The most significant difference between univel and standard voxel-based reconstruction and tracking methods (as used in MCNP) is that univel geometry enables use of the fast scan-line rasterization method, which allows rapid particle tracking through the univel geometry (Nigg 2003). Univel volumes along the particle track are investigated, and precise intersection points ('distance to boundary') are rapidly calculated as the particle moves from one anatomical region to the next. The photon and neutron transport are simulated using local material compositions set for each anatomical region within the patient model.

Another difference from the other BNCT TPSs is that radiation transport in seraMC is based on multi-energy group neutron and photon cross-sections instead of pointwise cross-sections (as in MCNP). The cross-section data in seraMC is based on the Evaluated Nuclear Data File (ENDF) library versions ENDF-B/IV and ENDF-B/V. The seraMC algorithm computes dose and fluence rates in the patient as a volume integral for each anatomical region (Wheeler 1999). A virtual edit mesh of cubic voxel cells (default size 1 cm^3) is imposed over all anatomical regions. The fluence and dose contribution, due to every particle path, that intersects with the voxel cell, are tallied in the cell. After the MC simulation, the pointwise dose is determined as a function of the volume-integrated values in each voxel cell. Point dose is determined as a function of the nearest seven edit voxels in orthogonal directions, except near the boundaries, where the nearest two voxels are used (Wheeler 1999). Fluence shape in the orthogonal directions is assumed to be a second-order polynomial. For dose calculation, flux-to-kinetic energy released in matter (KERMA) conversion factors from MACLIB (ENDF-B/IV) library are adopted. The interpolated surface dose may deviate from the real physical dose at the surface boundary, becauset the steep dose gradient is not taken into account in the interpolation and fitting schemes (Nigg 2003).

In Finland, the SERA system is applied to the dose planning calculations in clinical BNCT trials. The FiR 1 beam model is created with a 2-D discrete ordinate code transport code (DORT) (Rhoades and Childs 1988, Seppälä 2002) and transferred to the SERA system. In the DORT simulations, a coupled 67-group cross-section library Broad User Group Library ENDF/B-80 (BUGLE-80) was applied, which includes 47 neutron energy groups and 20 gamma energy groups specially defined for the light water reactor shielding calculations based on the ENDF-B/IV library (Roussin 1980). The new versions of the library (BUGLE-93 or BUGLE-96) have not been applied, albeit recommended by the BUGLE developers, since the new libraries are based on updated ENDF-B/VI data (White *et al.* 1996). The neutron beam model is validated with the neutron spectrum measurement, using several activation foils (Serén *et al.* 1999). Due to small differences between the measured and calculated neutron spectra and high levels uncertainty in the measurements at certain energies, the clinical beam model was not normalized according to the spectrum measured. The photon beam model has not been verified against measurements, since the contribution of the primary photons to the total biological dose is small in the phantom (or in the patient) (Seppälä 2002).

The SERA calculations have been validated for brain tumor dose planning (Seppälä 2002). The beam model is normalized with the Au-RR measurements at the reference measurement depth, 2 cm deep in the phantom. As mentioned in Section 4.3, the Au-RR and Mn-RR measurements are used as the primary dosimetric methods for calculation verification. At FiR 1, the original $^{55}Mn(n,\gamma)^{56}Mn$ and $^{197}Au(n,\gamma)^{198}Au$ reaction cross-sections (based on the International Reactor Dosimetry File-90 (IRDF-90) library) included in the SERA package are weighted with a Watt spectrum for fast neutrons, a 1/E spectrum for epithermal neurons, and a Maxwellian spectrum for thermal neutrons (Seppälä 2002). SERA calculations with the default-sized (1 cm^3) voxel cells have been found reliable in the homogenous medium inside the phantom, while 10–30% overestimation of the dose and the RRs has been observed on the phantom surface and near the air boundaries (Seppälä 2002, Seppälä *et al.* 2002). The effect of the reduced voxel cell size in the calculations on the surface is worth evaluating.

Due to the typically low number of fast neutrons in the BNCT beams, a biased fast neutron run function is included in SERA for better convergence of fast neutron calculations. If the biased fast neutron run is specified, a contribution to the D_{fast} from incident neutron energies greater than the given energy is added after a standard neutron transport run (Nigg 2003). In the FiR 1 neutron beam, the fast neutron flux is only bout 1/30 of the total neutron flux, and thus considerably higher calculation time is required to gain low statistical uncertainty at fast neutron energies. Thus, to obtain a practical dose calculation time in the clinical dose planning, the biased D_{fast} calculation option has been applied at FiR 1 (Seppälä 2002). However, notable differences between the D_{fast} values calculated with the SERA biased run option and MCNP were later reported (SERA underestimates D_{fast} by > 40%) (Casal *et al.* 2004, Albritton and Kiger 2006). A large difference (3.67 times) between the calculated and measured D_{fast} was reported by Riley *et al.* (2008), when SERA calculations were compared with measurements performed by

the MIT team at the FiR 1 beam. Consequently, D_{fast} determination with the SERA code in the FiR 1 beam requires verification.

5.2 *MCNP* − Monte Carlo code

One of the codes recommended for the BNCT dosimetric calculations (Voorbraak and Järvinen 2003) is the General *M*onte *C*arlo *N-P*article Transport Code (MCNP) (Briesmeister 2000, X-5 Monte Carlo Team 2008). The MCNP code was used as a simulation tool or as reference dose calculation method in Publications I–III. In Publication VI, electron transport accuracy of the MCNP was determined.

The MCNP system is maintained by a large group at the Los Alamos National Laboratory (Los Alamos, NM, USA) and was originally developed for coupled neutron-photon transport for the nuclear reactor calculations. Later on electron transport capabilities were included in the code and, furthermore, one earlier version of the code, Monte Carlo N-Particle Code Extended (MCNPX) (Waters 2002, Pelowitz *et al.* 2011), can also handle various other particles. The next version of the code, MCNP6 (Goorley *et al.* 2011), combines the capabilities of the MCNPX and MCNP version 5, but in addition contains new features not previously found in either code. The second beta version of MCNP6 was released in early 2012 (Goorley *et al.* 2011).

The MCNP code is widely used, due to its reliability and great flexibility in coupled photon-neutron transport calculations. The neutron energies in the code are from 10^{-11} MeV up to 20 MeV for all isotopes and up to 150 MeV for some isotopes, while the energy regime for photons is from 1 keV to 100 GeV and for electrons from 1 keV to 1 GeV. The point-wise continuous-energy cross-sections are applied for photons and neutrons based on more recent ENDF (ENDF-B/VI or ENDF-B/VII) data. All the reactions given for neutrons in the cross-section library are simulated. Neutron absorption is treated either in an analogue or implicit (the default) manner. The thermal neutron scattering in the default mode is treated as a free-gas model, which includes thermal motion of the nucleus, but neglects the complex chemical binding effects and interaction of the target atom with the nearby atoms in the scattering kinematics (Briesmeister 2000). For certain molecules and mixtures, the $S(\alpha,\beta)$ *thermal-scattering treatment* is available in the code, which includes the complete thermal neutron-scattering law to account for the molecular-binding effects of hydrogen in the materials. Accounting for the molecular-binding effects of hydrogen in the biological materials is essential in BNCT dose calculation (Goorley *et al.* 2002), and thus the $S(\alpha,\beta)$ treatment is applied for liquid water and solid plastics in all the MCNP simulations of this thesis. For photons, the MCNP code accounts for incoherent and coherent scattering, the possibility of fluorescent emission after photoelectric absorption, and absorption in electron-positron pair production (Breismeister 2000).

In terms of electron transport, MCNP is a class I CH code, and thus an electron's energy loss and direction are sampled from predetermined multiple-scattering distributions in case

of every electron collision. Radiative energy loss is simulated explicitly in an analogue manner. Electron (and positron) transport processes in MCNP5 account for angular deflection through multiple Coulomb scattering, collisional energy loss with optional straggling, and the production of secondary particles including K x-rays, knock-on and Auger electrons, bremsstrahlung, and annihilation gamma rays from positron annihilation at rest (X-5 Monte Carlo Team 2008). The most important electron transport algorithms are the Goudsmit-Saunderson (Goudsmit and Saunderson 1940) theory for angular deflections, the Landau (Landau 1944) theory of energy loss fluctuations, and the Blunck-Leisegang (Blunck and Leisegang 1950) enhancements of the Landau theory (correction for electron binding effects).

The multiple-scattering theory implies that, the electron step length must be long enough to encompass many collisions, but short enough that the mean energy loss within any one step is small. Thus, in the MCNP (as in all the ETRAN codes (Seltzer 1991)), the major electron energy step is broken into smaller substeps of equal lengths. The representation of the electron's trajectory as the result of many small steps is more accurate, since the angular deflections per (sub-) step are then smaller (X-5 Monte Carlo Team 2008). In the MCNP, the number of substeps is dependent on the average atomic number of the material. The user can increase, but not decrease, the number of substeps per energy step (the electron substep (ESTEP) parameter in the code). The MCNP manual recommends increasing the ESTEP parameter in case the expected number of substeps in a material region is less than 10. In particular, a very small material region may not accommodate enough substeps for an accurate simulation of the electron's trajectory. Thus, it may be useful to increase the ESTEP number in the IC response simulations for the gas cavity, as has been done in the first two IC response studies with MCNP by Roca *et al.* (2002) and Munck *et al.* (2002).

In the MCNP versions earlier than MCNP5 (X-5 Monte Carlo Team 2008) release 1.40, all parameters needed for sampling electron energyloss straggling were predetermined for standard energy boundaries and for the corresponding electron path lengths. The problem with this method is that an electron may not complete its major step before it reaches a geometric boundary and a systematic error in energy loss calculation occurs, since the actual major step length is less than the step length originally used for determining the collisional energy loss. Two optional methods for choosing energy boundaries were available by altering the 18th entry of the debug information card (DBCN): the default MCNP logic (DBCN 18 card = 0) and the ITS electron energy indexing developed previously for the ITS codes (DBCN 18 card = 1). Both these algorithms cause systematic errors in the electron transport calculations, due to the geometrical and energy grid resolution dependency (Jeraj *et al.* 1999, Chibani and Li 2002, Reynaert *et al.* 2002, Schaart *et al.* 2002). In MCNP5 version 1.4 (X-5 Monte Carlo team 2008), the electron transport has been improved by introducing a new detailed approach for electron transport (DBCN 18 card = 2): instead of calculating the electron energy straggling in the predetermined energy grid, the Landau distribution for energy straggling is sampled for each energy step, using the specific energy of the electron and the actual step length. Other electron transport events at the substep level (angular deflections, production of electron-

induced x-rays, and knock-on electrons) are still pre-computed in both logics. The new detailed electron transport model eliminates the step-size artifacts in a small geometric volume in water (Hughes 2005). Thus, in the recently released beta 2 version of MCNP6, the new detailed logic for Landau electron energy straggling is set as the default option for electron transport (Hughes 2011).

5.3 *JCDS* − treatment planning system

The JCDS system creates a detailed 3-D model of a patient, based on CT and MR image data for MC transport. Structures such as bone, soft tissue, and air are delineated, based on the Hounsfield unit (HU) values in the CT images (Kumada *et al.* 2004). MR images are used to delineate regions of interest within the structures. The JCDS system converts the patient model into a voxel model (Kumada *et al.* 2009). Each voxel cell is assigned to the proper material. The elemental data of each anatomical structure are defined according to ICRU report 46 (1992), but can also be modified manually. The particle fluences and the absorbed doses are calculated in the mesh elements superimposed over the patient model, using the Mesh Tally function of the MCNP5 code (X-5 Monte Carlo Team 2008, Kumada *et al.* 2006). Mesh Tally calculation requires shorter execution time, and thus higher resolution can be used in the patient voxel model, which enables accurate particle transport near tissue boundaries (Kumada *et al.* 2006). After the particle transport simulation, the JCDS system estimates the detailed dose distribution in the patient model by interpolating the mesh tally calculation results. JCDS also provides information on the patient's positional data, which can be utilized by the patient setting system (Kumada *et al.* 2004). The JCDS system is used as a comparative dose calculation method in Publication III.

In the next version of the code, JCDS-FX, the MCNP code as a calculation tool is replaced by the Japanese Particle and Heavy-Ion Transport code System (PHITS) (Iwasa *et al.* 2002), because the PHITS code can accurately simulate electrons, protons, and heavy particles in addition to photons and neutrons (Kumada *et al.* 2009, Kumada *et al.* 2011). The JCDS-FX system is also able to handle PET image data in addition to MR and CT data and it can handle a pixel-based voxel model of the patient, which further improves estimation of dose. Since such a small voxel geometry slows down the MC simulation considerably, the latest version of the JCDS-FX system includes a new geometry modeling function Multistep Lattice-Voxel (MLV) method, which enables creation of a voxel model of different voxel sizes (Kumada *et al.* 2011). In the MLV method, uniform material regions are described as single large voxels and regions consisting of two or more materials are described as pixel-sized voxel cells, each labeled with an appropriate material (Kumada *et al.* 2011). This modeling technique improves calculation time, since the total number of voxels in the patient model is decreased.

5.4 *PENELOPE* − Monte Carlo code

PENELOPE is a code system for MC simulation of coupled electron-photon transport, initially developed to simulate the PENetration and Energy LOss of Positrons and Electrons in matter. PENELOPE was also used as a reference calculation method in Publication VI.

The PENELOPE code performs particle transport in an arbitrary 3-D configuration of materials for electron, positron and photon energy ranges from 50 eV to 1 GeV. Photon interactions are simulated analogously event by event, in chronological order. For generation of the electron and positron tracks, a class II CH method is implemented: all interactions that involve changes in the kinetic energy or direction of flight are simulated in an analogous manner above certain threshold values given for scattering angle and energy loss. Below the threshold values, class I multiple-scattering methods are applied. The particle-tracking algorithm of PENELOPE operates independently of interface proximity and requires only knowledge of the material at the current position of the particle. Thus, the boundary-crossing artifacts are avoided. PENMAIN is a generic main program of PENELOPE, that performs simulations of electron-photon transport in complex material structures. It is well benchmarked against experimental data (Baro *et al.* 1995, Sempau *et al.* 1997, Sempau *et al.* 2003). Geometries and materials are modeled using the subroutine PENGEOM, which is able to handle complicated geometries very efficiently. The photoatomic database and the Compton momentum profiles are taken from the Evaluated Photon Data Library 97 (EPDL97) (Cullen *et al.* 1997) and Biggs *et al.* (1975) respectively. Atomic cross-sections for incoherent scattering of photons, inelastic scattering of electrons and positrons, and positron annihilation are evaluated directly from the analytical differential cross-sections (Salvat *et al.* 2003, 2008).

5.5 *EGSnrc* − Monte Carlo code

The EGS is a code system for the MC simulation of electron, positron, and photon transport (Nelson *et al.* 1985) in any element, compound or mixture. EGSnrc is an extended and improved version of the previous EGS4 system (Kawrakow and Rogers 2000) and has been used as a reference calculation method in Publication VI.

The EGSnrc system includes the user codes DOSRZnrc, FLURZnrc, CAVRZnrc, and SPRRZnrc, for scoring the dose in a generalized cylindrical geometry, particle fluence in the same geometry, a variety of quantities of specific interest to IC dosimetry calculations, and for calculation of Spencer-Attix spectrum-averaged stopping power ratios for any medium, respectively (Rogers *et al.*2011). The range of photon energies is between 1 keV and several hundred GeV and that of charged particles from a few tens of keV up to a few hundred GeV. The EGSnrc code employs the class II condensed method approach to simulate radiative and collisional energy loss (without the energyloss straggling) of electrons. The multiple scattering is simulated for steps of any size and moves from a single scattering model for short steps to an accurate multiple-scattering model at large

steps (Kawrakow *et al.* 2011). The user can choose between scattering based on Rutherford scattering or scattering accounting for relativistic and spin effects. As mentioned in Section 3.2.3, an accurate PRESTA-II algorithm is used for moving the electrons and positrons from one position to another. To avoid boundary-crossing artifacts, the electron/positron transport switches from CH to exact analogue modeling near boundaries. The distance from the boundary where the exact model is turned on can be set by a number of elastic-scattering mean free paths (the default value is 3). Bremsstrahlung production is modelled using either Bethe-Heitler cross-sections or the National Institute of Standards and Technology (NIST) cross-sections (Kawrakow *et al.* 2011). Compton scattering is simulated, using either the Klein-Nishina or bound Compton model. It is possible to use user-supplied atomic and molecular form factors for Rayleigh scattering. The total photon cross-sections can be chosen from EPDL97, XCOM, or any other user-supplied tabulation in addition to the default Storm and Israel tabulations.

6 Methods for BNCT dosimetry

A major difference between dosimetry of BNCT and conventional radiotherapy beams is that the epithermal neutron beams have unique spectral and angular distributions, (Rogus *et al.*1994, Riley *et al.*2003, Raaijmakers *et al.*1997, Woollard *et al.*2001) and thus the phantom geometries applied in the photon and electron beam dosimetry cannot be directly applied in BNCT. The phantom dimensions, which provide full back-scattering conditions at the reference measurement depth (*reference phantom*) and at every measurement point (*full-scanning phantom*) need to be determined.

As mentioned earlier, the accuracy of the IC measurements and at the same time, determination accuracy of the D_g and D_{fast}, is unsatisfactory. One reason for the inaccuracy may be inaccurately determined response for mixed neutron-photon beams, which should be determined through computer simulation of the measurement situation. However, the simulation codes, EGSnrc and PENELOPE, which are able to simulate IC response accurately, are not able to simulate neutron interactions. For IC response simulations in neutron beams, use of the MCNP code has been proposed (Munck af Rosenschöld *et al.*2002). The applicability of MCNP code (version 5) for IC response simulations has been investigated in comparison to EGSnrc and PENELOPE codes in Publication VI.

6.1 Reference phantom and water scanning phantom for BNCT

The MCNP code (version 4b) was used for determining the minimum dimensions for the reference phantom and a large water-scanning phantom (Publication I). To determine the impact of phantom size on the beam parameters at the measurement points, the water phantoms with several wall lengths were simulated and the results were compared with those obtained in a virtually infinite phantom, wherein the full-scattering conditions are gained. The induced D_g, D_{fast} (E > 0.5 eV), total dose rates to ICRU brain (ICRU, 1992), and the thermal neutron (E < 0.5 eV) and total neutron fluence rates were evaluated. The beam gamma component was not considered, because at its maximum (at the beam entrance), the beam gamma (primary photons) contribution to the total physical dose in the water phantom is only 2% (< 0.2 Gy/h) in the FiR 1 beam.

The calculated D_g components with depth in the phantom for the 14 cm diameter FiR 1 beam are plotted in Figure 4. It can be seen that the primary D_g in the phantom decreases gradually with depth, while the secondary (or induced) D_g decreases with deep gradients beyond the dose maximum, and thus at depths $\geq$ 6 cm, the contribution of primary photons to the total photon dose is D_g 3–10%.

It was found that the minimum dimension for the reference phantom is a 40 cm wall length for beam diameters from 14 cm to 20 cm in the FiR 1 beam. In the smaller phantoms, the uncertainty of the D_g increases, due to leakage from the geometry. For undisturbed measurements of the thermal neutron fluence at the reference depth, the margin between the beam aperture edge and phantom wall needs to be at least 3 cm and

for the D_{fast} at least 6–10 cm, regardless of the beam size. Correspondingly, undisturbed D_g measurements need a margin of approximately 10 cm. Thus, the size of a reference phantom needs to be defined based on the D_g measurement requirements. A lower limit for the phantom depth was not determined, but the 20 cm deep phantom was large enough to provide undisturbed doses and fluences at the reference point.
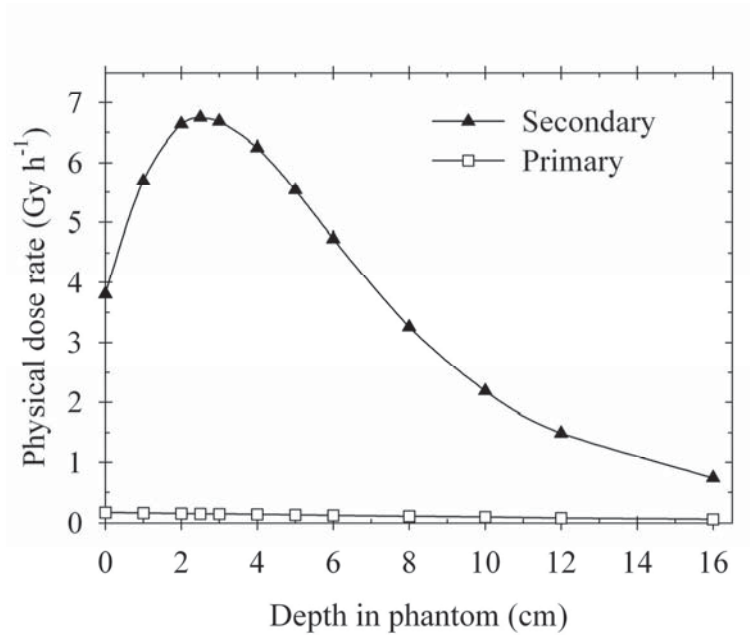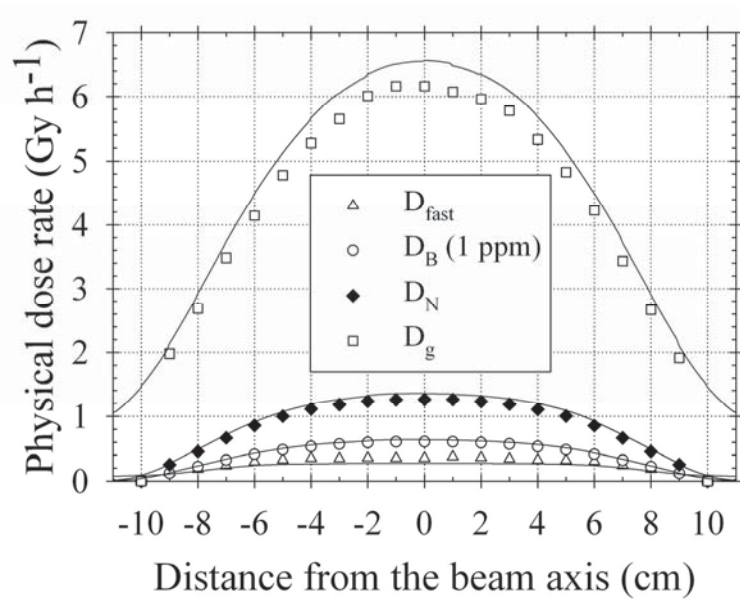

Figure 4 *Photon depth dose calculated with MCNP5 in the large water phantom (wall length 53.6 cm and height 49 cm) for the secondary and primary photons with the 14 cm diameter circular beam aperture. The statistical uncertainty is ≤ 0.6% (1σ).*

Only the largest phantom (56 cm × 56 cm and 28 cm deep) studied was large enough to fulfill requirements for a *large scanning phantom*. The most distant measurement point was found at a radial distance of 19.5 cm in the 14 cm beam, which sets s radial limit for the phantom size. The *large scanning phantom* in BNCT needs to extented at least 7 cm deeper than the most distant measurement point, which was found at 18 cm and 21 cm depths for the 14 cm and 20 cm beam sizes, respectively.

In the other studies of this thesis, the dose distributions were evaluated in the cylindrical water phantom (diameter 20 cm and length 20 cm) or in the similarly sized head geometry (an anthropomorphic phantom, ellipsoidal Snyder phantom, and a patient's head). At the FiR 1 facility, the main dosimetric phantoms are the large water-scanning phantom (wall length 51 cm and height 47 cm) with cylindrical extension (diameter 20 cm and length 20 cm) and the cylindrical PMMA phantom (diameter 20 cm and length 24 cm). To show the impact of these real phantom geometries on the neutron and photon dose components, the

radial dose profiles calculated with MCNP5 at a 2 cm depth in the water phantoms is plotted in Figure 5 for the 14 cm diameter FiR 1 beam. It is clear from Figure 5 that phantom geometry has no effect on the neutron dose components at radial distances within 4 cm from the beam axis. However, the D_g is 6–30% higher in the large phantom at every point. In the cylindrical phantom, photons leak out more from the phantom, whereas in the large phantom higher photon backscattering is obtained.


Figure 5 *Radial distributions of the physical neutron and photon dose components calculated with MCNP5 at the 2 cm depth in the cylindrical (symbol) and large (line) water phantoms for the 14 cm diameter FiR 1 beam. The statistical uncertainty (1σ) of the calculations is ≤ 0.6%.*

6.2 Suitability of the MCNP5 code for IC response simulations

In Publication VI, the purpose of the study was to evaluate the accuracy of the MCNP5 code in the electron transport calculations and suitability of the code for the IC response simulations, using either the ITS-based electron transport model (MCNP5$_{ITS}$) or the new detailed algorithm for electron energyloss straggling (MCNP5$_{new}$). The calculations with the EGSnrc and PENELOPE codes were used as a benchmark, due to their ability to provide results that agree closely with the experimental data for photon and electron beams (Doucet *et al.* 2003, Vilches *et al.* 2009, Rodríguez 2008, Sterpin *et al.* 2008) and their capability for simulating the IC response with high accuracy (Kawrakow *et al.* 2000, Sempau and Andreo 2006).

The accuracy of the MCNP electron transport was evaluated by comparing the depth dose curves in water, using discrete energies (0.05 MeV, 0.1 MeV, 1 MeV and 10 MeV) for the

broad (radius 10 cm) parallel electron beams in a water phantom subdivided into multiple thin (1/30 of electron's continuous slowing down approximation (CSDA) range, R_0) layers. For the IC response simulation evaluation, the absorbed dose was calculated in a small gas cavity, comparable to an IC gas cavity placed at the reference measurement depth in the water phantom and exposed to three different monodirectional high-energy photon beams: a ^{60}Co source, 6 MV linear medical accelerator, and a 2 MeV photon source. The 2 MeV monoenergetic photon beam was studied, because it approximates the hydrogen neutron capture gamma energy (2.2 MeV) which predominates in the water or TE phantom in BNCT, as can be seen in the photon spectrum plot in Figure 6.
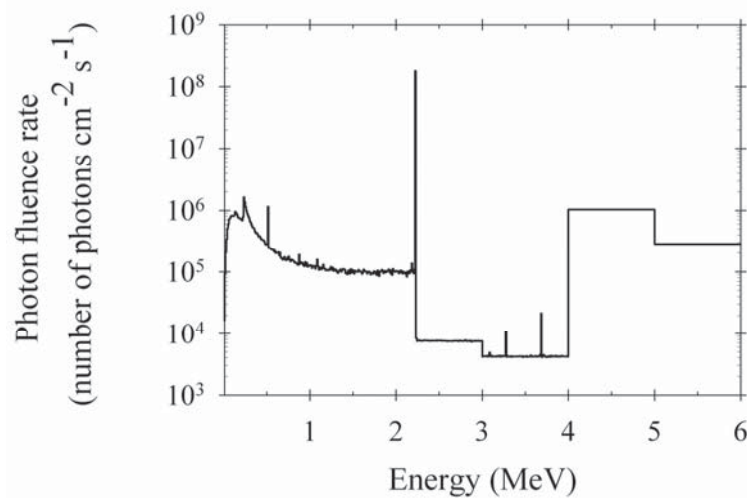

Figure 6 *MCNP5 calculation for the photon spectra at the 2.5 cm depth, where the photon dose maximum occurs in the cylindrical (diameter 20 cm) water phantom in the 14 cm diameter circular beam at the FiR 1 facility.*

The doses in three dosimetric gases were studied: air, argon, and methane-based TE-gas. The gas cavity was modeled to be comparable to the cylindrical part of the Exradin^{TM} M2 and T2 IC gas cavity (hollow cylinder of height 0.9 cm, outer radius 0.48 cm and inner radius 0.23 cm, volume 0.50 cm^3) as shown in Figure 7. In the ^{60}Co photon source, the influence of the ESTEP parameter set for gaseous material on the MCNP dose calculation was determined. The other simulation parameters applied in three codes are described in Publication VI.

At the 10 MeV beam energy, the MCNP5$_{new}$ results agreed with PENELOPE within 2% and with EGSnrc within 1%, whereas the MCNP5$_{ITS}$ results agreed with the reference codes within 2% only at depths up to 0.4R_0 and showed strong boundary-crossing artifacts at the deeper depths. At every lower beam energy, both the MCNP5 electron transport models deviated from the reference calculations by > 2%. The deviation was greatest at

the 0.1 MeV and 0.05 MeV energies and at the tails of the dose curves, especially in MCNP5$_{ITS}$.
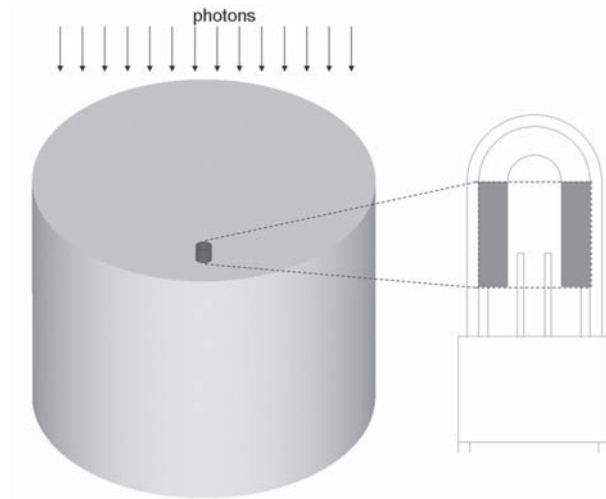

Figure 7 *Illustration of the simulation geometry (left) and a cross-sectional view of the Exradin^{TM} ionization chamber geometry (right). The gray area of the ionization chamber image corresponds to the gas volume studied (dark gray) placed in the water cylinder in the simulation geometry.*

Since the boundary-crossing artifacts were observed in the MCNP5 results, further simulations were performed by calculating the depth doses in the single scoring cells and comparing the results with those obtained for multiple layers. When the excessive boundary crossing was discarded, the dose calculation improved dramatically at the dose curve tails, but still the deviation from the reference codes was large (up to 20%) for the 0.1 MeV and 0.05 MeV electron beams. As was expected, the boundary-crossing artifacts were more notable in the MCNP5$_{ITS}$ than in the MCNP5$_{new}$, because the energy loss sampling in MCNP5$_{new}$ is independent of interfaces. The boundary-crossing artifacts with the MCNP5$_{new}$ were found only for the 0.1 MeV and 0.05 MeV beams.

For the IC response simulations, it was found that the MCNP5$_{ITS}$ dose estimate agreed with both the reference codes in every gas, except in argon at 2 MeV beam energy, in which case the dose was overestimated by 1.4% (± 1%). The MCNP5$_{ITS}$ dose calculations were nearly independent (maximum change 2%) of the ESTEP value chosen, whereas the MCNP5$_{new}$ dose estimate was highly dependent on the gaseous material and the ESTEP value selected for the gas. The MCNP5$_{new}$ agreed with the reference codes only if the default ESTEP value was applied for argon and if the ESTEP value was increased to 500 for TE-gas and air. When the ESTEP value was increased, the MCNP5$_{new}$ dose estimate decreased and, thus disagreed with the reference codes by 15% at most. The reason for the dose reduction at high ESTEP number was that the electron fluence was reduced at the smallest energies along with increase in the ESTEP number (as shown in Figure 8 for

argon), most probably because implementation of the Goudsmit–Saunderson multiple-scattering theory in MCNP5 is not valid for very short substep lengths.
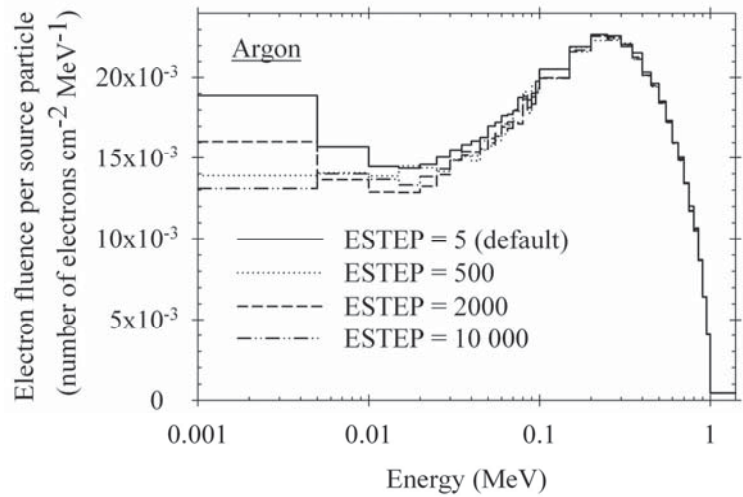
Figure 8 *Electron energy spectra in the argon-filled gas cavity in the water phantom exposed to the ^{60}Co beam calculated with MCNP5$_{new}$, using various ESTEP values (number of substeps per electron energy step) for argon. The error-bar of the electron fluence is 1–3% (lσ) per energy bin.*

7 Dose planning calculations

A combination of simple phantoms and more realistic conditions is recommended for the quality assurance and analysis of a BNCT TPS (IAEA 2001, Albritton and Kiger 2006). The basic features of the TPS, such as the effects of different cross-section libraries and fluence-to-dose conversion factors can be analyzed in simple phantoms with simple neutron sources. A more complex phantom with several materials and boundaries, and possibly irregular surface structures, is required for more realistic performance analysis. For the final assurance of the TPS, the dose calculation evaluation needs to be performed with a realistic neutron source in clinical patient cases.

The dose calculation performance of the SERA system was evaluated in comparison to measurements (Publication IV) and reference calculations, using either the MCNP code (Publications II and IV) or the JCDS system (Publication III). In Publication II, the dose calculation was evaluated in simple mono-energetic and -directional neutron sources in two ellipsoidal Snyder (Snyder *et al.* 1969) head phantoms. The aim was to evaluate the effect of the cross-section libraries and the dose calculation methodologies. In the publication III, the SERA dose calculations were compared with the JCDS system in a brain tumor patient case applying the clinical FiR 1 neutron beam. The aim was to determine the influence of the actual patient geometry in the dose calculations and verify the volumetric dose calculations in each region of interest. In the Publication IV, the SERA calculations were evaluated in a simple cylindrical water phantom and in a more complex irregular anthropomorphically shaped water head phantom by comparisons to measurements and MCNP calculations in the FiR 1 beam.

7.1 Calculation comparison with mono-energetic neutron beams

In Publication II, the neutron fluence and dose distributions in two ellipsoidal phantoms were investigated for six mono-directional and -energetic neutron beams of energies (25 meV, 1, 5, 10, 100 keV and 1 MeV), which were also applied in the BNCT simulation studies by Goorley *et al.* (2002) and Wojnecki and Green (2002). MCNP code version 4C2 was applied for the reference calculations with cross-sections from the ENDF-B/VI data library. In SERA, the cross-sections data from ENDF-B/IV and ENDF-B/V libraries are reprocessed into 94 neutron energy groups, as mentioned already in Section 5.1. The neutron cross-sections in SERA are listed as the total elastic scattering and the total absorption cross-sections instead of exact nuclear reaction cross-sections for the nuclides. In the water phantom, thermal (E < 0.414 eV) and total neutron fluences, as well as D_{fast}, D_g, and the total dose were compared. The more realistic head phantom was modeled, including the skin, skull, and brain regions with material compositions according to ICRU report 46 (ICRU 1992) (listed in Table 2). The biological doses were evaluated and the following w_i values applied: 1 for D_g, 3.2 for D_{fast} and D_N, 1.3 for D_B in brain, and 2.5 for D_B in skin.

Table 2 *Elemental compositions (percentage by mass) of body tissues applied for the Snyder phantom, according to ICRU report 46 (ICRU 1992).*

Tissue	H	C	N	O	Other
Brain	10.7	14.5	2.2	71.2	0.2 Na, 0.4 P, 0.2 S, 0.3 Cl, 0.3 K
Skin	10.0	20.4	4.2	64.5	0.2 Na, 0.1 P, 0.2 S, 0.3 Cl, 0.1 K
Cranium	5.0	21.2	4.0	43.5	0.1 Na, 0.2 Mg, 8.1 P, 0.3 S, 17.6 Ca

In the water phantom, high discrepancy (17–24%), between the SERA and MCNP neutron fluences was obtained at the thermal (25 meV beam) and fast (1 MeV beam) neutron energy, due to differences in the oxygen and hydrogen elastic-scattering cross-sections for water at these energy ranges (plotted in Figure 9 and Publication II). At neutron beam energies between 1 keV and 100 keV, the codes agreed generally well (within 5–6%) and large differences in the cross-sections were not observed. At thermal neutron energy, the total neutron cross-section is lower for SERA, due to constant elastic scattering cross-sections, suggesting that the thermal neutrons are less likely to interact with the medium and have longer mean free paths. Consequently, SERA tended to overestimate the neutron fluence in comparison to MCNP at neutron beam energies < 1 eV. The only other major difference in the cross-sections for water was in the oxygen elastic-scattering in the energy region >100 keV, where the cross-section peaks are flattened out in multi-group interpretation. The flattened cross-section peaks resulted in higher neutron fluence, due to lower collision probabilities and longer mean free paths, as observed for the 1 MeV neutron beam.
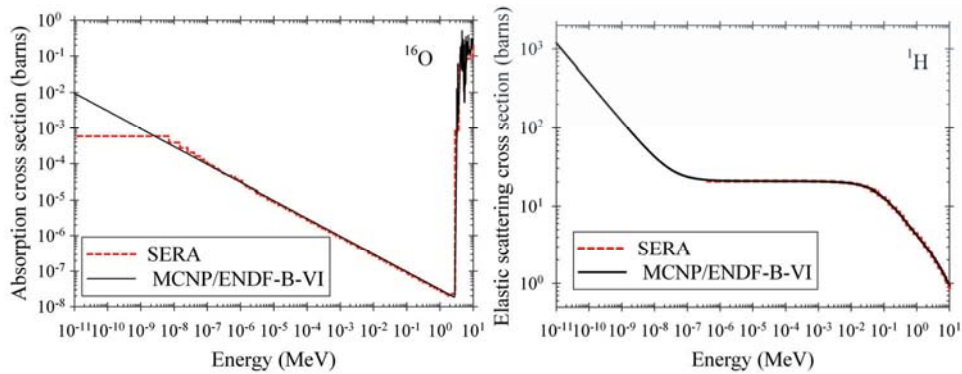
Figure 9 *Neutron elastic-scattering cross-section for ^1H and absorption cross-sections for ^{16}O applied in the SERA and MCNP. The SERA cross-section data were provided by the code developers and the ENDF-B/VI cross-section data is taken from Rose (1991).*

When the absorbed doses were compared, the largest differences between the SERA and MCNP results were observed for the D_g and D_{fast} values. SERA provided 4–22% higher D_g than MCNP for every neutron beam studied, because the hydrogen neutron absorption cross-section is higher in SERA at energies < 2.4 eV and thus photon production has higher

probability of occuring. For fast neutron beams (> 10 keV), SERA provided a maximum of 21% higher (at 1 MeV) and 43% lower (at 100 keV) D_{fast} values than did the MCNP. Deviation between the codes was due to flattened cross-section peaks in SERA at > 400 keV and due to different calculation methods at 100 keV. At beam energies of 1–10 keV, the maximum difference in total weighted doses between SERA and MCNP was only 2–3%, due to minor contribution of the D_g component to the total weighted dose. At the 25 meV beam energy, SERA overestimated the total dose by up to 17% in comparison to MCNP, due to overestimation of the D_g component as explained above. For the fast neutron beams, high differences for the total absorbed doses were obtained, due to the high contribution of the D_{fast} and D_g.

In the more complex Snyder head phantom, the neutron reaction cross-sections for ^{14}N, ^{12}C and ^{10}B need to be compared, in addition to cross-sections for ^{1}H and ^{16}O, since they contribute to neutron transport within the phantom. The neutron fluence and total weighted dose comparison results in the Snyder head were similar to those calculated in the water phantom. At beam energies of 1–100 keV, the maximum difference between the total weighted doses by SERA and MCNP was somewhat higher (6%) than in the water phantom. High differences at the 25 meV and 10 MeV beam energies were obtained for all the individual dose components, mainly due to differences in the hydrogen and oxygen cross-sections, as explained earlier, but also due to similar differences in the nitrogen and carbon cross-sections (Figure 10 and Publication II).
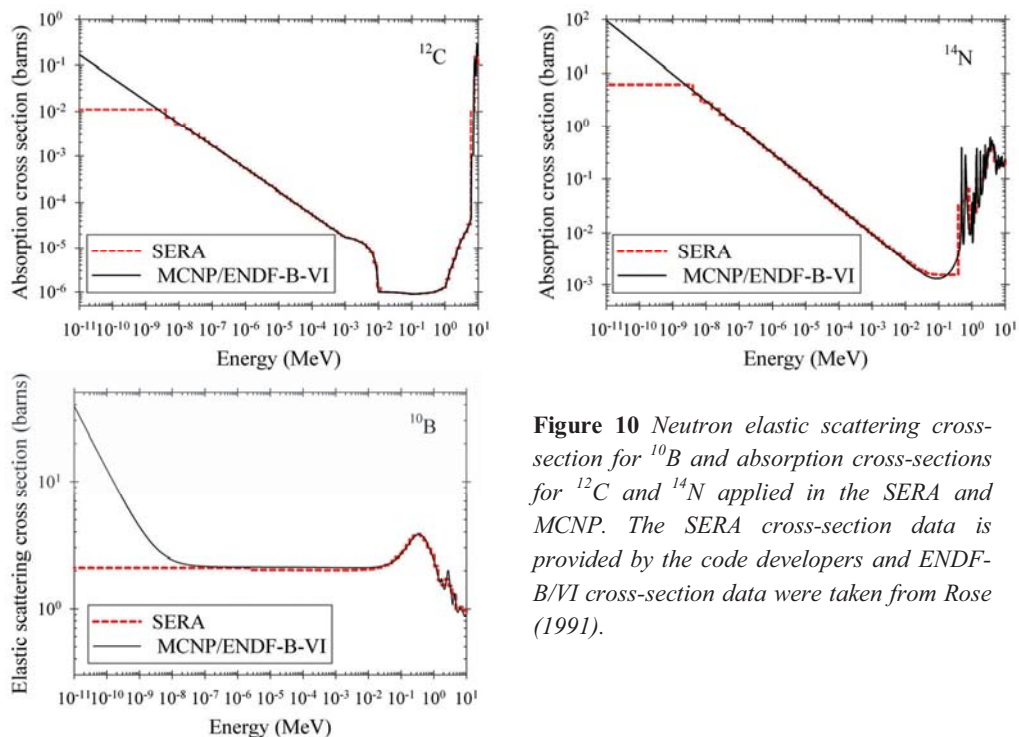

Figure 10 *Neutron elastic scattering cross-section for ^{10}B and absorption cross-sections for ^{12}C and ^{14}N applied in the SERA and MCNP. The SERA cross-section data is provided by the code developers and ENDF-B/VI cross-section data were taken from Rose (1991).*

For beam energies at 1–100 keV, SERA overestimated the D_B and D_N by a maximum of 9–12% and D_g by a maximum of 5–7%. Since at these energies, the neutron absorption cross-sections for ^{10}B and ^{14}N are very similar in the codes, the calculation difference was partly due to differences in neutron transport and partly to differences in the dose calculation methods.

7.2 Dose calculation verification in a clinical beam

In the previous section, the neutron source specification was simply forward-directed and defined exactly the same way in the two codes without any normalization. The SERA and MCNP calculations are compared, applying a real neutron source, the FiR 1 epithermal neutron beam, in the Publications III and IV. In the FiR 1 beam model, the energies and angular distributions for neutrons and photons are averaged for the surface source model applied in SERA and MCNP. The source model is located inside the beam collimator, at the surface 5 cm inward from the beam aperture. The only difference between the SERA and MCNP source descriptions is that in MCNP, the photon and neutron sources are modeled separately in independent simulation runs. As mentioned earlier, this clinical source model is normalized by the ratio of measured and calculated Au-RR at the 2 cm depth in the cylindrical PMMA phantom (diametric Ø 20 cm, length 24 cm), since the patient's head is similar to that size and the foil placement is accurate in the solid phantom. In the dosimetric calculations at the FiR 1 beam, the MCNP source model is normalized with the same RR ratio. The normalization factors (RR ratios) are slightly different for SERA and MCNP, 0.94 and 0.96, respectively, in cylindrical geometry.

In brain cancer BNCT, as well as in the study described in the previous section and in previously published phantom studies for the FiR 1 beam (Seppälä 2002, Uusi-Simola 2009, Kortesniemi 2002), the phantom is usually placed as near as possible to the beam aperture plane, the ASD being zero. For HN cancer patients, the ASD is increased to 5 cm, due to lack of space in the patient treatment position. The normalization factors for SERA and MCNP were defined for increased ASD of 5 cm, both of which were the same as defined for the ASD of 0 cm (Publication IV).

In every study of this thesis, the neutron dose calculations with MCNP were performed identically, applying the track length estimate tally F4 with the tally multiplier card counting total heating in MeV per collision for the hydrogen, boron, and nitrogen neutron reactions. The only difference was that, in Publications III and IV, only the ^{1}H(n, n') proton-recoil was accounted for in D_{fast}, whereas in Publication II, neutron interactions with oxygen in water and carbon in brain were also included. In the FiR 1 beam, the proportion of the carbon and oxygen doses of the total D_{fast} in brain tissue is only 1–2% and 4–5%, respectively (plotted in Figure 11). The D_g was calculated in the same way in the Publications II and IV, applying the total energy deposit tally F6, whereas in the Publication III, the D_g was calculated according to clinical JCDS dose planning, applying the F4 tally with the 1977 American National Standards Institute/American Nuclear Society (ANSI/ANS) (ANS-6.1.1 Working Group, 1977) flux-to-dose conversion factors

for photons in the tally multiplier card. The RRs were calculated with MCNP, using the F4 tally with the tally multiplier card counting the total number of (n,γ) reactions in gold and manganese. In SERA, the RR cross-sections specially modified for the FiR 1 neutron spectrum were applied, as mentioned already in Section 5.1, whereas in MCNP, the standard pointwise ENDF-B cross-sections were used.

The SERA dose planning calculations were evaluated in the cylindrical water phantom and in the water-filled anthropomorphic head phantom in comparison to the IC and activation foil measurements, and the MCNP5 calculations in Publication IV. The major purpose was to verify the SERA dose planning calculations with the increased ASD of 5 cm in these two phantom geometries. In addition, the influence of reduced voxel size and biased fast neutron simulation function in SERA were examined.
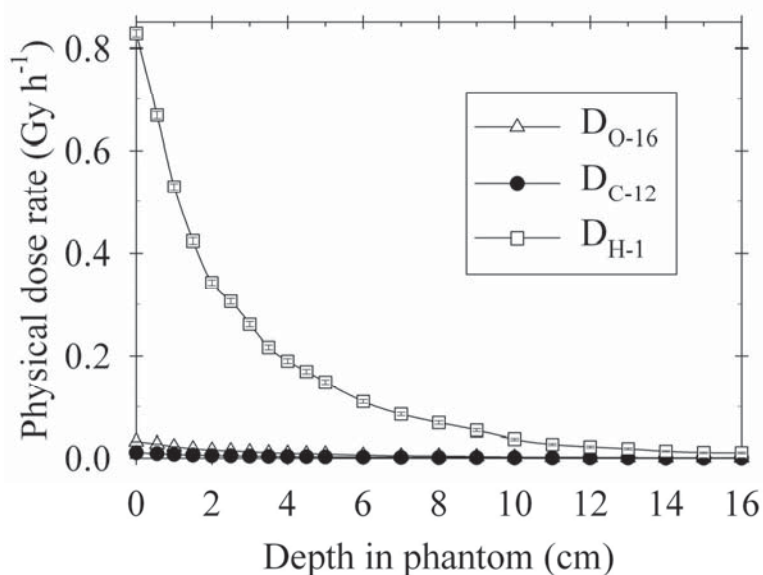
Figure 11 *Dose components in brain tissue due to fast neutron interactions with ^{16}O (D_{O-16}), ^{12}C (D_{C-12}) and ^{1}H (D_{H-1}) calculated with MCNP5 in the cylindrical water phantom with the 14 cm diameter circular FiR 1 neutron beam.*

In the Publication III, actual dose plans calculated with the SERA and JCDS systems were compared. The main differences between the SERA and JCDS codes are in patient model creation and the MC engines. The SERA system creates the univel model, which has a resolution of one image pixel, whereas the JCDS creates a voxel model. Even if a voxel size can be reduced to an image pixel size, the dose calculation time in the JCDS becomes impractical if pixel-sized voxels are used, and thus the voxel size must be compromised between calculation time and spatial accuracy. The JCDS uses the MCNP code as the MC engine. Differences related to MC transport between the codes have already been analyzed in two previous sections and in Publications II and IV. However, the dose calculation

results provided by the JCDS are not pure MCNP results, but were interpolated by the code for points of interest. Thus, in the JCDS and SERA dose calculation comparisons in patients, the same differences were included as in the MCNP and SERA comparisons (different MC transports, cross-section library forms, and dose calculation parameters), but the effects of the various patient geometry and dose output methods (individual interpolations) were also shown.

7.2.1 Cylindrical water phantom

In the cylindrical water phantom, the SERA calculations were compared with the Mn-RR and Au-RR measurements, and the D_g measurements with the Mg(Ar) chamber and the MCNP calculations.

The SERA and MCNP calculations for the Au-RR were within ± 4% and ± 5% for ASDs of 0 cm and 5 cm, respectively, while the Mn-RR agreed somewhat better within ± 3% and ± 4%, respectively, at depths of 0.5–10 cm in the phantom. Due to inaccuracies in the FiR 1 beam model (the thermal neutron fluence was underestimated and epithermal overestimated), shown already by Serén *et al.* (1999), disagreement was found between the MCNP and experiments on the phantom surface with ASD = 0.

The SERA and MCNP predictions for the D_g agreed within 2–3% at depths > 0.5 cm in the phantom. High discrepancy (5–13%), which increased with depth in the phantom, was observed between the measured and calculated D_g values at certain depths, despite a newly defined calibration factor applied for the IC signal interpretation.

The neutron-induced dose components were not directly measured, but the SERA and MCNP calculations were compared. With both ASDs studied, the D_B and D_N values agreed within 3–4% at depths > 0.5 cm in the phantom. The difference between the codes was nearly the same as that observed for the Au-RR and Mn-RR calculations, and thus the difference was due to the neutron transport simulations, not to the varying dose calculation methods.

To prove the adequacy of the Au-RR and Mn-RR measurements as verification methods for dose planning calculations at FiR 1, the RR depth profiles were compared with individual dose component profiles normalized to unity. Exactly the same distribution was found for the Mn-RR, D_B and D_N values with depth in the phantom (Publication IV, figure 7).

For the D_{fast}, large (34–60%) deviation was observed between SERA and MCNP5, as expected, since the biased fast neutron run was applied in SERA. When the biased fast neutron run was discarded, the SERA D_{fast} agreed notably better (within 8%) with the MCNP5 results on the phantom surface at depths up to 2.5 cm, but the dose calculations showed poor statistical accuracy at deeper depths. Computing times for statistically accurate D_{fast} calculations without biased fast neutron runs are clinically impractical (30

fold compared with thermal neutron run). Although the calculations tended to underestimate D_{fast}, the MCNP5 results were in line with the experimental data, with an uncertainty of 30% obtained by the MIT group at FiR 1 (Binns *et al.* 2005, Riley *et al.* 2008).

The doses obtained with SERA, using two dose-plotting commands, the point-edit and isodose contours, were compared. The results agreed within 3–5% in the phantom for every dose component. As shown in Figure 12, the point-edit tends to overestimate the dose compared with the isodose. Both SERA results agreed equally well with the MCNP5 calculations. All the rest of the SERA dose results in this thesis were obtained with the point-edit command, as in the previous dosimetric studies, despite the point-edit function in SERA shows erratic behavior in interpolating the results at the voxel boundaries. In clinical dose planning at FiR 1, the point-edit command is rarely used. Instead, the isodose contours and dose volume histograms are applied. The dose volume command of SERA was verified against the JCDS code in the Publication III.

7.2.2 An anthropomorphic RSVP^{TM} phantom

To investigate the influence of more complex geometries on dose planning calculations, the SERA calculations were compared with the Mn-RR and Au-RR measurements in an anthropomorphic Radiosurgery Verification Phantom (RSVP^{TM}, The Phantom Laboratory, Salem, NY, USA). For the simulations, the same procedures were applied as in the patient treatments: the phantom model was created based on CT images of the phantom and the two-field dose plan was calculated.

The SERA calculations with the default voxel size (1 cm^3) for the Mn-RR agreed within 5% with the measurements at the points of relevance inside the phantom. When the SERA calculations were repeated with the reduced voxel size (0.5 cm × 0.5 cm × 0.5 cm and 0.25 cm × 0.25 cm × 0.25 cm), the deviation from the measurements increased inside the phantom, due to unphysical fluctuation of the calculation results (shown in Publication IV, Figure 8). The fluctuation was not related to statistical uncertainty of the results, since the number of simulation particles per each voxel was the same as in the 1 cm^3 voxel (0.25 cm voxel) or greater (in the 0.5 cm voxel). Instead, the fluctuation could have been caused by the interpolation scheme included in the code, clearly indicating that reduced voxel sizes should not be applied when doses inside the phantom or patient are analyzed.

However, when the activation measurements were considered on the phantom surface, agreement between the SERA calculation and the measurements increased at nearly every measurement point with the highest neutron fluence, when the voxel size was reduced from 1 cm to 0.5 cm or 0.25 cm.
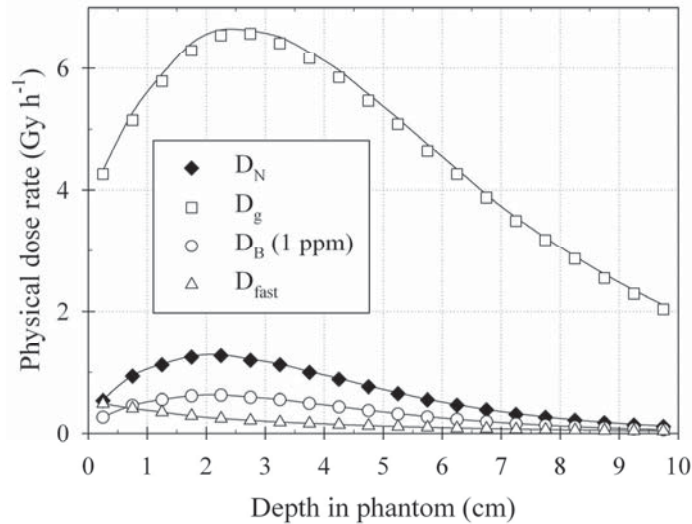
Figure 12 *Difference between SERA dose calculation results obtained with point-edit (line) and isodose contour (symbol) commands. The boron dose (D_B) was calculated for 1 µg/g (ppm) of ^{10}B.*

7.2.3 Brain cancer dose planning: SERA verification against JCDS

For the TPS comparison, a brain cancer patient dose plan was first performed with the SERA system, following the Finnish dose planning protocol of BPA-mediated BNCT for recurrent brain tumors (Joensuu *et al.* 2003, Kankaanranta *et al.* 2011). The univel patient model created with SERA was converted into grayscale images to reconstruct exactly the same patient model with the JCDS. Each grayscale was labeled as a single body region with tissue composition from ICRU Report 46 (ICRU, 1992). The body regions are listed in Table 3. Two neutron fields (anterior and posterior to the patient) of diameter 14 cm were applied in the dose plan and weighted 65:35, respectively. The dose calculation parameters applied are listed in Table 3 and the simulation parameters in Table 4. In SERA, the biased D_{fast} calculation was applied according to the clinical protocol.

Table 3 *Applied body tissues and ^{10}B concentrations for the segmented regions in the patient model and weighting factors in the dose calculation. The elemental compositions of the body tissues are taken from ICRU report 46 (ICRU 1992). The planning target volume (PTV) includes tumor, edema, and a 2 cm margin.*

Region	Body tissue from ICRU	^{10}B concentration (µg/g)	Weighting factors for the dose components		
			D_B	D_N	D_{fast}
Skin	Skin	28.5	2.5	3.2	3.2
Brain	Adult brain	19	1.3	2.68	3.16
Cranium	Cranium	-	-	-	-
PTV	Adult brain	66.5	3.8	2.68	3.16

53

Table 4 *Simulation parameters in the SERA and JCDS systems. The calibration factor is defined as the ratio of measured to calculated $^{197}Au(n,\gamma)$ reaction rate in the cylindrical PMMA phantom.*

	SERA	JCDS
Patient model resolution	0.1 cm	0.2 cm
Dose calculation voxel size	1 cm × 1cm × 1 cm	0.5 cm × 0.5 cm × 0.5 cm
Calibration factor	0.94	0.96
Number of simulation histories	5×10^7	$\sim 10^8$

The epithermal neutron fluence rates calculated for the individual beams with SERA and JCDS agreed within ± 2% at the patient surface, and the agreement was within ± 5% at depths up to 7.0 cm. SERA overestimated the thermal neutron fluence rate in comparison to JCDS by 14–36% on the patient surface and at depths up to 0.5 cm, while agreement between the codes was mainly within 5% at depths of 2–7 cm. Unlike in the phantom study (Publication IV), differences between the codes for D_N and D_B deviated systematically from the thermal neutron fluence calculation difference. Somewhat better agreement between the codes was found for the D_B estimates than for D_N and the thermal neutron fluences. SERA overestimated the D_g by up to 9% in comparison to JCDS at all depths (at the surface even more), due to the different flux-to-dose conversion factors applied in SERA and JCDS dosimetry (plotted in Figure 13).
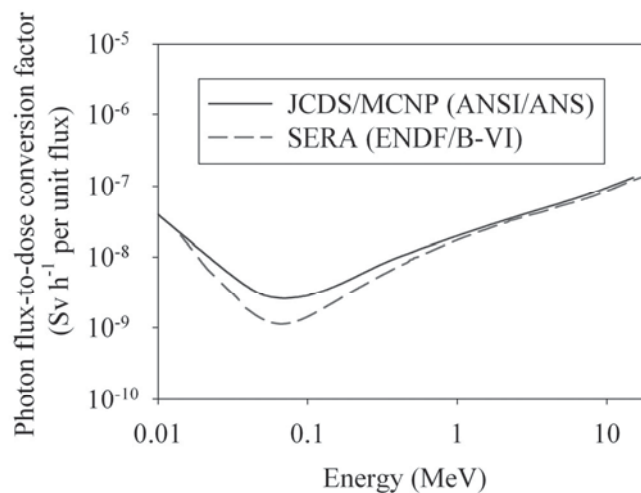
Figure 13 *Photon flux-to-dose conversion factors from the ENDF-B/VI (Rose 1991) library applied in SERA and from the 1977 ANSI/ANS library (*ANS-6.1.1 Working Group 1977*) used in JCDS.*

At the phantom surface and depths < 0.5 cm, SERA underestimated the fast neutron fluence by 4–13% in comparison to the JCDS. At deeper depths, the fast neutron fluence rates agreed within 8–10% at depths up to 10 cm. However, deviation between the D_{fast}

values was substantially larger (up to 35%), due to erroneous biased fast neutron run in SERA. If the biased fast neutron run was omitted and initial simulation neutron number (of all energies) is increased from 50 to 100 million, the D_{fast} calculation difference was reduced to 1–6% at shallow depths (< 2 cm in tissue). At deeper depths, the statistical accuracy of the SERA results was poor.

The total weighted dose rates to brain and tumor obtained with SERA and JCDS for the anterior field are shown in Figure 14. At depths inside the skull, the total weighted brain doses agreed within 10% at depths up to 15 cm (5% isodose) and tumor doses within 5% at depths up to 7.3 cm (37% isodose) for both the fields. The total weighted brain doses agreed within 3–4% at all depths.

The combined two-field dose plans are compared in Table 5. The differences between the codes for the total maximum weighted doses were small, 3% for the normal brain dose and 4% for the PTV and tumor doses, while the corresponding average dose differences were larger: 8%, 4% and 10%. Large (up to 32%) calculation differences were found for the D_{fast}, which covers only < 1% of the total maximum tumor and PTV doses, but about 6% of the total maximum brain dose. About 99% of the total tumor and PTV doses and over 90% of the total brain dose were produced by the thermal neutron-induced dose components (D_B, D_N, and D_g). The differences between the codes for the maximum D_B, D_N, and D_g were, respectively, 1%, 3%, and 13% in brain and 4%, 2%, and 8% in tumor.
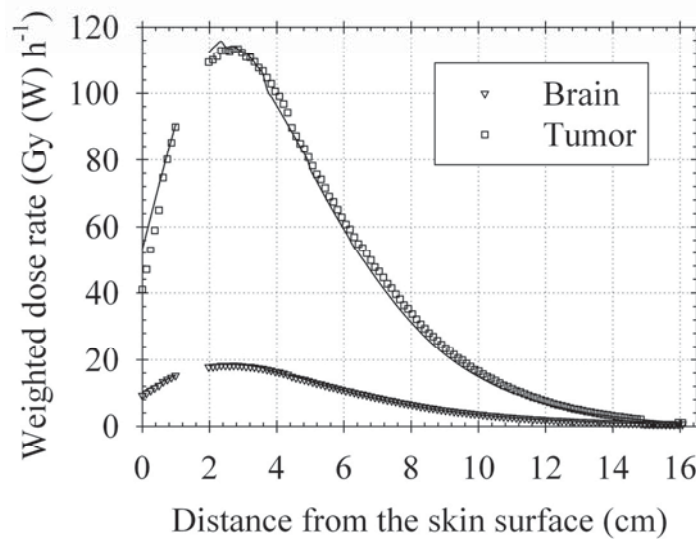
Figure 14 SERA (line) and JCDS (symbol) calculations for the total depth distributions in brain and tumor for the anterior field, using a 14 cm diameter circular FiR 1 beam. The boron dose (D_B) was calculated for 19 mg/g (ppm) of ^{10}B in brain and 66.5 µg/g (ppm) ^{10}B in tumor.

Table 5 SERA and JCDS dose results for weighted dose rates in two-field treatment plan at dose minimum point (P_{min}), at dose maximum point (P_{max}), and average in the regions of tumor, planning target volume (PTV), and brain.

		Volume (cm)	D_g (Gy/h)			D_{fast} (Gy(W)/h)			D_B (Gy(W)/h)			D_N (Gy(W)/h)			Total (Gy(W)/h)		
			Average	P_{min}	P_{max}	Average	P_{min}	P_{max}	Average	P_{min}	P_{max}	Average	P_{min}	P_{max}	Average	Min	Max
SERA	Tumor	24	4.8	4.0	5.3	0.5	0.3	1.1	88.3	53.6	108.3	1.9	1.2	2.3	95.6	59.1	116.3
	PTV	141	4.4	2.9	5.3	0.5	0.2	1.1	77.5	30.3	108.9	1.7	0.7	2.4	84.0	34.1	116.9
	Brain	1543	2.1	0.4	5.26	0.2	0.0	1.1	2.6	0.0	10.5	0.6	0.0	2.3	5.6	0.5	18.7
JCDS	Tumor	22	4.2	3.6	4.4	0.7	0.4	0.9	96.2	63.2	112.8	2.0	1.3	2.4	103.1	68.5	120.5
	PTV	133	3.8	1.5	4.4	0.7	0.2	0.9	82.0	20.8	112.5	1.7	0.4	2.4	90.6	23.0	120.5
	Brain	1380	1.7	0.4	4.1	0.2	0.0	0.9	2.4	0.1	10.4	0.5	0.0	2.3	4.8	0.5	17.7

8 Applicability of the D-D and D-T fusion neutron sources for BNCT

As already mentioned in Section 3.1.1, compact D-D and D-T fusion neutron sources have been under development at LBNL for over a decade (Reijonen *et al.* 2004, 2005). The applicability of some designs of the sources for brain cancer BNCT was examined by Verbeke *et al.* (2000). For moderation of the fusion neutrons down to epithermal neutron energy, materials similar to those used for moderation of the reactor-based neutrons, such as aluminum, aluminum fluorides, lithium and lithium fluorides, iron, magnesium fluoride, metallic aluminum and bismuth and its fluorides, lead, and its fluorides have been suggested (Verbeke *et al.* 2000, Cerullo *et al.*2004, Durisi *et al.*2007, Publication V). In addition, use of fission converter to multiply the neutron yield has been investigated (Lou *et al.* 2003).

For reasons mentioned in Section 3.3.2, the tumor BNCT treatments have been of interest. The applicability of D-D and D-T fusion-based neutron generators for external liver BNCT was evaluated by means of dose calculations with the SERA system (Publication V). The neutron generator model studied was developed to allow neutron yield of 10^{12} neutrons per second from D-D fusion and 10^{14} neutrons per second from D-T fusion. Iron and Fluental^{TM} were used as moderator materials. At first, an iron layer was used to decrease the fast neutron energy down to energies below 1 MeV. For D-T neutrons, the advantage of iron is that while the neutrons are slowed down, they are also multiplied, due to the (*n,2n*) reaction, which occurs above 8 MeV. After the iron layer, a Fluental^{TM} layer was used to decrease the neutron energies further down to epithermal energy range. Finally, the neutron beam was collimated with bismuth and a lithiated polyethylene collimator. Rectangular beam apertures (20 cm × 20 cm and 25 cm × 25 cm) were applied and the optimum collimator thickness was studied.

The patient model was created based on axial abdominal CT scans. Dose calculations were performed for the single beams and three combined beams. The maximum BNCT dose to healthy liver was limited to 12.5 Gy (W) and it was proposed that BNCT would be a possible treatment for liver tumors, if a > 30 Gy tumor dose throughout the liver were achieved. The boron concentration of the healthy liver tissue and tumor were assumed to be the same as those measured in an actual patient BNCT (Pinelli *et al.* 2002): 8 ± 1 ppm and 47 ± 2 ppm, respectively.

With a single irradiation beam, the deepest penetration was achieved with the 25 cm × 25 cm beam size and 15 cm thick collimator with D-D and D-T sources, which led to tumor doses of 11 Gy (W) and 10 Gy (W), respectively, at the deepest depth in the liver (12 cm from the skin). The irradiation time with the D-D source was calculated to be unrealistically long, over 3000 minutes, but with the D-T source clinically relevant, at 56 minutes.

When the three beams were combined, using a D-D source, the largest liver volume (> 57%) was covered with a 30 Gy (W) isodose, using either a 20 cm or 25 cm diameter beam. For a D-T source, a 25 cm diameter beam and 15 cm thick collimator were needed to cover the equivalent liver volume. The maximum tumor dose was 68–71 Gy (W) in every case and the minimum tumor dose was about 8 Gy (W) (11% isodose) at the most distant point in the liver. The irradiation times required for the three-beam treatments were 3500–7500 minutes for the D-D source and 63–128 minutes for the D-T source. Clearly, more powerful D-D fusion neutron sources are required for clinical applications. The D-D neuron yield should be at least 6×10^{13} neutrons per second and D-T neutron yield 10^{13} −2 $\times 10^{13}$ neutrons per second for clinically adequate 1 hour treatment time, which requires, respectively, 60 times and 1−2 times more powerful sources than those studied here.

8.1 Comparison of the fusion-based and FiR 1 neutron beams

To compare the fusion-based neutron sources with the FiR 1 beam, the depth dose distributions according to the brain cancer BNCT protocol were calculated with MCNP5 in a water phantom, using the fusion neutron beams described in previous section and Publication V. The collimator size was reduced to 15 cm × 15 cm in diameter to be better comparable with the clinical 14 cm diameter FiR 1 beam.

The depth dose distributions from the fusion-based neutron beams and the FiR 1 beam for brain tissue and tumor are compared in Figure 15. The fusion neutron sources caused higher surface doses due to a harder neutron spectrum than that of the FiR 1 beam. Using the boron concentration (1.5 times that of blood or brain) and the CBE factor of 2.5 commonly applied for skin, the skin dose was about 11 Gy (W) for the fusion neutrons, which is a lower dose than that resulting in the acute skin toxicity TD (15–20 Gy for 100 cm^2 of skin) reported for BNCT (González *et al.* 2009). Due to the more energetic neutron spectrum, the fusion neutron beams also penetrated deeper than the FiR 1 beam. For the fusion neutrons, the maximum tumor dose was obtained at the 3 cm depth and the advantageous depth (the depth at which the tumor dose is as large as the maximum brain dose) is at 10 cm, whereas the corresponding values for the FiR 1 beam are 2 cm and 9 cm, respectively. The fusion neutron sources clearly provided a lower tumor (68–70 Gy (W)) dose maximum than the FiR 1 beam (76 Gy (W)). To achieve an equivalent treatment time with the fusion neutron generators and the FiR 1 beam, the fusion neutron yield needs to be 3×10^{13} neutrons per second for the D-D source and 4×10^{13} neutrons per second for the D-T source. The geometry studied has been estimated to yield 10^{12} neutrons per second D-D fusion neutrons and 10^{14} neutrons per second, at an accelerator voltage of 120 kV and ^{2}H current of 330 mA . This number for the D-T source is theoretically high enough for clinical BNCT, while a clinical D-D fusion neutron source requires almost 30 times more beam power.
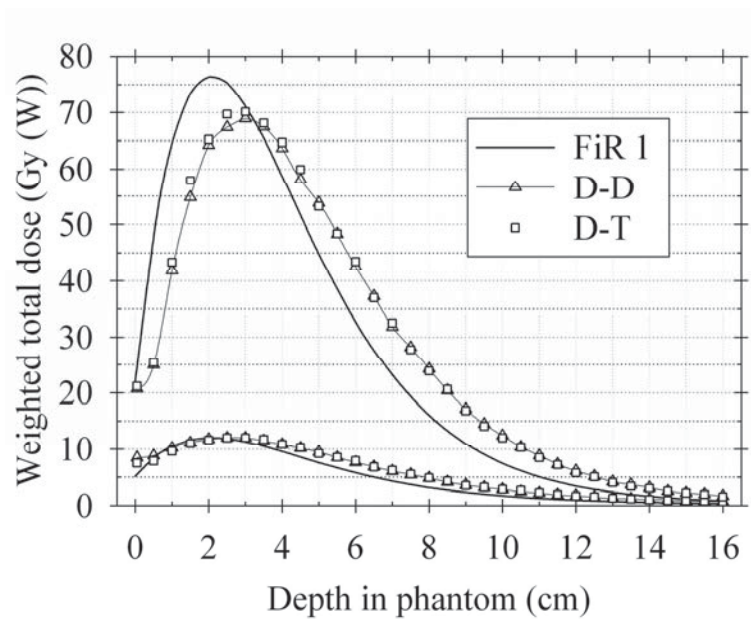
Figure 15 *Total weighted doses for brain (lower set of curves) and tumor (upper set of curves) calculated with MCNP5 for FiR 1 (14 diameter circular) and for the D-D and D-T fusion neutron beams (15 cm diameter rectangular) normalized to maximum dose to brain (12 Gy(W)). The weighting factors and boron concentrations (19 ppm for brain and 66.5 for tumor) are according to the FiR 1 dosimetry for brain cancer treatments (Kankaanranta et al. 2011).*

9 Discussion

9.1 Dose planning

Various cross-section file forms applied in SERA and MCNP caused negligible calculation deviation in the BNCT dose at the energy range of clinical epithermal neutron beams. However, in neutron moderation, it should be noted that multienergy group forms applied in SERA flatten out the cross-section resonance peaks at high energies (> 100 keV and > 1 MeV).

When the SERA and MCNP calculations were compared using a clinical epithermal neutron beam of the FiR 1 facility, the thermal neutron-induced D_B and D_N and the D_g agreed within 4% at every depth in the water phantom, except on the phantom surface. The erratic biased fast neutron run option in the SERA system leads to significant underestimation (up to 30–60%) of D_{fast}, while the standard SERA neutron run provides reliable D_{fast} calculations, but the simulation time must be increased by 30-fold to obtain statistically accurate results.

Use of ^{55}Mn(n,γ) activation RR measurements as the primary dose planning verification method is justified, since the RR distribution acts exactly like the D_B and D_N dose (which cover most of the total weighted healthy tissue dose at FiR 1) distribution with depth in the phantom. The reduced voxel cell size (< 1 cm) in the SERA edit mesh improves dose calculation accuracy on the phantom surface and is recommended for *in vivo* dosimetry calculations.

The differences in patient dose calculations between SERA and the JCDS system are very similar to those observed in the phantom study between SERA and MCNP. The JCDS-style dosimetry (the applied flux-to-dose conversion factors) underestimated D_g by 20–30% in comparison to SERA. The difference between SERA and JCDS for the total weighted tumor, PTV, and healthy brain doses are only 3–4%, regardless of the discrepancy in D_g and biased fast neutron calculation in SERA. The best agreement with SERA is obtained if the F6 energy deposit tally is applied for the D_g calculations in the MCNP and the source models are normalized according to the FiR 1 protocol.

The SERA comparison studies show that the dose calculation accuracy can be considered sufficient for reliable BNCT dose planning with ASDs from 0 to 5 cm, despite slight overestimation of the epithermal and underestimation of the thermal neutrons in the beam model, and miscalculation of the dose on the surface. Moreover, the dose calculation with the MCNP code and the JCDS system is very similar to that of SERA. Since both codes have similar accuracy in comparison to measurements, MCNP can be applied as a reference calculation method at the FiR 1 beam.

In these studies, the neutron doses in MCNP were calculated, using the track length estimate tally F4 with the tally multiplier card counting total heating in MeV per collision

for hydrogen, boron, and nitrogen. The photon doses were calculated with the F6 total energy deposit tally or by applying flux-to-dose conversion factors from the 1977 ANSI/ANS. In SERA, the corresponding dose components were calculated from the neutron and photon fluences by applying flux-to-dose conversion factors from the MACLIB (ENDF-B/IV) library. If different dose calculation methods are applied in MCNP, the agreement between the codes may differ from that observed in this thesis. Limitation of SERA dose calculation verification is that the radial dose or fluence distributions have not been compared in this thesis.

9.2 Photon dose

An alarming fact related to the discrepancy between the measured and calculated D_g at the FiR 1 beam is that the difference increases with the phantom depth. An inaccurately determined effective point of the Mg(Ar) chamber partially explained the increasing difference (Koivunoro *et al.* 2011). With the 0.3 cm shift in the effective point, the difference becomes smaller, but still increases with phantom depth (from 5% to 9%).

Measurements by the visiting research group from MIT, using $C(CO_2)$ IC, provided linear deviation between the experimental and calculated D_g for the FiR 1 beam in the water phantom. The measurement results of the MIT team are published in Binns *et al.* (2005). The $C(CO_2)$ measurement predicts 6–9% higher D_g values than the SERA and MCNP calculations at depths up to 16 cm in the phantom. Agreement between the two ICs for D_g is from -3% to 1% at depths up to 10 cm, except that at the most shallow measurement point the $C(CO_2)$ chamber predicts an 8% higher dose.

Deviation between the measured and calculated D_g indicates that the FiR 1 photon beam model may be inaccurately determined in terms of photon spectra or intensity. As mentioned earlier, the photon beam model is not verified against measurements and the same normalization factor (based on neutron activation measurements) as for the neutron beam model was applied. However, in-air measurements with the $C(CO_2)$ and Mg(Ar) chambers in the FiR 1 beam predict considerably higher D_g values (0.34–0.37 Gy/h) than the MCNP calculations (0.20 Gy/h) (previously unpublished result). The beam model verification can be performed through measurements of the photon spectrum with the Mg(Ar) chamber applying multiple buildup caps with different thicknesses, as has been reported for the Tsing Hua Open-Pool Reactor (THOR) BNCT facility in Taiwan (Liu *et al.* 2011).

The increasing discrepancy with phantom depth between the D_g calculations and measurements may also indicate that the Mg(Ar) chamber signal is inaccurately interpreted. Either the chamber response for the epithermal neutron beam is incorrectly determined or the chamber is neutron-sensitive (unlike assumed). As mentioned earlier, the chamber response for the FiR 1 beam should be determined through simulations of the real measurement situation (discussed in the next section). The thermal neutron sensitivity of the chamber could be measured in a pure neutron beam, which can be created at the FiR 1

mixed beam with a thick moderator of material, which absorbs but does not create photons via neutron interactions. Thermal neutron sensitivity was reported previously for chambers of the same type (Raaijmakers and Konijnenberg 1995). In addition, neutron activation of the Mg(Ar) chamber structures caused 2% increase in the IC signal at the epithermal neutron beam of the THOR reactor (Liu *et al.* 2010), which is not taken into account at the FiR 1 beam.

9.3 IC response simulations

Munck af Rosenschöld *et al.* (2002) used MCNP version 4 for simulations of the Mg(Ar) and TE(TE) chamber responses of photons in an epithermal neutron beam of the Studsvik reactor in Sweden. The photon quality correction factors, which determine the chamber response in an epithermal neutron beam relative to the reference ^{60}Co beam, were determined. One limitation of the study was that the calculation results were not compared with experimental data or reference calculations. In the study by Roca *et al.* (2002), the same chambers were modeled with the MCNPX code and their response was calculated and measured in the ^{60}Co reference beam. For the TE(TE) chamber, the difference between the calculated and measured current inside the gas cavity were within 2%, whereas for the Mg(Ar) chamber, MCNPX overestimated the dose by 7% in comparison to the measurement. The authors suspected that the systematic discrepancy in the case of the Mg(Ar) chamber was caused by overestimation of the chamber's sensitive volume. In the study by Munck af Rosenschöld *et al.* (2002), the electron transport algorithm applied was not reported, whereas the ITS-based electron transport was applied in the study by Roca *et al.* (2002).

Based on the results in Publication VI, the MCNP electron transport is not accurate enough for IC response simulations in the clinical photon beams, since in conventional radiotherapy, the IC response can be calculated with an accuracy of well below 1% using the other codes. However, MCNP may still be a useful tool for improving the dose determination accuracy in BNCT, since the calculation uncertainty (2% ± 1%) for dosimetric gases and the energy range of BNCT is low, compared with the current uncertainty of the IC measurements in the BNCT beam.

The TE(TE) chamber response simulations for neutron dose requires a simulation code, that handles transport of various charged particles created in the neutron interactions. The codes could include e. g. PHITS, MCNPX and GEANT4. So far, the neutron response has been determined according to formalism presented by ICRU (ICRU 1989), based on gas-to-wall conversion factors, the energy required to produce an ion pair by secondary charged particles, and the neutron fluence-dependent KERMAs (ratio for tissue and chamber wall) at the measurement points. The uncertainty of the relative sensitivity of the chamber for the BNCT beam was estimated to be 10% (Kosunen *et al.* 1999), which could be improved by the chamber response simulations. Since uncertainty in the neutron dose determination is mostly due to subtraction of the photon dose measured with the Mg(Ar) chamber from the total dose measured with the TE(TE) chamber, more accurate Mg(Ar) chamber

measurements would already improve TE(TE) detector measurement accuracy considerably.

9.4 Fusion neutron sources

The fusion neutron generator model and BSA system studied in Publication V would presumably yield 10^{14} neutrons per second from D-T fusion, which should be a sufficient number for clinical brain or liver cancer BNCT. This neutron generator model is not adequate for clinical BNCT if the D-D fusion reaction is utilized (yield 10^{12} neutrons per second). However, this theoretical study of neutron moderation has limitations. The more realistic study by Durisi *et al.* (2007) for D-D neutron generators includes some space between the neutron source and BSA and an electric insulator. With this realistic configuration, the neutron fluence rate in the patient side is somewhat lower than in the ideal configuration presented in the Publication V. A neutron generator utilizing the D-T fusion reaction seems more realistic than D-D fusion, since almost two orders of magnitude less power is required for sufficient neutron yield for BNCT application. However, with the D-T fusion reaction some practical aspects need to be overcome. The neutron generators developed at LBNL, which utilize D-D fusion, operate on an open system, so that deuterium gas is constantly pumped out of the generator to maintain the fusion reaction. In D-T fusion, the generator needs to be a sealed system, since tritium is a highly reactive radioactive isotope and potentially dangerous, if inhaled or ingested. Another practical issue may be activation of the BSA and the neutron source structures, due to high (14.1 MeV) initial neutron energy.

9.5 BNCT of liver

Results of Publication V show that a tumor dose of 30 Gy (W) cannot be delivered throughout the liver volume with the epithermal neutron beams and boron concentrations studied. Since epithermal neutron penetration is limited, the entire liver treatment can be achieved with BNCT only by enhancing the tumor-to-tissue boron concentration ratio. With less or more energetic neutron beams, the skin dose would increase and thus limit the treatment time. In the study, the boron concentrations were assumed to be similar to those measured for the first liver cancer patient in Italy (Pinelli *et al.* 2002). In that case, the BPA-fructose complex (300 mg/kg) was injected through the colic vein in 2 hours, which led to a boron concentration ratio of 6:1 between the tumor and healthy liver at irradiation time. The concentration ratio was clearly higher than that commonly assumed (3.5:1) for the peripheral BPA-F infusion (Imahori *et al.* 1998, Kabalka *et al.* 1997, Ishiwata *et al.* 1992, Kato *et al.* 2004). A boron concentration ratio between tumor and healthy liver of 18:1 would be needed to cover nearly all of the liver volume with a greater than 30 Gy (W) dose, if the boron concentration in healthy tissue were 8 (Publication V). It has been suggested that boron could be administered to liver tumors more selectively, using locoregional infusion via the hepatic artery (Zanon *et al.* 2001).

Later on, a patient with multiple liver tumors received intra-arterial administration of BPA and BSH, with a vessel-embolizing agent, lipiodol, directly via the right hepatic artery, followed by neutron irradiation (Suzuki *et al.* 2007). The boron concentration of the blood just before irradiation was 11.6 ppm and of liver 23.8 ppm estimated with the γ-telescope. Recently, a 15:1 boron concentration ratio between liver tumor and healthy liver was demonstrated in rabbits using intra-arterial administration of boron-entrapped water-in-oil-in-water emulsion (Yanagie *et al.* 2011). Moreover, a cationized gelatin-hemagglutinating virus of Japan (HVJ) envelope with BSH has shown a boron concentration ratio of up to 35:1 between liver tumor and healthy tissue *in vivo* (Fujii *et al.* 2011), while intravenous and intraperitoneal injection of two boron carriers (BPA and GB-10) demonstrated a boron concentration ratio between tumor and healthy liver of at most of 2.3 ± 0.9 ppm (Garabalino *et al.* 2010). The authors, however, hypothesized that preferential uptake of the boron compound by tumor tissue may not be as essential to BNCT success as previously reported. The Argentinian research group showed in small animal studies that in BNCT mediated by the chemically non-selective boron compound GB-10, selective tumor lethality results from tumor blood vessel damage rather than from selective tumor uptake, since GB-10-BNCT selectively damages tumor vessels, sparing precancerous and normal tissue vessels (Trivillin *et al.* 2006). GB-10, a stable polyhedral borane dianion, used in the second Brookhaven GBM clinical trial in 1961, has no targeting features, is of low toxicity even at high concentrations, and is commercially available under investigational new drug (IND) status in the US (Hawthorne and Lee 2003).

The advantageous of BNCT over external photon radiotherapy in liver cancer is that, as a biologically targeted treatment modality, BNCT should treat both visible and undetectable tumors. The demand for a minimum 30 Gy (W) tumor dose throughout the liver may be unnecessary, since BNCT doses to tumor may be more effective than calculated doses indicate. Complete treatment responses have been achieved with calculated tumor doses as low as 12–14 Gy (W) given twice (32–76 days apart) for HN cancer patients (Kankaanranta *et al.* 2007, 2011). According to Publication V, high BNCT doses (up to 70 Gy (W)) can be delivered to liver tumors located at shallow depths from the skin, while the minimum tumor dose in liver would be about 11 Gy (W) using an epithermal neutron beam.

10 Conclusions

In this thesis, BNCT dose calculation with the SERA system was evaluated against reference dose calculation methods and measurements in various geometries (Publications II–IV). The minimum phantom dimensions for undisturbed neutron and photon dose measurements at the reference measurement depth and at every measurement point were determined with MC simulations (Publication I). The accuracy of the MCNP5 code for IC response simulations was determined (Publication VI). The suitability of compact fusion reaction-based neutron generators for liver BNCT was evaluated (Publication V). The calculated dose distributions from the fusion neutron sources and the FiR 1 beam were compared (Section 8.2).

The multi-energy group representation of the nuclear interaction cross-sections applied in SERA correlates well with the continuous cross-sections of the reference code MCNP in the main energy range of an epithermal neutron beam. The neutron capture cross-section for hydrogen is overestimated in SERA at < 1 eV in comparison to MCNP, which may lead into higher photon dose, while the elastic scattering cross-sections are lower for the main tissue elements (^{1}H, ^{12}C, ^{14}N, ^{16}O) and ^{10}B below 10^{-2} eV or 10^{-3} eV energy, which may cause overestimation of neutron fluence and dose.

The dose calculations with the SERA system are accurate against reference calculations for the thermal neutron-induced dose components (D_B, D_N and D_g), which produce 99% of the tumor dose and > 90% of the healthy tissue dose at points of relevance for treatment at the FiR 1 facility. For these dose components, the deviation between SERA and the reference calculations is within 4% in the phantoms and in a brain cancer patient model elsewhere, except on the phantom or skin surface. The SERA calculations for the thermal neutron fluence are accurate (within 5%) in comparison to the activation foil measurements. Large (> 5%) deviation is found between the measured and calculated photon dose, which produces from 25% up to > 50% of the healthy tissue dose at certain depths. The erratic biased fast neutron run option in the SERA system leads in significant underestimation (up to 30–60%) of the fast neutron dose. Currently, no reliable measurement method exists for fast neutron detection of the FiR 1 beam, since the measurement accuracy is > 30%, due to low fast neutron contamination.

For the FiR 1 neutron beam, the minimum reference phantom size is a 40 cm × 40 cm cross-section and 20 cm depth, wherein the undisturbed measurements are achieved at the reference depth (2 cm) for the neutron and photon dose components. A water scanning phantom of size 56 cm × 56 cm cross-section and 28 cm depth is required for undisturbed measurements of the depth and transverse profiles up to 5% isodose of the total dose.

The MCNP5 code is applicable for the IC response simulations (with accuracy of 2% ± 1%) in BNCT dosimetry. Nevertheless, the electron transport models of MCNP5 are not accurate enough for IC response simulations in conventional radiotherapy applications, where better accuracy is required and can be achieved with the other codes.

The D-D and D-T fusion-based neutron generators may be applicable for BNCT treatments, if yields of $> 10^{13}$ neutrons per second from D-D or D-T fusion can be obtained. The simulations indicate that noninvasive BNCT of liver tumors is a technically possible treatment with epithermal neutron beams, while the 30 Gy (W) tumor dose cannot be delivered at the deepest parts of the liver, if accumulation of boron in the tumor compared with the healthy liver is sixfold or less.

The patient dose calculation practice is accurate, compared with reference calculation methods for the major dose components induced by thermal neutrons in the FiR 1 beam. Calculation of the thermal neutron fluence, which creates the most crucial patient dose, is also accurate against experimental data. Final verification of the fast neutron and photon dose calculation is restricted to high uncertainties in the existing measurement methods. Determination accuracy of the absorbed patient dose at FiR 1 cannot be substantially improved by focusing on measurement and calculation methods, since the most crucial inaccuracy is due to inability to define exact boron distribution in the tumor and healthy tissues during treatment. The earlier conclusions and the results of this thesis on the matter confirm the statement.

References

Agostinelli S *et al.* 2003 Geant4—a simulation toolkit *Nucl. Instrum. Methods Phys. Res.* **A** **506** 250–303

Ahnesjö A and Aspradakis M M 1999 Dose calculations for external photon beams in radiotherapy *Phys. Med. Biol.* **44** R99–R155

Aihara T, Hiratsuka J, Morita N, Uno M, Sakurai Y, Maruhashi A, Ono K and Harada T 2006 First clinical case of boron neutron capture therapy for head and neck malignancies using 18F-BPA PET *Head Neck.* **28** 850-5

Andreo P, Burns D T, Hohlfeld K., Huq M S, Kanai T, Laitano F, Smyth V and Vynckier S 2000 Absorbed Dose Determination in External Beam Radiotherapy: an International Code of Practice for Dosimetry Based on Standards of Absorbed Dose to Water IAEA Technical Report Series No 398 (IAEA Vienna)

Aschan C 1999 Applicability of thermoluminescent dosimeters in X-ray organ dose determination and in the dosimetry of systemic and boron neutron capture radiotherapy PhD thesis *Report Series in Physics* HU-P-D77 (Helsinki, Finland: Helsinki University)

Albritton J R and Kiger W S 2006 Development of reference problems for neutron capture therapy treatment planning systems *Advances in Neutron Capture Therapy Proceedingd of ICNCT-12* 496–9

Allen B J, Wallace S A, Carolan M G , 1997 Can epithermal boron neutron capture therapy treat primary and metastatic liver cancer? In: Larsson B, Crawford J, Weinreich R (Eds.) Advances in Neutron Capture Therapy Vol. I Medicine and Physics (Amsterdam: Elsevier) p. 118

ANS-6.1.1 Working Group, M. E. Battat (Chairman) 1977 American National Standard Neutron and Gamma-Ray Flux-to-Dose Rate Factors *ANSI/ANS-6.1.1-1977(N666)* (LaGrange Park, Illinois: American Nuclear Society)

Auterinen I, Serén T, Anttila K, Kosunen A and Savolainen S 2004a Measurement of free beam neutron spectra at eight BNCT facilities worldwide Applied Radiation and Isotopes, Volume 61, Issue 5, November 2004 1021-6

Auterinen I, Serén T, Uusi-Simola J, Kosunen A and Savolainen S. 2004b A toolkit for epithermal neutron beam characterisation in BNCT *Rad. Prot. Dosim.* **110** 587-93.

Auterinen I *et al.* 2001 Metamorphosis of a 35 year-old triga reactor into a modern BNCT facility *Frontiers in Neutron Capture Therapy* ed MF Hawthorne, K Shelly and RJ Wiersema Vol. 1 (New York: Kluwer Academic/Plenum Publishers) pp. 267-75

Barth R F *et al.* 1989 Pre-clinical studies on boron neutron capture therapy *Basic Life Sci.* **50** 95-105

Barth R F 2009 Boron neutron capture therapy at the crossroads: challenges and opportunities *Appl. Radiat. Isot.* **67** S3-6

Barth R and Joensuu H 2007Boron neutron capture therapy for the treatment of glioblastomas and extracranial tumours: As effective, more effective or less effective than photon irradiation? *Radiotherapy and Oncology* **82** 119-22

Barth R F *et al.* 1989 Pre-clinical studies on boron neutron capture therapy *Basic Life Sci.* **50** 95-105

Benczik J 2000 Relative biological effectiveness of reactor produced epithermal neutrons for the canine brain *PhD Thesis* (Helsinki, Finland: University of Helsinki)

Berger M J 1963 Monte Carlo Calculation of the Penetration and Diffusion of Fast Charged Particles *Methods in Computational Physics* **135**

Berger M J 1993 Proton Monte Carlo transport program PTRAN National Institute for Standards and Technology *Report NISTIR 5113* (Gaithersburg, MD)

Binns P J *et a*l. 2005 An international dosimetry exchange for boron neutron capture therapy Part I: Absorbed dose measurements *Med Phys.* **32** 3729-36

Bleuel D L 2003 Determination and production of an optimal neutron energy spectrum for boron neutron capture therapy *PhD Thesis* (Berkeley, CA: University of California)

Bleuel D L, Donahue R J, Ludewigt B A, Vujic J 1998 Designing accelerator-based epithermal neutron beams for boron neutron capture therapy *Med Phys.* **25** 1725-34

Blomgren H, Lax I, Näslund I and Svanström R 1995 Stereotactic high dose fraction radiation therapy of extracranial tumors using an accelerator. Clinical experience of the first thirty-one patients *Acta Oncol.* **34** 861-70.

Blue T E and Yanch J C 2003 Accelerator-based epithermal neutron sources for boron neutron capture therapy of brain tumors *J. Neurooncol.* **62** 19-31

Briesmeister J F, Ed. 2000 MCNP—a general Monte Carlo code N-particle transport code, Version4C, *Report LA-13709* (Los Alamos National Laboratory)

Brooks R A, Di Chiro G, Keller M R 1980 Explanation of cerebral white--gray contrast in computed tomography *J. Comput. Assist. Tomogr.* **4** 489-91

Busse P M *et al.* 2003 A critical examination of the results from the Harvard-MIT NCT program phase I clinical trial of neutron capture therapy for intracranial disease *J. Neurooncol.* **62** 111-21

Bohm T D, Griffin S L, DeLuca P M Jr., DeWerd L A 2005 The effect of ambient pressure on well chamber response: Monte Carlo calculated results for the HDR 1000 plus *Med Phys.* **32** 1103-14

Bortolussi S *et al.* 2011 Boron uptake measurements in a rat model for Boron Neutron Capture Therapy of lung tumours *Appl. Radiat. Isot.* **69** 394-8

Boutillon M and Perroche A -M 1993 Ionometric determination of absorbed dose to water for cobalt-60 gamma rays *Phys. Med. Biol.* **38** 439

Capote R, Sánchez-Doblado F, Leal A, Lagares J I, Arráns R, Hartmann G H 2004 An EGSnrc Monte Carlo study of the microionization chamber for reference dosimetry of narrow irregular IMRT beamlets *Med Phys.* **31** 2416-22.

Carrier J F, Archambault L, Beaulieu L, Roy R 2004 Validation of GEANT4, an object-oriented Monte Carlo toolkit, for simulations in medical physics *Med. Phys.* **31** 484-92

Carrier R and Cormack D 1995 Historical Overview Physics in Canada Special Issue 51

Cerullo N, Esposito J and Daquino G G 2004 Spectrum shaping assessment of accelerator-based fusion neutron sources to be used in BNCT treatment *Nuclear Instruments and Methods in Physics Research Section B: Beam Interactions with Materials and Atoms* **213** 641-5

Chadwick M B *et al.* 2006 ENDF/B-VII.0: Next Generation Evaluated Nuclear Data Library for Nuclear Science and Technology *Nuclear Data Sheet* **107**

Chanana A D *et al.* 1999 Boron neutron capture therapy for glioblastoma multiforme: interim results from the phase I/II dose escalation studies *Neurosurgery* **44** 1182–92

Chetty I J *et al.* 2007 Report of the AAPM Task Group No. 105: Issues associated with clinical implementation of Monte Carlo-based photon and electron external beam treatment planning *Med. Phys.* **34** 4818-53

Coderre J A, Elowitz E H, Chadha M, Bergland R, Capala J, Joel D D, Liu H B, Slatkin D N and Chanana A D 1997 Boron neutron capture therapy for glioblastoma multiforme using boronophenylalanine and epithermal neutrons: trial design and early clinical results *J. Neurooncol.* **33** 141-52

Coderre J A and Morris G M 1999 The radiation biology of boron neutron capture therapy *Radiat. Res.* **151** 1-18

Cohen L, Hendrickson F R 1989 Neutron therapy for nonresectable radioresistant tumors *Arch. Surg.* **124** 294-300

Culbertson C N, Green S, Mason A J, Picton D, Baugh G, Hugtenburg R P, Yin Z, Scott M C, Nelson J M 2004 In-phantom characterisation studies at the Birmingham Accelerator-Generated epIthermal Neutron Source (BAGINS) BNCT facility *Appl. Radiat. Isot.* **61** 733-8

Dancey J E, Shepherd F A, Paul K, Sniderman K W, Houle S, Gabrys J, Hendler A L and Goin J E 2000 Treatment of nonresectable hepatocellular carcinoma with intrahepatic 90Y-microspheres *J. Nucl. Med.* **41** 1673-81

Doucet R, Olivares M, DeBlois F, Podgorsak E B, Kawrakow I and Seuntjens J 2003 Comparison of measured and Monte Carlo calculated dose distributions in inhomogeneous phantoms in clinical electron beams *Phys. Med. Biol.* **48** 2339–54

Duderstadt J and Martin W 1979 Transport Theory (New York: Wiley)

Durisi E, Zanini A, Manfredotti C, Palamara F, Sarotto M, Visca L and Nastasi U 2007 Design of an epithermal column for BNCT based on D–D fusion neutron facility *Nucl. Inst. and Methods in Physics Research Section A: Accelerators, Spectrometers, Detectors and Associated Equipment* **574** 363-9

Fong Y *et al.* 1997 Liver resection for colorectal metastases *J. Clin. Oncol.* **15** 938-46

Forton E, Stichelbaut F, Cambriani A, Kleeven W, Ahlback J, Jongen Y 2009 Overview of the IBA accelerator-based BNCT system *Appl. Radiat. Isot.* **67** S262-5

Fragoso M, Wen N, Kumar S, Liu D, Ryu S, Movsas B, Munther A and Chetty IJ 2010 Dosimetric verification and clinical evaluation of a new commercially available Monte Carlo-based dose algorithm for application in stereotactic body radiation therapy (SBRT) treatment planning *Phys. Med. Biol.* **55** 4445-64

Garabalino MA, Monti Hughes A, Molinari AJ, Heber EM, Pozzi EC, Cardoso JE, Colombo LL, Nievas S, Nigg DW, Aromando RF, Itoiz ME, Trivillin VA and Schwint AE 2011 Boron neutron capture therapy (BNCT) for the treatment of liver metastases: biodistribution studies of boron compounds in an experimental model *Radiat Environ Biophys*. **50** 199-207

Goorley T *et al.* (2011) Initial MCNP6 Release Overview, Los Alamos National Laboratory *LAUR-11-05198* (Nuclear Technology) in press

Gragg RL, Humphrey RM and Meyn RE 1977 The response of Chinese hamster ovary cells to fast neutron radiotherapy beams. II. Sublethal and potentially lethal damage recovery capabilities. *Radiat. Res*. **71** 461-70

Griffin T and Phillips MH 1998 Particle Beam Radiation Therapy: Clinical Applications. In Perez CA and Brady LW (eds): *Principles and Practice of Radiation Oncology, 3rd Edition*, (Philadelphia: J B Lippincott Co) pp. 607-616

Grofsmid D, Dirkx M, Marijnissen H, Woudstra E and Heijmen B 2010 Dosimetric validation of a Monte Carlo based IMRT planning system *Med. Phys.* **37** 540–9

Halbleib J A, Kensek R P, Valdez G D, Seltzer S M, and Berger M J 1992 ITS: the integrated TIGER series of electron/photon Monte Carlo transport codes Version 3.0, *IEEE Trans. Nucl. Sci.* **39** 1025-30

Hatanaka H and Sano K 1973 A revised boron-neutron capture therapy for malignant brain tumors. I. Experience on terminally ill patients after cobalt-60 radiotherapy *Z Neurol* **204** 309-332 Hawthorne MF and Lee MW 2003 A critical assessment of boron target compounds for boron neutron capture therapy *J Neurooncol.* **62** 33-45

Henriksson R, Capala J, Michanek A, Lindahl SA, Salford LG, Franzén L, Blomquist E, Westlin JE and Bergenheim AT 2008 Swedish Brain Tumour Study Group. Radiother Oncol. **88** 183-91

Herfarth KK Debus J and Wannenmacher M 2004Stereotactic radiation therapy of liver metastases: update of the initial phase-I/II trial. *Front Radiat Ther Oncol* **38** 100-5

Hideghéty K, Sauerwein W, Haselsberger K, Grochulla F, Fankhauser H, Moss R, Huiskamp R, Gabel D, de Vries M 1999 Postoperative treatment of glioblastoma with BNCT at the Petten irradiation facility (EORTC protocol 11961) *Strahlenther Onkol.* **175** S111-4

Hughes H G 2005 Improved Logic for Sampling Landau Straggling in MCNP5 *ANS Mathematics and Computation Topical Meeting* (Avignon, France, 12-15 September 2005)

Hughes H G 2011 Controlling MCNP6 Transport with DBCN Options Second Beta Release *LAUR-11-01887* https://laws.lanl.gov/vhosts/mcnp.lanl.gov/pdf_files/la-ur-11-01887_dbcn_mcnp6b2.pdf

IAEA 2001 Current status of neutron capture therapy *TECDOC-1223* (Vienna: IAEA)

IAEA 2005 Radiation Oncology Physics: A Handbook for teachers and students (editor E.B. Podgorsak)

ICRU 1978 Dose Specification for Reporting External Beam Therapy with Photons and Electrons *ICRU Report 29* (Bethesda, MD: ICRU)

ICRU 1987 Use of Computers in External Beam Radiotherapy Procedures with High-energy Photons and Electrons *ICRU Report No 42* (Bethesda, MD: ICRU)

ICRU 1989 Clinical neutron dosimetry Part I: determination of absorbed dose in a patient treated by external beams of fast neutrons ICRU *Report No 45* (Bethesda, MD: ICRU)

ICRU 1992 Radiation Dosimetry: Electron, Photon, Electron, Proton and Neutron Interaction Data for Body Tissues *ICRU Report No 46* (Bethesda, MD: ICRU)

ICRU 1993 Prescribing, Recording, and Reporting Photon Beam Therapy *ICRU Report No 50* (Washington, DC: ICRU)

ICRU 2001 Dosimetry of High-Energy Photon Beams Based on Standards of Absorbed Dose to Water *ICRU Report No 64* (Bethesda, MD: ICRU)

Fujii H, Matsuyama A, Komoda H, Sasai M, Suzuki M, Asano T, Doki Y, Kirihata M, Ono K, Tabata Y, Kaneda Y, Sawa Y and Lee CM 2011 Cationized gelatin-HVJ envelope

with sodium borocaptate improved the BNCT efficacy for liver tumors in vivo *Radiat Oncol.* **6** 8

Imahori Y, Ueda S, Ohmori Y, Sakae K, Kusuki T, Kobayashi T, Takagaki M, Ono K, Ido T and Fujii R 1998 Positron emission tomography-based boron neutron capture therapy using boronophenylalanine for high-grade gliomas: part II. *Clin. Cancer Res.* **4** 1833-41

Ishiwata K *et al.* 1992 A unique in vivo assessment of 4-[10B]borono-Lphenylalanine in tumor tissues for boron neutron capture therapy of malignant melanomas using positron emission tomography and 4-borono-2-[18F]fluoro-L-phenylalanine *Melanoma Res.* **2** 171–179

Iwase, H Niita, K and Nakamura T 2002 Development of a general-purpose particle and heavy ion transport Monte Carlo code *J. Nucl. Sci. Technol.* **39** 1142–1151

Joensuu H *et al.* 2003 Boron neutron capture therapy of brain tumors: clinical trials at the finnish facility using boronophenylalanine. *J. Neurooncol.* **62** 123-34

Fippel M and Nüsslin F 2001 Evaluation of a clinical Monte Carlo dose calculation code based on the ICCR benchmark test," *Med. Phys.* **28** (AAPM Annual Meeting Issue) Abstr. 1198

Gifford K A, Horton J L Jr, Wareing T A, Failla G and Mourtada F 2006 Comparison of a finite element multi group discrete-ordinates code with Monte Carlo for radiotherapy calculations *Phys. Med. Biol.* **51** 2253–65

Goitein M and Busse J 1975 Immobilization error: Some theoretical considerations *Radiology* **117** 407 412

González, S J *et al.* 2005 Voxel model in BNCT treatment planning: performance analysis and improvements *Phys. Med. Biol.* **50** 441–458

Goorley J T, Kiger W S 3rd and Zamenhof R G 2002 Reference dosimetry calculations for neutron capture therapy with comparison of analytical and voxel models *Med. Phys.* **29** 145-56

Heath E, Seuntjens J and Sheikh-Bagheri D 2004 Dosimetric evaluation of the clinical implementation of the first commercial IMRT Monte Carlo treatment planning system at 6 MV *Med. Phys.* **31** 2771–9

Kabalka GW *et al.* 1997Evaluation of fluorine-18-BPA-fructose for boron neutron capture treatment planning. *J Nucl Med* **38** 1762–67

Kadri O, Ivanchenko V, Gharbi F and Trabelsi A 2009 Incorporation of the Goudsmit–Saunderson electron transport theory in the Geant4 Monte Carlo code *Nucl. Instrum. Methods B* **267** 3624-32

Kankaanranta L, Saarilahti K, Mäkitie A, Välimäki P, Tenhunen M and Joensuu H 2011 Boron neutron capture therapy (BNCT) followed by intensity modulated chemoradiotherapy as primary treatment of large head and neck cancer with intracranial involvement *Radiother Oncol.* **99** 98-9

Kankaanranta L *et al.* 2007 Boron neutron capture therapy in the treatment of locally recurred head and neck cancer *Int. J. Radiat. Oncol. Biol. Phys.* **69** 475-82

Kankaanranta L *et al.* 2012 Boron neutron capture therapy in the treatment of locally recurred head and- neck cancer: final analysis of a phase I/II trial *Int J Radiat Oncol Biol Phys.* **82** e67-75

Karila J 2006 Thermoluminescent dosimetry in boron neutron capture therapy *Licenciate thesis* (Helsinki, Finland: University of Helsinki)

Kato I, Ono K, Sakurai Y, Ohmae M, Maruhashi A, Imahori Y, Kirihata M, Nakazawa M and Yura Y 2004 Effectiveness of BNCT for recurrent head and neck malignancies. *Appl Radiat Isot.* **61** 1069-73

Kawrakow I 2000a Accurate condensed history Monte Carlo simulation of electron transport. II. Application to ion chamber response simulations *Med. Phys.* **27** 499-513

Kawrakow I 2000b Accurate condensed history simulation of electron transport: I. EGSnrc, the new EGS4 version *Med. Phys.* **27** 485–98

Kawrakow I 2001 VMC++ , electron and photon Monte Carlo calculations optimized for radiation treatment planning *Advanced Monte Carlo for Radiation Physics, Particle Transport Simulation and Applications: Proceedings of the Monte Carlo 2000 Meeting Lisbon* (edited by A. Kling, F.Barao, M. Nakagawa, L. Tavora, and P. Vaz) (Berlin: Springer) pp. 229–236

Kawrakow I and Rogers D W O 2003 The EGSnrc Monte Carlo system: Monte Carlo simulations of electron and photon transport *NRC Report PIRS-701* (Ottawa: NRC)

Kawrakow I and Fippel M 2000 Investigation of variance reduction techniques for Monte Carlo photon dose calculation using XVMC *Phys. Med. Biol.* **45** 2163–2183

Kirby D, Green S, Palmans H, Hugtenburg R, Wojnecki C and Parker D 2010 LET dependence of GafChromic films and an ion chamber in low-energy proton dosimetry. *Phys Med Biol.* **55** 417-33

Kononov OE, Kononov VN, Bokhovko MV, Korobeynikov VV, Soloviev AN, Sysoev AS, Gulidov IA, Chu WT and Nigg DW 2004 Optimization of an accelerator-based epithermal neutron source for neutron capture therapy. *Appl Radiat Isot* **61** 1009-13

Kortesniemi M 2002 Solutions for Clinical Implementation of Boron Neutron Capture Therapy in Finland, *PhD thesis Report Series in Physics HU-P-D95* (Helsinki, Finland: University of Helsinki) thesis.helsinki.fi/julkaisut/mat/fysik/vk/kortesniemi/solution.pdf

Kosunen A, Kortesniemi M, YläMella H, Seppälä T, Lampinen J, Serén T, Auterinen I, Järvinen H and Savolainen S 1999 Twin ionisation chambers for dose determination in phantom in an epithermal neutron beam *Rad. Prot. Dos.* **81** 187-94

Kosunen A 1999 Metrology and quality of radiation therapy dosimetry of electron, photon and epithermal neutron beams *PhD thesis* (Helsinki: STUK A164)

Kotiluoto P, Hiismäki P and Savolainen S 2001 Application of the new MultiTrans SP3 radiation transport code in BNCT dose planning *Med. Phys.* **28** 1905–10

Kotiluoto P 2007 Adaptive tree multigrids and simplified spherical harmonics approximation in deterministic neutral and charged particle transport *PhD thesis* (Espoo: VTT Publications 639)

Kouri M *et al.* 2004 Undifferentiated sinonasal carcinoma may respond to single-fraction boron neutron capture therapy *Radiother Oncol* **72** 83–5

Kumada H, Yamamoto K, Matsumura A, Yamamoto T, Nakagawa Y, Nakai K and Kageji T 2004 Verification of the computational dosimetry system in JAERI (JCDS) for boron neutron capture therapy *Phys. Med. Biol.* **49** 3353–65

Kumada H, Yamamoto K, Matsumura A, Yamamoto T, Nakagawa Y, Kageji T 2006 Improvement of JCDS, a computational dosimetry system in JAEA for neutron

capture therapy *Advances in Neutron Capture Therapy 2006* In: Proceedings of ICNCT-12 512-515

Künzler T, Fotina I, Stock M and Georg D 2009 Experimental verification of a commercial Monte Carlo-based dose calculation module for high-energy photon beams *Phys Med Biol.* **54** 7363-77

Leal A, Sanchez-Doblado F, Arrans R, Rosello J, Pavon E C and Lagares J I 2003 Routine IMRT verification by means of an automated Monte Carlo simulation system *Int. J. Radiat. Oncol. Biol. Phys.* **56** 58–68

Liu Y-H, Lin Y-C, Nievaart S, Roca A, Tsai E-E, Liu H-M, Moss R and Jiang S-H 2010 The activation contamination in the metal-based ionization chambers as gamma dosimeters in the mixed filed dosimetry *Radiation Measurements* **45** *1427-1431*

Li H S, Liu Y W, Lee C Y, Lin T Y and Hsu F Y 2009 Verification of the accuracy of BNCT treatment planning system THORplan *Appl. Radiat. Isot.* **67** S122–5

Locher G L 1936 *Am. J. Roentgenol. Radium Ther.* **36** 1-13

Lou TP, Vujic JL, Koivunoro H, Reijonen J and Leung KN 2003 Fission multipliers for D-D/D-T neutron generators *Sixth International Meeting on Nuclear Applications of Accelerator Technology* (AccApp'03): Accelerator Applications in a Nuclear Renaissance 2003 (San Diego, CA)

Ma CM and Nahum AE 1991 Bragg-Gray theory and ion chamber dosimetry for photon beams *Phys Med Biol.* **36** 413-28

Madoc-Jones H *et al.* 1996 A Phase–I dose escalation trial of Boron Neutron Capture Therapy for subjects with metastatic subcutaneous melanoma of the extremities *In: Cancer Neutron Capture Therapy* ed Yutaka Mishima (New York: Plenum Press) 707

Marek M and Viererbl L 2004 Spatial characterization of BNCT beams *Appl Radiat Isot.* **61** 1051-5

Matsumura A, Yamamoto T, Tsurubuchi T, Matsuda M, Shirakawa M, Nakai K, Endo K, Tokuue K and Tsuboi K 2009 Current practices and future directions of therapeutic strategy in glioblastoma: survival benefit and indication of BNCT *Appl Radiat Isot.* **67** S12-4

Mainegra-Hing E, Kawrakow I and Rogers DW 2003 Calculations for plane-parallel ion chambers in ^{60}Co beams using the EGSnrc Monte Carlo code *Med Phys.* **30** 179-89

Menéndez PR *et al.* 2009 BNCT for skin melanoma in extremities: updated Argentine clinical results *Appl Radiat Isot.* **67** S50-3

Mishima Y, Honda C, Ichihashi M, Obara H, Hiratsuka J, Fukuda H, Karashima H, Kobayashi T, Kanda K and Yoshino K 1989 Treatment of malignant melanoma by single thermal neutron capture therapy with melanoma-seeking 10B-compound *Lancet.* **2** 388-9

Miyatake S *et al.* 2005 Modified boron neutron capture therapy for malignant gliomas performed using epithermal neutron and two boron compounds with different accumulation mechanisms: an efficacy study based on findings on neuroimages *J Neurosurg.* **103** 1000-9

Miyatake SI *et al.* 2006 Clinical results of BNCT for malignant meningiomas *Advances in neutron capture therapy* In: Proceedings 12th international congress on neutron

capture therapy, Takamatsu, Japan ed Nakagawa Y, Kobayashi T and Fukuda H pp. 51–3

Munck af Rosenschold P M, Ceberg C P, Giusti V and Andreo P 2002 Photon quality correction factors for ionization chambers in an epithermal neutron beam *Phys. Med. Biol.* **47** 2397–409

Nahum A E 1988 Simulation of dosimeter response and interface effects *Monte Carlo Transport of Electrons and Photons* ed T. M. Jenkins, W. R. Nelson, A. Rindi, A. E. Nahum, and D. W. O. Rogers (New York: Plenum)

Nakagawa Y and Hatanaka H 1997 Boron neutron capture therapy: clinical brain tumour studies *J. Neurooncol.* **33** 105–15

Nelson W R, Hirayama H and Rogers D W O 1985 The EGS4 Code system *Report SLAC-265* (Stanford, CA: Stanford Linear Accelerator Center)

Nigg D W et al. 1999a Collaborative neutronic performance characterization of the FiR 1 clinical epithermal neutron beam facility for BNCT *INEEL BNCT Research Program Annual Report 1998* INEEL-EXT-99-00293 ed J R Venhuizen (Idaho Falls: Martin Idaho Technologies Company) pp 13–38

Nigg D W, Wemple C A, Wessol D E and Wheeler F J 1999b SERA—an advanced treatment planning system for neutron therapy and BNCT *Trans. ANS* **80** 66–8

Nigg D W 2003 Computational dosimetry and treatment planning considerations for neutron capture therapy *J. Neurooncol.* **62** 75-86

Nordlinger B *et al.* 1987 Hepatic resection for colorectal liver metastases *Ann Surg* **205** 256–263.

Palmans H 2006 Perturbation factors for cylindrical ionization chambers in proton beams. Part I: corrections for gradients *Phys Med Biol.* **51** 3483-501

Palmans H 2004 PTRAN, a Monte Carlo code for transport simulation of 50 to 250 MeV protons & McPTRAN.MEDIA, McPTRAN.CAVITY and McPTRAN.RZ, a series of derived codes *Lecture Notes for the NPL Workshop on Monte Carlo Codes* (17–18 March 2004) (National Physical Laboratory) http://www.npl.co.uk/ionrad/training/montecarlo/workshop/ptran notes.pdf

Palmans H, Symons JE, Denis JM, de Kock EA, Jones DT and Vynckier S 2002 Fluence correction factors in plastic phantoms for clinical proton beams *Phys Med Biol.* **47** 3055-71

Panettieri V, Sempau J and Andreo P 2008 Chamber-quality factors in 60Co for three plane-parallel chambers for the dosimetry of electrons, protons and heavier charged particles: PENELOPE Monte Carlo simulations *Phys Med Biol.* **53** 5917-26

Pelowitz D *et al.* 2011 MCNPX 2.7.0 Extensions, *LA-UR-11-2295* (Los Alamos, NM: Los Alamos National Laboratory)

Pinelli T *et al.* 2002 TAOrMINA: from the first idea to the application on the human liver *Research and Development in Neutron Capture Therapy* In: Proceedings of the 10th International Congress on Neutron Capture Therapy, Essen, Germany ed W Sauerwein, R Moss and A Wittig (Bologna: Monduzzi Editore) pp. 1065–1072

Protti N *et al.* 2009 Calculations of dose distributions in the lungs of a rat model irradiated in the thermal column of the TRIGA reactor in Pavia *Appl Radiat Isot.* **67** S210-3

Raaijmakers C P, Konijnenberg M W, Verhagen H W and Mijnheer B J 1995 Determination of dose components in phantoms irradiated with an epithermal neutron beam for boron neutron capture therapy *Med. Phys.* **22** 321-9

Raaijmakers CP, Watkins PR, Nottelman EL, Verhagen HW, Jansen JT, Zoetelief J and Mijnheer BJ 1996 The neutron sensitivity of dosimeters applied to boron neutron capture therapy *Med Phys.* **23** 1581-9.

Reijonen J, Gicquel F, Hahto SK, King M, Lou T-P and Leung KN 2005 D–D neutron generator development at LBNL *Applied Radiation and Isotopes* **63** 757-763

Reijonen J *et al.* 2004 First PGAA and NAA experimental results from a compact high intensity D–D neutron generator *Nuclear Instruments and Methods in Physics Research Section A: Accelerators, Spectrometers, Detectors and Associated Equipment* **522** 598-602

Rhoades W A and Childs R L 1988 The DORT two-dimensional discrete ordinates transport code *Nucl. Sci. Eng.* **99** 88-89

Riley KJ *et al.* 2008 An international dosimetry exchange for BNCT part II: computational dosimetry normalizations. *Med Phys.* **35** 5419-25

Roca A, Nievaart V A, Moss R L, Stecher-Rasmussen F and Zamfir N V 2008 Validating a MCNPX model of Mg(Ar) and TE(TE) ionisation chambers exposed to 60Co gamma rays *Radiat. Prot. Dosimetry* **129** 365-71

Rodríguez M L 2008 PENLINAC: Extending the capabilities of the Monte Carlo code PENELOPE for the simulation of therapeutic beams *Phys Med Biol.* **53** 4573–4593 Rogers DWO 1993 How accurately can EGS4/PRESTA calculate ion chamber response? *Med. Phys.* **20** 319–323

Rogers D W O 2006 Fifty years of Monte Carlo simulations for medical physics *Phys. Med. Biol.* **51** 287-301

Rogus R D, Harling O K and Yanch J C 1994 Mixed field dosimetry of epithermal neutron beams for boron neutron capture therapy at the MITR-II research reactor *Med. Phys.* **21** 1611-25

Rose PF (Comp. and Ed.) 1991 ENDF-201, ENDF/B-VI Summary Documentation *BNL-NCS-17541, 4th Edition*

Roussin R W 1980 BUGLE-80: Coupled 47 Neutron, 20 Gamma-Ray, P3, Cross-Section Library for LWR Shielding Calculations *Informal Notes* Available from the Radiation Safety Information Computational Center at Oak Ridge National Laboratory as *DLC-075/BUGLE-80*

La Russa DJ, McEwen M and Rogers DW 2007 An experimental and computational investigation of the standard temperature-pressure correction factor for ion chambers in kilovoltage x rays *Med Phys.* **34** 4690-9

La Russa DJ and Rogers DW 2006 An Egsnrc investigation of the P(TP) correction factor for ion chambers in kilovoltage X rays *Med Phys.* **33** 4590-9

Rusthoven KE *et al.* 2009 Multi-institutional phase I/II trial of stereotactic body radiation therapy for liver metastases *J Clin Oncol.* **27** 1572-8

Ryynänen P 2002 Kinetic mathematical models for the 111In labelled bleomycin complex and 10B in boron neutron capture therapy, PhD thesis *Report Series in Physics, HUPD102* (Helsinki, Finland: University of Helsinki)

Salvat F, Fernandez-Varea JM and Sempau J 2008 *PENELOPE-2008: A code system for Monte Carlo simulation of electron and photon transport* (Issy-les-Moulineaux: OECD Nuclear Energy Agency) (available in pdf format on the web at http://www.nea.fr)

Sarfaraz M, Kennedy AS, Cao ZJ, Sackett GD, Yu CX, Lodge MA, Murthy R, Line BR and Van Echo DA 2003 Physical aspects of yttrium-90 microsphere therapy for nonresectable hepatic tumors *Med Phys.* **30** 199-203

Sarfaraz M, Kennedy AS, Lodge MA, Li XA, Wu X and Yu CX 2004 Radiation absorbed dose distribution in a patient treated with yttrium-90 microspheres for hepatocellular carcinoma *Med Phys.* **31** 2449-53

Sauerwein W and Zurlo A 2002 EORTC Boron Neutron Capture Therapy Group.The EORTC Boron Neutron Capture Therapy (BNCT) Group: achievements and future projects *Eur J Cancer.* **38** S31-4

Savolainen S *et al.* 2001 Dosimetry chain for the dogs irradiated in the epithermal neutron beam at the Finnish BNCT Facility *Frontiers in Neutron Capture Therapy* **2** ed MF Hawthorne, K Shelly and R J Wiersema (New York: Kluwer Academic/Plenum Publishing Corporation) pp. 1245-50

Savolainen S *et al.* 2012 Boron neutron capture therapy (BNCT) in Finland: Technological and physical prospects after 20 years of experiences *Phys Med.* May 19 (Epub ahead of print)

Schneider U, Pedroni E and Lomax A 1996 The calibration of CT Hounsfield units for radiotherapy treatment planning *Phys Med Biol.* **41** 111-24

Seltzer S M 1988 An overview of Monte Carlo methods *Monte Carlo Transport of Electrons and Photons* ed T M Jenkins, W R Nelson and A Rindi (New York: Plenum) pp 153–81

Seltzer S M 1991 Electron-photon Monte Carlo calculations: The ETRAN code *Appl. Radiat. Isot.* **42** 917-935

Sempau J, Acosta E, Baró J, Fernández-Varea J M and Salvat F 1997 An algorithm for Monte Carlo simulation of coupled electron-photon transport *Nucl. Instr. Meth. B* **132** 377–90

Sempau J and Andreo P 2006 Configuration of the electron transport algorithm of PENELOPE to simulate ion chambers *Phys. Med. Biol.* **51** 3533–48

Seppälä T 2002 FiR 1 Epithermal Neutron Beam Model and Dose Calculation for Treatment Planning in Neutron Capture Therapy, PhD thesis *Report Series in Physics, HU-P-D103* (Helsinki, Finland: University of Helsinki) ethesis.helsinki.fi/julkaisut/mat/fysik/vk/seppala/fir1epit.pdf

Seppälä T, Vähätalo J, Auterinen I, Kosunen A, Nigg D W, Wheeler F J and Savolainen S 1999 Modelling of brain tissue substitutes for phantom materials in neutron capture therapy (NCT) dosimetry *Radiation Physics and Chemistry* **55** 239-246

Seppälä T *et al.* 2002 Dose planning with comparison to in vivo dosimetry for epithermal neutron irradiation of the dog brain *Med Phys.* **29** 2629-40

Seppälä T *et al.* 2004 A dosimetric study on the use of bolus materials for treatment of superficial tumors with BNCT *Appl Radiat Isot.* **61** 787-91

Seppälä T, Kotiluoto P, Savolainen S, Auterinen I, Hiismäki P, Serén T, Kosunen A, Aschan C, Kortesniemi M and Toivonen M 2001 Determining and reporting the

doses in the treatments of glioma patients in the epithermal neutron beam at the Finnish BNCT facility (FiR 1) *IAEATECDOC-1223* 275-87

Serén T, Auterinen I, Seppälä T and Kotiluoto P 1999 Spectrum measurements and calculations in the epithermal neutron beam at the FiR 1 BNCT facility *15th Europeon TRIGIA Conf., VTT Symp.* **197** ed S Salmenhaara (Espoo: Libella) pp. 167–79

Schefter TE, Kavanagh BD, Timmerman RD, Cardenes HR, Baron A and Gaspar LE 2005 A phase I trial of stereotactic body radiation therapy (SBRT) for liver metastases *Int J Radiat Oncol Biol Phys.* **62** 1371-8

Simpson DR, Lawson JD, Nath SK, Rose BS, Mundt AJ and Mell LK 2009 Utilization of advanced imaging technologies for target delineation in radiation oncology *J Am Coll Radiol.* **6** 876-83

Singletary AE *et al.* 2003 A role for curative surgery in the treatment of selected patients with metastatic breast cancer *Oncologist* **8** 241–251

Slatkin DN 1991 A history of boron neutron capture therapy of brain tumours. Postulation of a brain radiation dose tolerance limit *Brain.* **114** 1609-29

Snyder WS, Ford M R, Warner G G and Fisher Jr. HL 1969 Estimates for absorbed fractions for monoenergetic photon sources uniformly distributed in various organs of a heterogeneous phantom *J. Nucl. Med*, **3** 47

Sterpin E, Salvat F, Cravens R, Ruchala K, Olivera GH and Vynckier S 2008 Monte Carlo simulation of helical tomotherapy with PENELOPE *Phys Med Biol.* **53** 2161–80

Stewart JG and Jackson AW 1975 The steepness of the dose response curve both for tumor curve and normal tissue injury *Laryngoscope* **85** 1107-11

Stubbs RS, Cannan RJ and Mitchell AW 2001 Selective internal radiation therapy (SIRT) with 90Yttrium microspheres for extensive colorectal liver metastases *Hepatogastroenterology.* **4** 333-7

Suzuki M, Sakurai Y and Hagiwara S 2007 First attempt of boron neutron capture therapy (BNCT) for hepatocellular carcinoma *Jpn. J. Clin. Oncol.* **37** 376–381

Suzuki M *et al.* 2008 A novel concept of treatment of diffuse or multiple pleural tumors by boron neutron capture therapy (BNCT) *Radiother Oncol* **88** 192–195.

Suzuki M, Sakurai Y, Masunaga S, Kinashi Y, Nagata K, Maruhashi A and Ono K 2006 Feasibility of boron neutron capture therapy (BNCT) for malignant pleural mesothelioma from a viewpoint of dose distribution analysis *Int J Radiat Oncol Biol Phys.* **66** 1584-9

Tanaka H *et al.* 2009 Characteristics comparison between a cyclotron-based neutron source and KUR-HWNIF for boron neutron capture therapy *Nuclear Instruments and Methods in Physics Research Section B* **267** 1970-77

Tillikainen L, Helminen H, Torsti T, Siljamäki S, Alakuijala J, Pyyry J and Ulmer W 2008 A 3D pencil-beam-based superposition algorithm for photon dose calculation in heterogeneous media *Phys Med Biol.* **53** 3821-39

Timmerman R, Papiez L and Suntharalingam M 2003 Extracranial stereotactic radiation delivery: expansion of technology beyond the brain *Technol Cancer Res Treat.* **2** 153-60

Timonen M 2010 Proton magnetic resonance spectroscopy of a boron neutron capture therapy 10B carrier, L-p-boronophenylalanine-fructose complex PhD thesis *Report*

Series in Physics, HU-PD171 (Helsinki, Finland: University of Helsinki) (available at https://helda.helsinki.fi/bitstream/handle/10138/23208/protonma.pdf?sequence=1)

Trivillin VA, Heber EM, Nigg DW, Itoiz ME, Calzetta O, Blaumann H, Longhino J and Schwint AE 2006 Therapeutic success of boron neutron capture therapy (BNCT) mediated by a chemically non-selective boron agent in an experimental model of oral cancer: a new paradigm in BNCT radiobiology *Radiat Res.* **166** 387-96

Tsukamoto T, Tanaka H, Yoshinaga H, Mitsumoto T, Maruhashi A, Ono K and Sakurai Y 2011 A phantom experiment for the evaluation of whole body exposure during BNCT using cyclotron based epithermal neutron source (C-BENS) *Appl Radiat Isot.* **69** 1830-3

Uusi-Simola J 2009 Finnish Dosimetric Practice for Epithermal Neutron Beam Dosimetry in Boron Neutron Capture Therapy, PhD thesis *Report Series in Physics, HU-P-D160* (Helsinki, Finland: University of Helsinki) (available at http://www.doria.fi/bitstream/handle/10024/44583/finnishd.pdf?sequence=1)

Van Dyk J *et al.* 2004 Commissioning and quality assurance of computerized planning systems for radiation treatment of cancer *IAEA TRS-430* (Vienna, Austria: International Atomic Energy Agency)

Verhaegen F and Seuntjens J 2003 Monte Carlo modelling of external radiotherapy photon beams. *Phys Med Biol.* **48** R107-64

Verbeke JM, Vujic J and Leung K-N 2000 Neutron Beam Optimization for Boron Neutron Capture Therapy Using the D-D and D-T High-Energy Neutron Sources *Nuclear Technology* **129** 257

Vilches M, García-Pareja S, Guerrero R, Anguiano M, and Lallena A M 2009 Multiple scattering of 13 and 20 MeV electrons by thin foils: A Monte Carlo study with GEANT, Geant4, and PENELOPE *Med Phys.* **36** 3964–70

Vitale GC, Heuser LS and Polk Jr, HC 1986 Malignant tumors of the liver *Surg. Clin. North Am.* **66** 723-41

Voorbraak W and Järvinen H 2003 Recommendations for the dosimetry of boron neutron capture therapy (BNCT) *NRG Report 21425/03.55339/C* (Petten, The Netherlands: NRG)

Vähätalo J 2004 Studies of 4-dihydroxyborylphenylalanine and its radiolabelled analogues to implement clinical trials of boron neutron capture therapy in Finland, PhD thesis *ISBN 952-10- 1965-4* (Helsinki, Finland: University of Helsinki) (available at https://helda.helsinki.fi/bitstream/handle/10138/21087/studieso.pdf?sequence=1)

Wang CK, Blue TE and Blue JW 1990 An experimental study of the moderator assembly for a low energy proton accelerator neutron irradiation facility for BNCT *Basic Life Sci* **54** 271-80

Wang LL and Rogers DW 2007 Monte Carlo study of si diode response in electron beams *Med Phys*. **34** 1734-42 Wang LL and Rogers DW 2008a Calculation of the replacement correction factors for ion chambers in megavoltage beams by Monte Carlo simulation *Med Phys.* **35** 1747-55

Wang LL and Rogers DW 2008b The replacement correction factor for the BIPM flat cavity ion chamber and the value of W/e *Med Phys.* **35** 4410-6

Wareing T, Vassiliev O, Failla G, Davis I, McGhee J, Barnett D, Horton J and Mourtada F 2007 TU-EE-A1-01:validation of a prototype deterministic solver for photon beam

dose calculations on acquired CT data in the presence of narrow beams and heterogeneities *Med. Phys.* **34** 2565

Warenius HM, White R, Peacock JH, Hanson J, Britten RA and Murray D 2000 The influence of hypoxia on the relative sensitivity of human tumor cells to 62.5 MeV (p-->Be) fast neutrons and 4 MeV photons *Radiat Res.* 1**54** 54-63

Waters L S (ed) 2002 MCNPX User's Manual Version 2.4.0 Los Alamos National Laboratory document *LA-CP-02-408* (Los Alamos, NM: Los Alamos National Laboratory)

White JE *et al. 1996* BUGLE-96: Coupled 47 Neutron, 20 Gamma-Ray Group Cross-section Library Derived from ENDF/B-VI for LWR Shielding and Pressure Vessel Dosimetry Applications *RSICC Data Library Collection DLC-185* (Oak Ridge National Laboratory)

Wojnecki C and Green S 2002 A preliminary comparative study of two treatment planning systems developed for boron neutron capture therapy: MacNCTPlan and SERA *Med Phys.* **29** 1710-5

X-5 Monte Carlo Team 2008 MCNP - A General Monte Carlo N-Particle Transport Code, Version 5 - Volume I: Overview and Theory *LA-UR-03-1987* (Los Alamos, NM: Los Alamos National Laboratory) revised 2/2008. http://mcnp-green.lanl.gov/pdf/MCNP5_Manual_Volume_I_LAUR-03-1987.pdf

Yamamoto T, Nakai K and Matsumura A 2008 Boron neutron capture therapy for glioblastoma *Cancer Lett.* **262** 143-52

Yanagie H *et al.* 2011 Feasibility evaluation of neutron capture therapy for hepatocellular carcinoma using selective enhancement of boron accumulation in tumour with intra-arterial administration of boron-entrapped water-in-oil-in-water emulsion *Appl Radiat Isot.* **69** 1854-7

Yanch JC, Zhou XL and Brownell GL 1991 A Monte Carlo investigation of the dosimetric properties of monoenergetic neutron beams for neutron capture therapy *Radiat. Res.* **126** 1-20

Yanch JC, Zhou XL, Shefer RE and Klinkowstein RE 1992 Accelerator-based epithermal neutron beam design for neutron capture therapy *Med Phys* **19** 709-21

Zamenhof R, Redmond E II , Solares G, Katz D, Riley K, Kiger S and Harling O 1996 Monte Carlo-based treatment planning for boron neutron capture therapy using custom designed models automatically generated from CT data. *Int. J. Radiat. Oncol. Biol. Phys*. **35** 383–397

Zanon C, Grosso M, Clara R, Alabiso O, Chiappino I, Miraglia S, Martinotti R, Bortolini M, Rizzo M and Gazzera C 2001 Combined regional and systemic chemotherapy by a mini-invasive approach for the treatment of colorectal liver metastases *Am J Clin Oncol.* **24** 354-9

Zonta A *et al.* 2009 Extra-corporeal liver BNCT for the treatment of diffuse metastases: what was learned and what is still to be learned. *Appl Radiat Isot.* **67** S67-75